# Processive Acceleration of Actin Filament Barbed End Assembly by N-WASP

**Nimisha Khanduja**

Dissertation submitted to Faculty of Virginia Polytechnic and State University in partial fulfillment of the requirements for the degree of

Doctor of Philosophy
In
Biological Sciences

Jeffrey. R. Kuhn Co-Chair

Daniela Cimini Co-chair

Brenda S. J. Winkel

William Huckle

Amrinder Nain

9th December 2013

Blacksburg, Virginia

Key Words: Cell Movement; Actin Motility; Microscopy, Fluorescence, TIRF

**Processive Acceleration of Actin Filament Barbed End Assembly by N-WASP**

Nimisha Khanduja

# Abstract

Actin-based cell motility plays crucial roles throughout the lifetime of an organism. The dynamic rearrangement of the actin cytoskeleton triggers a plethora of cellular processes including cellular migration. Neural Wiskott Aldrich syndrome protein (N-WASP) is involved in transduction of signals from receptors on the cell surface to the actin cytoskeleton. N-WASP activated actin polymerization drives extension of invadopodia and podosomes into the basement layer. In addition to activating Arp2/3 complex, N-WASP binds actin filament barbed ends, and both N-WASP and barbed ends are tightly clustered in these invasive structures.

We used nanofibers coated with N-WASP WWCA domains as model cell surfaces and single actin filament imaging to determine how clustered N-WASP affects Arp2/3-independent barbed end assembly. Individual barbed ends captured by WWCA domains of N-WASP grew at or below their diffusion limited assembly rate. At high filament densities, overlapping filaments formed buckles between their nanofiber tethers and myosin attachment points. These buckles grew 3.4-fold faster than the diffusion-limited rate of unattached barbed ends. N-WASP constructs with and without the native poly-proline (PP) region showed similar rate enhancements. Increasing polycationic $Mg^{2+}$ or Spermine to enhance filament bundling increased the frequency of filament buckle

formation, consistent with a requirement of accelerated assembly on barbed end bundling.

Our preliminary data shows that tethered N-WASP construct containing one WH2 domain does not generate processive bundles or filament loops leading us to believe that tandem WH2 is required for processivity. We propose that this novel N-WASP assembly activity provides an Arp2/3-independent force that drives nascent filament bundles into the basement layer during cell invasion. Discovery of this bundle mediated unique pathway involved in invasion and metastasis will provide new targets for therapeutic development.

## Dedication

This thesis is dedicated to my beloved family who has supported me in everyway, especially to my late grandparents who believed in the richness of learning.

**Acknowledgements**

From the time I started as a PhD candidate at Virginia Tech till today there have been a number of people who have supported me and influenced me. I would like to take this time to mention some of their names and thank them for their effort and guidance.

First and foremost I offer my sincerest gratitude to my supervisor, Dr Jeffery Kuhn, who introduced me to the world of scientific research and has supported me throughout my studies. I am grateful for his continuous guidance, encouragement and inspiration. Thank for being so approachable and always being there to point me in the right direction.

I would like to express my heartfelt gratitude to Dr Daniela Cimini who has always gone that extra mile to advise me and find time in her schedule whenever I needed her guidance.

I would also like to thank Dr. William Huckle for his unrestricted support and constant motivation throughout my studies.

I am grateful to Dr. Amrinder Nain who has always been a constant support and provided an outside perspective that challenged me and helped me grow my knowledge.

Also, I would like to give my heartfelt gratitude to Dr. Brenda Winkel who was not only a role model but also a source of constant inspiration and support.

I would also like to thank Dr Capelluto for his guidance during the initial phase of my research.

I cannot complete this acknowledgment without mentioning some people who supported me with their love and friendship and motivated me to be the person I am today. I want to start with giving a special thanks to my loving parents and my brother for always

supporting me and encouraging me and being there for me during good and difficult times. I want to thank my dear colleagues in the Kuhn Lab-Xiaohua Hu, Sihui Zhang, Ying Li, Brent Bowden, Jane Canter, Casey Knowles, and especially Tracy James, a true friend and confidante. Beyond lab I want to say my thanks to Nidhi Parikh for being a loving and caring housemate for many years. I would also like to thank the faculty and staff in the Department of Biological Science for providing me the resources during my study. Lastly, I want to mention my loving husband for fully supporting, trusting and believing in me.

# Table of Contents

# List of Figures

# List of Tables

# Chapter 1

# Literature Review

## Overview: Cell Migration In Biology

Directed cell migration accompanies us from conception to death. In eukaryotes, cell migrations depend upon the actin cytoskeleton: a cohesive meshwork of protein filaments extending through the cytoplasm of cell (Bray 2001). Many cellular events, including migration, utilize localized actin polymerization to assemble a branched network of actin microfilaments that produces a protrusive force towards the plasma membrane. The dynamic assembly of a branched network of these actin filaments in eukaryotic cells drives cell migration and participates in endocytosis, phagocytosis, vesicle trafficking, cell maintenance, changes in cell shape, cytokinesis, and maintenance of polarity (Goley and Welch 2006).

In some cases, the pathways regulating cell motility are also instrumental in the dissemination of tumor cells away from their primary site of growth. This migration of primary tumor cells and their invasion into other tissues is called metastasis. Metastases resulting in the formation of secondary tumors account for more than 90% of the fatalities associated with cancer progression (Mehlen and Puisieux, 2006; Weigelt et al., 2005).

Because most cells rely on the actin migration machinery for general housekeeping functions, alterations to the actin machinery can result in metastasis. Up-regulation or activation of motility proteins encourages cells to move away from their initial place to invade surrounding tissues. Cell motility results from changes in the dynamics of the

protein, actin, polymerizing just under the plasma membrane in response to stimuli (Friedl and Gilmour, 2009).

Actin polymerizes into fiber like filaments that are approximately 6 nm in diameter. These filaments are cross-linked by other cellular proteins to form a wide variety of actin cytoskeletal based structures. These structures include protrusions at the leading edge of migrating cells, mainly the lamellopodia and filopodia, invasive structures like invadopodia and podosomes, stress fibers of adherent cells, neuronal growth cones and thin filament muscle fibers. All of these structures are dynamic and are able to reorganize themselves in response to internal/external stimuli.

The migration of cells involves protrusion of their leading edge and retraction of their trailing edge (Mitchison and Cramer, 1996). The cell protrusions of great interest are lamellopodia, filopodia and invadopodia. Lamellopodia are thin sheet like extension containing a dendritic actin network. Filopodia, on the other hand, are fingerlike membrane protrusions containing bundled actin filaments. Similarly, invadopodia are membrane protrusions containing a mix of bundled and branched actin that cause proteolysis of extracellular matrices (ECM). After development, invadopodia are found mainly in cancer cells.

The assembly and disassembly of actin filaments is accomplished by a plethora of proteins associated with the actin cytoskeleton that effect the actin filament nucleation, branching, elongation, capping, severing and crosslinking of actin filaments. Much of the understanding of actin mediated movement and regulatory protein function comes from decades of biochemical dissection of individual or combination of these purified proteins.

The understanding of complex cell movement can be understood and modeled from what we learned from these experiments.

## Structures for Cellular Migration

Cells make various structures to migrate under different conditions. Under such conditions cells become polarized and generate distinct membrane protrusions to migrate.

*Lamellipodia and Filopodia:* At the front of a migrating cell, a broad sheet-like membrane protrusion called the lamellipodium and filopodia, spike-like membrane protrusions that extend out from the lamellipodium, dominate the leading edge. These protrusive structures contain actin filaments with elongating barbed ends orientated towards the plasma membrane. Different actin architecture underlies these two different structures as illustrated in Figure 1.1. While lamellopodia consist of a meshwork of branched actin filaments, filopodia consist of bundled actin filaments.

*Invadopodia and Podosomes*: Cells produce specialized point-like membrane protrusions on their basal side to degrade ECM. Invadopodia and podosomes (which can be subsumed under the umbrella term `invadosomes') are subcellular actin-rich structures that are specialized for matrix degradation and are formed by cancer and normal cells, respectively (Gimona et al., 2008). Although both membrane structures are sites of matrix degradation, invadopodia are longer membrane protrusions with longer lifetime, and therefore more degradative (Murphy and Courtneidge, 2011).

## Actin Cytoskeleton and Cell Motility

Actin was first identified as part of the protein complex acto-myosin responsible for producing the contractile force in skeletal muscle (Straub, 1942). Most non-muscle cells

contain 100 $\mu$M cytosolic actin. The core constituent of actin cytoskeleton is the monomeric globular actin (G actin, where G for globular). The G actin monomer is a globular protein composed of a single polypeptide chain of 375 amino acids with a molecular weight of 42 kDa. The actin monomer has four sub-domains and forms a hinged molecule with a deep "ATP-binding cleft" on one side where ATP can enter and leave (Bray, 2001). Actin monomers can self-associate both laterally and longitudinally through a combination of hydrophobic and hydrogen bonds to generate a double-helical polymer filament that can grow up to several micrometers in length through further monomer addition. Actin subunits in the two helical strands are arranged in parallel (as apposed to anti-parallel) to give the filament an overall directional polarity. This polarity is key to the mechanism of actin assembly in cells (Bray, 2001). Based on the arrowhead pattern created when actin is decorated by rigor myosin S1 heads, one end of actin called the barbed end favors rapid monomer addition. The other- or pointed-end favors only slow growth. Actin filaments in cells orient their barbed ends outward and toward the cell surface. This orients the rapidly growing barbed end to push the cell membrane outward (Small et al., 1978a).

## Actin Dynamics

Under appropriate conditions actin monomers self-assemble to form filaments. Polymerization only occurs if the concentration of G-actin exceeds the critical concentration ($C_C$). The $C_C$ is defined as the concentration of actin monomers coexisting with polymer at equilibrium (Oosawa, 1983). In other words, at levels of actin below the $C_C$, actin will fail to polymerize and remain in monomer state. Inside cells, a large number of ABPs sequester actin and allow monomeric actin to exist at concentrations

100–1,000 times the $C_C$ *in vitro (Pollard et al., 2000a)*. The time course of the actin polymerization usually consists of four steps, namely, activation, nucleation and elongation (Gaszner et al., 1999) as illustrated in figure 1.2.

Activation results from the binding of $Mg^{2+}$, $K^+$ or $Ca^{2+}$ to the intermediate affinity cation-binding sites, and *in vitro*, the exchange of $Ca^{2+}$ for $Mg^{2+}$ at the high affinity cation-binding site (Carlier et al., 1986a). Activation reduces electrostatic repulsion between monomers by neutralizing the negative charges on actin (Carlier et al., 1986b; Frieden, 1983) and also induces a conformational change that facilitates the nucleation process (Gaszner et al., 1999).

Nucleation is an energetically unfavorable process of aggregating actin monomers to form a relatively stable oligomer (seed or nucleus)(Oosawa, 1983). A nucleus supports addition of monomeric actin at both ends leading to the formation of actin filaments. Spontaneous nucleation is kinetically unfavorable and is the rate-limiting step in polymerization, because the actin dimer intermediate is very unstable.

Elongation refers to the association and dissociation of actin monomers at both ends of the actin filament. Association predominantly occurs at the barbed end of the filament and dissociation at the pointed end. A short delay exists between the incorporation of ATP-G-actin onto a filament end and hydrolysis of the bound nucleotide. A longer delay exists for release of the generated inorganic phosphate. ATP hydrolysis primarily occurs at the barbed (growing) end of filaments. The structural polarity of F-actin and the irreversible nucleotide hydrolysis during actin assembly has implications for the rate and direction of filament growth at opposite ends of the actin filament. The $C_C$ for the pointed end is much higher than for the barbed end under physiological conditions. This

difference in $C_C$ may result in a continual flux of F-actin subunits from the pointed to the barbed end producing unidirectional growth of the actin filament. This head-to-tail polymerization or *treadmilling* (Wegner, 1976) of actin is modulated by a number of ABPs within cells (dos Remedios et al., 2003).

The rate of filament elongation is the constant ($k_{on}$, per $\mu$M per sec) multiplied by the concentration of free actin in solution. The depolymerization of filaments given by the rate constant $k_{off}$ (in per sec) is independent of the concentration of filaments. When the Cc is reached the rate of polymerization is equal to rate of depolymerization and is given by $k_{on} \times Cc = k_{off}$ or $k_{off}/ k_on = Cc$. Therefore at concentration greater than the critical concentration filaments elongate at rates that depend linearly on the concentration of actin.

Actin polymerization is ultimately driven by ATP hydrolysis. As filaments elongate, actin subunits hydrolyze their bound ATP and release the free phosphate. Rapid hydrolysis and slow phosphate release drives the different polymerization kinetics at each filament end. Actin monomers can bind to one molecule of ATP each, but ATP hydrolysis is extremely slow (several days) when actin is in its monomeric (G) state (Korn et al., 1987; Small et al., 1978b). During actin polymerization, one ATP bound G-actin assembles to the barbed end of another G-actin (Figure 1.2) resulting in a polarized filamentous actin (F –actin, F for filamentous) (Bugyi and Carlier, 2010; Holmes et al., 1990). Once polymerized, Mg-ATP-actin subunits at the barbed end rapidly hydrolyze their γ-phosphate (Blanchoin and Pollard, 2002) with a half-time of 2 seconds and slowly form Mg-ADP-actin by releasing their γ-phosphate with a half-time of 6 min (Blanchoin and Pollard, 1999; Melki et al., 1996). ADP bound actin has lower binding affinity for

filament ends. Therefore ADP-bound actin is more likely to disassociate from the filament than is ADP-Pi-bound actin or ATP-actin. After ADP actin monomers dissociate from either end of a filament, or the filament completely disassembles in a process called severing, ADP-bound G actin monomers are far less likely to re-polymerize. The ATP nucleotide held by the monomers must later be replaced by ATP in a process called 'nucleotide exchange'. Freshly recharged ATP-bound monomer is then available for re-polymerization. Because actin barbed ends are directed toward the plasma membrane, this cycle of polymerization and depolymerization drives actin filament growth towards the membrane (Small et al., 1978b). As a result, the growing actin filaments push the membrane forward to drive cell migration. The critical concentrations and rates of hydrolysis, association, and dissociation are different at each end of the filament. ATP provides the energy to maintain this difference in affinity for monomer addition between the barbed and pointed ends (Millard et al., 2004a).

Several line of evidence originally suggested that actin polymerization against the plasma membrane drives protrusions (Peskin et al., 1993). If the barbed end were constantly associated with the membrane, there would be little room for the addition of new actin monomers. In fact, because of Brownian motion, the relative position of barbed end and the plasma membrane fluctuates. In the "Brownian Ratchet" model of Mogilner and Oster (Mogilner and Oster, 1996), when the fluctuation of the membrane and barbed end provides a large enough gap, one actin monomer can add to the barbed end and push the membrane forward. Meanwhile, long enough actin filaments can bend to provide further space for actin monomer insertion at the barbed end. The lengthened actin filament then applies an elastic force to push the membrane forward. While actin

polymerization provides the force necessary for membrane expansion, the geometry of polymerized actin filaments dictates the morphology of the membrane protrusions.

## Actin Regulatory Proteins

A large repertoire of actin-binding proteins regulates the dynamic assembly and spatial organization of actin filaments to orchestrate the motility of eukaryotic cells. These proteins can: (i) promote the nucleation of actin monomers, like the Arp2/3 complex or formins; (ii) initiate the depolymerization of actin filaments, like the actin-depolymerizing factor (ADF/cofilin) family; (iii) bind to monomeric actin, like profilin and beta-thymosin; (iv) regulating filament assembly by capping barbed or pointed ends, such as the capping protein CapZ.

Most actin regulatory proteins bind preferentially either to actin monomers or to actin filaments to control organization and assembly actin cytoskeleton. For example, actin sequestration proteins bind to actin monomers and temporarily prevent their assembly, thereby maintaining the pool of unpolymerized actin. Other actin regulatory protein bind filaments and can stabilize actin nuclei, assist in filament elongation, sever filaments, cap filament ends, or organize filaments into a network or bundle them.

## Profilin

Profilin is an important spatial and temporal regulator of actin filament growth. Profilin, discovered in 1977 (Carlsson et al., 1977), is a 12-15 kD protein known to form a 1:1 complex with G-actin. Surprisingly, profilin can simultaneously both suppress and promote actin assembly through its actin monomer binding activity.

Profilin can positively regulate actin polymerization through its nucleotide-exchange activity. Profilin binds between subdomains 1 and 3 on an actin monomer and opens up the hinged ATP binding cleft of actin. By freeing a path for nucleotide to leave or enter actin, profilin catalyzes the exchange of actin-bound ADP to ATP. Profilin thereby converts poorly polymerizing ADP-actin monomers into readily polymerizing ATP-actin monomers (Goldschmidt-Clermont et al., 1992; Mockrin and Korn, 1980).

Profilin also suppresses spontaneous, or *de novo*, actin nucleation. Profilin binds to monomeric actin along the latitudinal actin-actin contact site and effectively suppresses actin dimer and trimer formation – essential pathways for the *de novo* formation of actin filament nuclei. Once actin nuclei are generate by other actin binding proteins (see below), profilin–actin complexes rapidly associate with the filament barbed end (but not the pointed end). After profilin-actin dimers are assembled on to a filament barbed end, profilin rapidly dissociates from its bound actin subunit, leaving the actin-actin binding interface free. Another profilin-actin dimer can then readily add to the barbed end to repeat the cycle.

In addition to its actin binding activity, profilin has two other binding domains: one for the phosphoinositide-phosphates, PtdIns(4,5)$P_2$ and PtdIns(3,4,5)$P_3$ (Lassing and Lindberg, 1985) and one for amino acid sequences rich proline, or so-called poly-L-proline stretches (Mahoney et al., 1999; Metzler et al., 1994). It is through the poly-L-proline-binding domain that profilin interacts with the many proteins. Profilin-actin complexes are fed into growing actin polymers by proteins such as formin and VASP that contain one or more stretches of proline-rich domains. These proteins can drive actin polymerization to much faster rates than available through unaided polymerization.

Profilin is essential for this mode of polymerization because it recruits the actin monomers to the proline-rich sites. Through their multiple poly-proline profilin binding sites, these proteins can recruit multiple profilin-actin dimers at once, increasing the pool of monomeric actin available for polymerization near the barbed end. These actin accelerating proteins have also been show to "feed" profilin-actin to the barbed end at the correct orientation for binding and thus greatly accelerate polymerization over the *de novo* assembly of randomly oriented actin to the barbed end.

## The Nucleator of Actin: Arp2/3 Complex

Because profilin so effectively suppresses spontaneous filament nucleation, eukaryotic cells rely on filament nucleators or nucleation factors (NF) to generate actin nuclei. Currently, there are three known classes of nucleation factors: Arp2/3 complex, Formins and Spire. Arp2/3 complex and Formins are expressed in all eukaryotes while Spire seems to be restricted to metazoans. These molecules control the time and location of actin polymerization, and additionally influence the structures of the actin networks that they generate.

Arp2/3 complex is a seven-subunit protein that is a major initiator of actin polymerization (Goley and Welch, 2006). The arp2/3 induces actin branches on pre-existing filaments to generate a new actin barbed end nucleus that propels the edge of the cell forward (Pollitt and Insall, 2009)**.** The Arp2/3 complex is intrinsically inactive, relying on signaling pathways converging on the members of the Wiskott-Aldrich syndrome family protein (WASP, N-WASP, WAVE, and WASH proteins) (Millard et al., 2004a).

The Arp2/3 complex was first purified from *Acanthamoeba castellanii* and was shown to consist of a stable assembly of seven polypeptides, including two main Arp (actin related proteins) subunits Arp2 and Arp3 (Goley and Welch, 2006; Mullins et al., 1997). The remaining five subunits were originally named by size, but are now referred to as ArpC1 (actin-related protein complex-1), ArpC2, ArpC3, ArpC4 and ArpC5 (Robinson et al., 2001) (Goley and Welch, 2006).

While many actin other nucleators have been identified, Arp2/3 complex is the major nucleator in lamellipodia formation (Lai et al., 2008; Suraneni et al., 2012)), invadopodia (Yamaguchi et al., 2005), podosomes (Kaverina et al., 2003) and pseudopods (Li et al., 2011).

When activated by a nucleation promoting factor (NPF), the Arp2/3 complex binds to the side of existing actin filament (mother filament) and nucleates a new branch of actin filament, known as the daughter filament (Amann and Pollard, 2001a). The actin-like Arp2 and Arp3 subunits form the pointed end of the new daughter filament, while ARPC2 and ARPC4 make contact with the mother filament (Weed et al., 2000). The new daughter filament and its mother filament form a "y"-shaped branch with both barbed ends pointing in the same direction (Amann and Pollard, 2001a) (Mullins et al., 1998a). This combination of filament nucleation and branching by the Arp2/3 complex is referred to as autocatalytic branching or dendritic nucleation for the "tree"-like shape these actin networks take (Goley and Welch, 2006).

The Arp2 and Arp3 subunits have both an inactive (open) conformation and an active (closed) conformation. In the inactive state conformation, the Arp2 and Arp3 are too far apart to interact with actin (Rodal et al., 2005), while in the active (closed) state,

Arp2 and Arp3 converge to form a pseudo-actin dimer that nucleates a new daughter actin filament. The activity of the Arp2/3 complex is tightly controlled through the signal dependent association with many NPFs – and their central role lies in stabilizing Arp2 and Arp3 in their active, closed conformation (Goley and Welch, 2006).

## Regulation of Arp2/3

Because Arp2/3 complex is such a potent actin nucleator, its activity must in turn be tightly regulated to control actin polymerization. The fact that purified Arp2/3 complex is inactive initially suggested that additional activators were required (Machesky et al., 1999). In fact, a number of nucleation-promoting factors (NPFs) that activate the Arp2/3 complex have been identified.

The largest group of NPFs is Wiskott-Aldrich Syndrome Protein (WASP)-family of proteins (Padrick and Rosen, 2010). Eight members of this protein family have been identified, namely, WASP, neural WASP (N-WASP) and Scar/WAVE-1, -2, and -3, WASH, WHAMM, and JMY (Campellone and Welch, 2010). These are capable of overcoming the rate-limiting step of actin polymerization by directly binding and controlling the nucleation promoting activity of the Arp2/3.

Based on the mechanism by which the NPFs activate the Arp2/3 complex, their branching effects, and how the signal-transduction pathways control them, the NPFs fall into two classes: I and II. Class I NPFs are activated by the Rho-family GTPases, CDC42 and Rac and are diverse in their overall domain organization. They possess a common WCA domain, which consists of a WASP-homology-2 (WH2 or W; also called V for verprolin-homology) domain that binds to actin monomers (Boczkowska et al., 2008; Rodal et al., 2005), and a central (C; cofilin-homology or connector) and acidic (A)

region, together known as CA, that bind to Arp2/3 (Boczkowska et al., 2008) (Goley and Welch, 2006). The WCA domain is sufficient for the activation of the Arp2/3 complex *in vitro* to polymerize branched actin filaments. While the CA region holds Arp2 and Arp3 in their active, closed conformation, the W domain holds an actin monomer in the proper orientation to form a pseudo-trimer of actin, Arp2, and Arp3 that function as the nucleus for the new filament.

The class II NPFs include the *saccharomyces cerevisiae* actin binding protein 1 (Abp 1), Pan1, and metazoan cortactin (Duncan et al., 2001; Kessels et al., 2001; Uruno et al., 2001). Like the class I NPFs they have an acidic region but instead of the monomeric actin-binding domain they contain a filamentous actin-binding region that activates the Arp2/3 complex. It is believed that the class II NPFs bind simultaneously to the Arp2/3 complex with a WASP family protein and remain attached to the Arp2/3 complex to inhibit branch dissociation (Weaver et al., 2001).

The canonical Class I Arp2/3 activator, WASP, was first identified as a rare X-chromosome linked disorder that leads to Wiskott-Aldrich syndrome, a combination of immune deficiency and low blood platelet count (Derry et al., 1994; Millard et al., 2004a). WASP is a 501-amino-acid proline-rich protein expressed in haematopoietic cells. A second, more ubiquitously expressed isoform was later isolated from brain and called N-WASP. (Miki et al., 1996). A protein related to WASP was identified in a genetic screen in *Dictyostelium* and named Scar, as disruption of the Scar gene suppresses abnormalities caused by loss of one of the cARs (cAMP receptors)(Bear et al., 1998). Later, the mammalian homologue of Scar was identified and named WAVE (WASP family verprolin homologous protein)(Machesky and Insall, 1998)((Miki et al.,

1998b). Mammals express two other isoforms of Scar/WAVE, bringing the total number of WASP family members to five: namely WASP, N-WASP, Scar/WAVE1, Scar/WAVE2 and Scar/WAVE3 (Suetsugu et al., 1999).

## Nucleation Promoting Factors: N-WASP

Another WASP family protein member, N-WASP, was first identified in a screening for Ash/Grb2 binding proteins (Miki et al., 1996). N-WASP is ubiquitously expressed but enriched in neural tissues (hence the name). The members of WASP family of proteins are characterized by conserved domain architecture (Innocenti et al., 2004). The C-terminus of N-WASP binds to and activates the Arp2/3 complex (Machesky et al., 1999) and consists of one or two WASP homology 2 (WH2) domains (historically referred to as V for their homology to verprolin), which bind to monomeric actin. The single or double WH2 domain is followed by a short central (C) region and an acidic (A) domain, which bind and activate the Arp2/3 complex. Polyproline repeats within the proline-rich domain (PRD) immediately upstream of the WCA region provide sites for the binding of proteins containing Src homology 3 (SH3) domain (Takenawa and Suetsugu, 2007a) or profilin (as discussed above).

The N-terminal region contains domains that provide a connection with regulatory proteins (see "Regulation of N-WASP" below). As such, they differ among WASP family members. WASP and N-WASP contain a WASP homology 1 (WH1) domain, also known as an Ena/VASP homology 1 (EVH1) domain, and a CRIB domain, which binds to proline-rich protein and the small GTPase Cdc42 (Takenawa and Suetsugu, 2007a).

The N terminus of N-WASP contains an EVH1/WH1 domain that binds the WASP-interacting protein, WIP (Ramesh et al., 1997). The N terminus of N-WASP also

binds $PIP_2$, actin filaments, and, through its IQ domain, calmodulin (Egile et al., 1999b). The GTPase-binding domain (GBD) includes a Cdc42/Rac interactive binding (CRIB) motif and surrounding sequences. The GBD preferentially binds Cdc42 and basic sequence (B) binds $PIP_2$ (Rohatgi et al., 2000). The PRD binds profilin and SH3 domain-containing proteins, including the adaptors Nck and Grb2, and tyrosine kinases (Takenawa and Suetsugu, 2007a).

## Regulation of N-WASP

Under resting conditions, WASP and N-WASP are folded by an intramolecular interaction between the C-terminal WCA region and the N-terminal region. Folded WASP and N-WASP are inactive because the WCA region is masked, thereby inhibiting access of the ARP2/3 complex to the WCA region (Figure 1.3). This prevents binding of the Arp2/3 complex to the CA region and thus inhibits WASP and N-WASP's Arp2/3 activation activity. The N-terminal basic region on N-WASP also interacts with the acidic A domain, contributing to the auto-inhibition of N-WASP. The X-ray crystal structure of inactive N-WASP shows that the inactive molecule is folded on itself preventing the WCA from interacting with Arp2/3 complex (Kim et al., 2000) (Miki and Takenawa, 1998).

Intramolecular auto-inhibition of N-WASP can be relieved by competitive binding of small Rho-family GTPase, Cdc42, (Kolluri et al., 1996) and $PIP_2$ (Rohatgi et al., 1999) to the N-terminus regulatory domain of N-WASP. Binding of Cdc42 to the CRIB domain activates WASP and N-WASP by causing a dramatic conformational change – hence the release of WCA domain (Kim et al., 2000). The basic region can also interact with negatively charged phospholipid, $PIP_2$, on the plasma membrane. This interaction with

$PIP_2$ greatly enhances Cdc42 dependent activation of N-WASP. Thus, Cdc42 and $PIP_2$ release the autoinhibiton of N-WASP, which in turn activates the Arp2/3 complex, resulting in actin polymerization near the plasma membrane (Figure 1.3). Rac1, another Rho-family GTPase, can also exclusively release the autoinhibition of N-WASP. This activation of N-WASP activation by purified Rac1 is more potent than Cdc42 activation of N-WASP, suggesting that Cdc42 is the major activator of WASP, while Rac1 activates N-WASP (Tomasevic et al., 2007).

In addition to Cdc42 activation of N-WASP, the Nck adapter protein is reported to activate N-WASP independently of Cdc42 and through a different binding site. Nck SH3 domains bind directly to the proline rich motif of WASP/N-WASP (Rivero-Lezcano et al., 1995, Rohatgi et al., 2001). In the presence of $PIP_2$, Nck activates N-WASP to promote Arp2/3 dependent actin polymerization. All three SH3 domains of Nck are required for maximum activation of N-WASP (Rohatgi et al., 2001). This multivalent interaction has recently been shown to promote N-WASP-Nck polymer formation, which triggers Arp2/3 complex activation *in vitro*. With the help of a trans-membrane protein nephrin in cells, N-WASP-Nck complex is organized into a polymeric platform just beneath the plasma membrane that activates Arp2/3 complex (Li et al., 2012).

## N-WASP and Cancer

The ability to cells to migrate and invade tissues allows cancer cells to proliferate within tissues (growth), expand to adjacent tissues (invasion), and travel to distant organs (metastasis)(Hanahan and Weinberg, 2000). Most tumors remain benign while cells are restricted to their immediate environment. These “stage zero” cancers may often be surgically removed. Consequently, metastasis or the spreading of cancerous cells, is

leading cause of 90% of cancer deaths. (Chambers et al., 2002). Tumor invasion is a complex process involving invasion of cells at edge of a tumor through the extracellular matrix that fences the tumor. Invasion begins with formation of cell protrusions that degrade the extracellular matrix. As the first step in metastasis, it is important to gain a deeper understanding of the proteins contributing to such protrusions – as they control the invasive and metastatic potential of cancer cells.

Invadopodia are small, invasive, actin-rich subcellular structures that play a pivotal role invasive cancer metastasis. They aide in degradation of and protrusion through the extracellular matrix (ECM) (Buccione et al., 2004). Similar structures known as podosomes, are produced in cells transformed with oncogenic src kinase, but can also be found in normal cells that traverse or remodel tissue such as macrophages and osteoclasts (Linder and Aepfelbacher, 2003). Initiation of invadopodia depends on branched actin assembly by the Arp2/3 complex. Invadopodia and podosomes share many common functional and molecular characteristics. Out of the five know members of the WASP family, N-WASP and WAVE-1 have been shown to be critical for invadopodia formation and ECM degradation respectively.

Both invadopodia and podosomes contain tightly-packed actin filaments that depend on N-WASP for their generation (Linder et al., 1999a; Mizutani et al., 2002a). N-WASP is activated in small punctae at the basal cell membrane during the initiation of invadopodium formation. While N-WASP localization implicates N-WASP activity in the initiation of invasion (Lorenz et al., 2004a), the precise functions of N-WASP in invadopodia remain to be determined.

N-WASP is specifically localized at invadopodia together with the Arp2/3 complex (Li et al., 2010b; Linder et al., 2000; Lorenz et al., 2004b) to generate a branched actin network (Baldassarre et al., 2006) similar to dendritic nucleation in a lamellipodium (Pollard et al., 2000b; Pollard and Borisy, 2003; Pollard and Cooper, 2009).

Despite the presence of Arp2/3, which generates branched actin structures, both invadopodia and podosomes contain a mix of bundled and branched actin (Gavazzi et al., 1989; Schoumacher et al., 2010). In support, invadopodia are also rich in actin crosslinking proteins (Schoumacher et al., 2010). The actin bundling protein fascin stabilizes invadopodia and enhances substrate degradation (Li et al., 2010b). Ultrastructure studies of podosomes similarly show tight clusters of actin filaments (Luxenburg et al., 2007). Thus, actin clusters or bundles may play an important role in the extension of both structures into the substrate.

## Biochemical approaches to study actin dynamics *in vitro*

Over the past decades tremendous progress has been made in understanding how actin networks assemble. Many methods have been developed to quantify actin polymerization processes *in vitro* including but not limited to centrifugal, densiometric and light scattering experiments, and fluorometric and microscopic assays. Some of the techniques that were used in analyzing the different states of actin are as follows.

Pyrenyl-actin assays: Also known as the pyrene assay, this technique was one of the first few techniques that was used to quantify the kinetics of actin polymerization (Cooper et al., 1983). Actin monomers are covalently labeled at their reactive Cys-374 residue with a fluorescence dye Pyrenyl-iodacetamide and subsequently mixed with unlabeled actin monomers. Polymerization of actin is initiated by transferring labeled

actin monomers into polymerization buffer containing salts (typically KCl). The fluorescence of pyrene labeled actin increases 20-30 fold when monomers are incorporated into filaments. This method can be used to determine different parameters related to the assembly and disassembly of actin filaments. Although a great amount of information can be extracted from these assays, these bulk assays only report total polymer mass. They do not provide direct information about the kinetics of individual filaments, filament length, or filament branching or bundling. Thus, this technique makes it difficult to visualize or estimate the change in actin architecture. Furthermore, the biochemical properties of proteins that alter elongation and nucleation cannot be precisely quantified, and some (such as cofilin) alter pyrene-actin fluorescence directly.

*In vitro* TIRF (total internal reflection fluorescence) microscopy: This is the best known technique to date to directly observe and verify single filament dynamics and verify binding protein interactions in real time. In early experiments, single actin filaments could be visualized by fluorescence microscopy using phalloidin, an actin binding toxin that can be conjugated to a fluorescent dye such as TRITC. Although frequently used, phalloidin stabilizes actin filaments and is known to alter the binding behavior of accessory proteins like Arp2/3 (Blanchoin et al., 2000; Mahaffy and Pollard, 2008).

In contrast to phalloidin-fixed actin studies, TIRF microscopy can observe the dynamics of single growing and shrinking actin filaments. TIRF microscopy uses an evanescent wave that only penetrates approximately one hundred nanometers into the specimen, thus greatly reducing the background fluorescence. For these microscopic assays, fluorescently labeled actin monomers are mixed with polymerization buffers and

applied to a flow cell precoated with inactivated NEM myosin heads. Monomers nucleate to form filaments that elongate and are captured along their lengths by myosin heads. TIRF microscopy visualizes these filaments that are captured at the coverslip surface and can continually monitor their growth, severing, bundling, branching, or shrinkage.

## Aim of Research

Why is N-WASP so critical to invadopodia formation? If it acts solely as an Arp2/3 activator in invadopodia, then why are they formed of a mixture of bundled and branched actin? Invasive cancer cells both degrade and produce large, punctate forces to push their way through the crosslinked basal lamina and escape a tumor. A dendritic actin network generated by Arp2/3 distributes the force of actin polymerization across a wide lamella. In contrast, rod-like actin bundles might provide the required stiffness and dense concentration of barbed ends to penetrate the substratum and invade the stroma. Because invadopodia formation appears to depend on a wide range of proteins, N-WASP's precise role in invadopodia remains a contentious issue.

Critical single-filament TIRF studies over the past few years have demonstrated that some actin regulators are insertional polymerases, accelerating the elongation of filaments while they cap or remained attached to the ends (Breitsprecher et al., 2008a; Hansen and Mullins, 2010a; Kovar and Pollard, 2004a; Shemesh et al., 2005). Formin family proteins were the first to shown such 'processive' activity, with individual Formin molecules remaining attached to a barbed end as the filament grew (Kovar and Pollard, 2004a; Shemesh et al., 2005). Similarly, Ena/VASP proteins also accelerate filament elongation, but interact with growing filaments by a different mechanism (Breitsprecher et al., 2008a; Breitsprecher et al., 2011; Hansen and Mullins, 2010a). In addition to

activating Arp2/3, the WCA domains of WASP family proteins share some homology with the processive actin assembling portion of Ena/VASP proteins (Machesky and Insall, 1999). Furthermore, N-WASP has two tandem WH2 that bind to actin monomers (Chereau et al., 2005; Marchand et al., 2001b) and fast-growing actin filament barbed ends (Co et al., 2007; Egile et al., 1999a; Hu and Kuhn, 2012b; Laurent et al., 1999). Could then N-WASP act as a processive actin assembler?

The Kuhn lab recently showed that, in the presence of Arp2/3 complex, nanofibers coated with GST-WWCA domains from N-WASP generated both branched and bundled actin networks (Hu and Kuhn, 2012a). In this *in vitro* reconstruction, filament bundles arose spontaneously from the dendritic network and appeared to attach processively to WWCA tethers. Surprisingly, this attachment generated enough force to buckle filaments within the bundle. Because N-WASP generated a mix of branched and bundled protruding actin, N-WASP's barbed end binding activity may play an important role in the extension of invadopodia or podosomes into the basement layer. However, it was unclear whether N-WASP attached to barbed ends directly or indirectly through Arp2/3. Therefore, we sought to determine whether actin filaments could bind processively to tethered WWCA domains in the absence of Arp2/3, how WWCA binding might affect barbed end polymerization rates, and whether the profilin-binding poly-proline domains of N-WASP were critical for this activity.

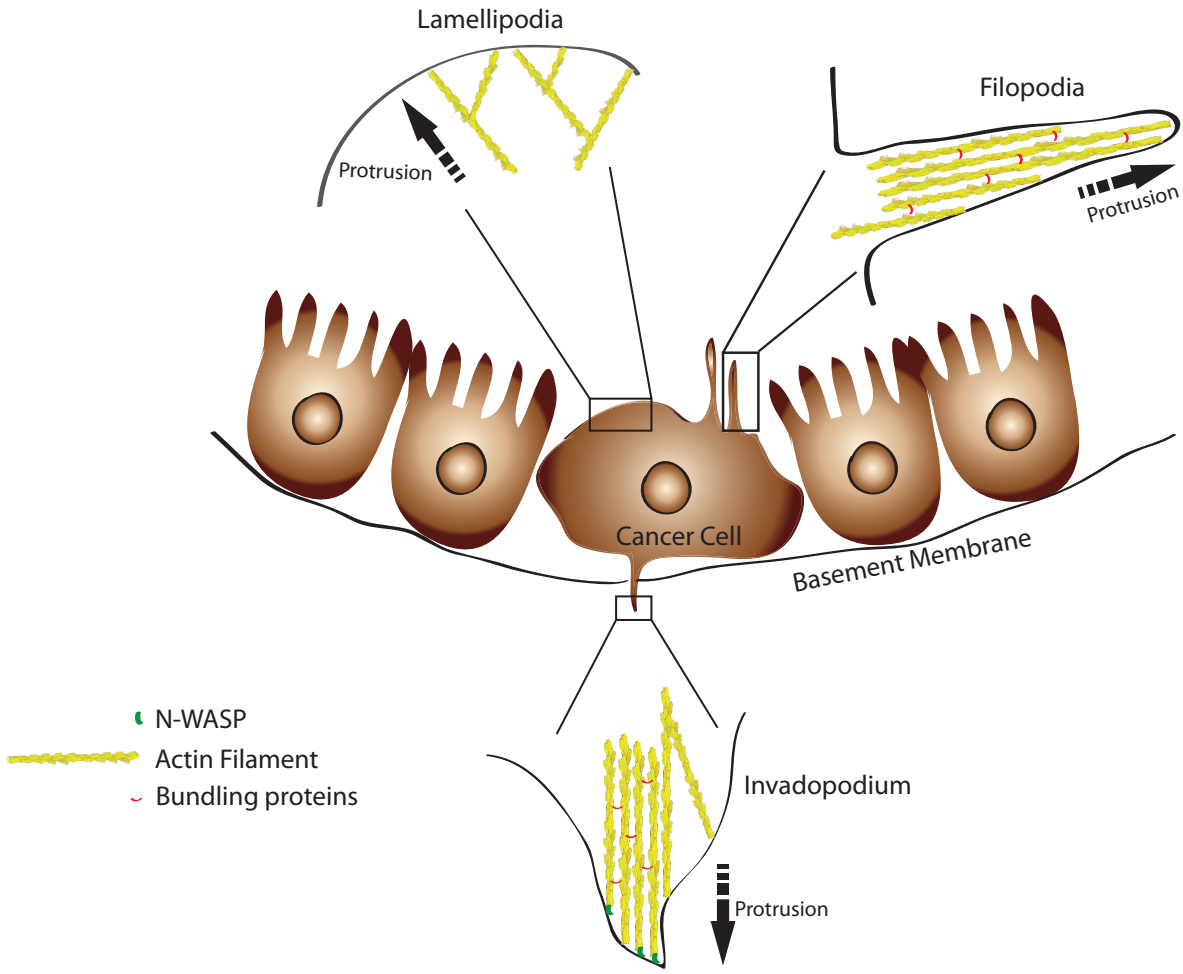


**Figure 1.1 Cell migration structures at a glance.** Lamellipodia are thin, sheet-like membrane protrusions found at the leading edge (front) of motile cells. Filopodia are slender cytoplasmic projections containing bundled actin and are associated with sensing environmental cues. Invadopodia, formed only in cancer cells, mediate matrix degradation and invasion.

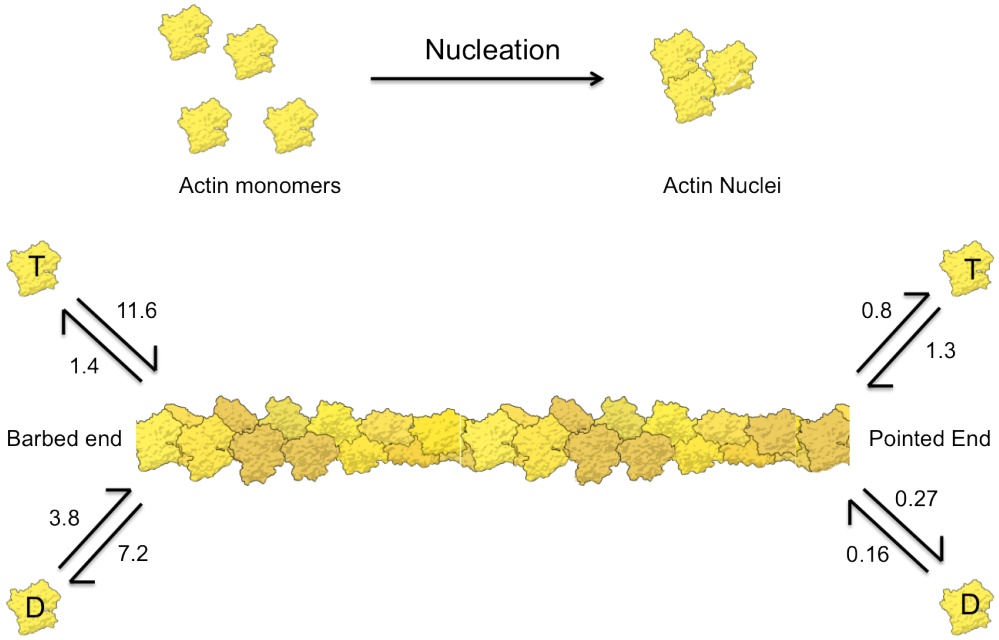


**Figure 1.2 Actin nucleation and elongation.** Spontaneous actin nucleation and elongation. Actin dimer and trimer are unstable. After nuclei formation, filament starts to elongate rapidly at barbed end and slowly at pointed end. Rate constants are shown for Mg-ATP actin (T) and Mg-ADP actin (D) with units of $\mu M^{-1}s^{-1}$ for *k*+ and $s^{-1}$ for *k*-. Adapted from Pollard, 1986, *J. Cell. Biol.*

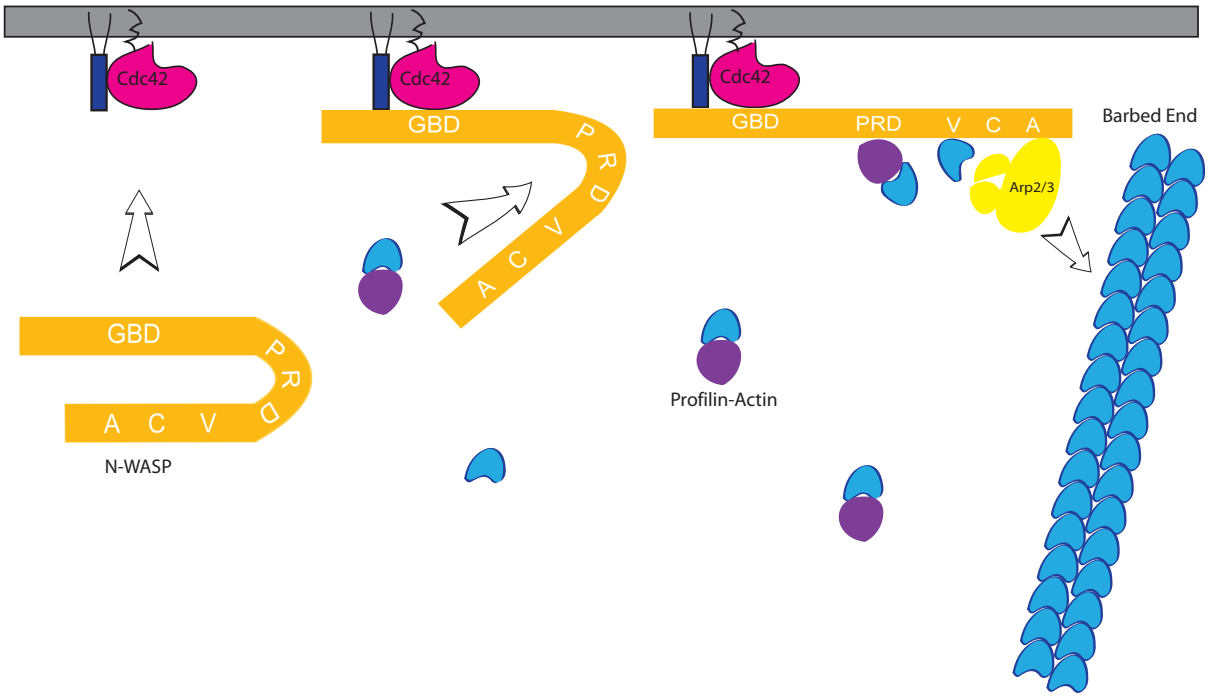


**Figure 1.3 The assembly of branched actin filament networks.** A model of how WASP family proteins stimulate Arp2/3 complex mediated nucleation of branched actin filament networks. Free N-WASP is in an autoinhibited conformation and cannot interact with Arp2/3 complex. This autoinhibition is released after activation through Cdc42 (pink) and $PIP_2$ (dark blue). N-WASP is then unfolded and activated. The profilin–actin complex then binds to the PRD of N-WASP. An ATP bound actin subunit binds to the V (also called WH2) region of N-WASP. N-WASP, now in the active conformation, binds to, and activates, the Arp2/3 complex, which binds to the side of a preexisting filament to initiate a new daughter filament. The barbed ends of these filaments are oriented towards the plasma membrane. The rapid actin polymerization at the barbed ends pushes the membrane forward.

# Chapter 2

# Processive Acceleration of Actin Barbed End Assembly by N-WASP

Nimisha Khanduja and Jeffrey R. Kuhn

MBoC, Mol. Biol. Cell November 13, 2013 mbc. E12-11-0781

## Abstract

N-WASP-activated actin polymerization drives extension of invadopodia and podosomes into the basement layer. In addition to activating Arp2/3, N-WASP binds actin filament barbed ends, and both N-WASP and barbed ends are tightly clustered in these invasive structures. We used nanofibers coated with N-WASP WWCA domains as model cell surfaces and single actin filament imaging to determine how clustered N-WASP affects Arp2/3-independent barbed end assembly. Individual barbed ends captured by WWCA domains grew at or below their diffusion limited assembly rate. At high filament densities, however, overlapping filaments formed buckles between their nanofiber tethers and myosin attachment points. These buckles grew about 3.4-fold faster than the diffusion-limited rate of unattached barbed ends. N-WASP constructs with and without the native poly-proline (PP) region showed similar rate enhancements in the absence of profilin, but profilin slowed barbed end acceleration from constructs containing the PP region. Increasing $Mg^{2+}$ to enhance filament bundling increased the frequency of filament buckle formation, consistent with a requirement of accelerated assembly on barbed end bundling. We propose that this novel N-WASP assembly activity provides an Arp2/3-independent force that drives nascent filament bundles into the basement layer during cell invasion.

## Introduction

Invadopodia (Mueller and Chen, 1991) and related podosomes (Tarone et al., 1985) are specialized ventral cellular projections that can degrade the extracellular matrix *via* localized activity of matrix metaloproteases. Both structures contain tightly-packed actin filaments that depend on neuronal Wiskott-Aldrich Syndrome protein (N-WASP) for

their generation (Co et al., 2007; Linder et al., 1999b; Lorenz et al., 2004b; Mizutani et al., 2002b). N-WASP is thought to organize invadopodia primarily through its Arp2/3 activating activity (Li et al., 2010b; Linder et al., 2000; Lorenz et al., 2004b), which generates a branched actin network (Baldassarre et al., 2006) reminiscent of dendritic nucleation in a moving cell's lamellipodium (Pollard et al., 2000b; Pollard and Borisy, 2003; Pollard and Cooper, 2009). Despite the presence of Arp2/3, both invadopodia and podosomes contain a mix of bundled and branched actin (Gavazzi et al., 1989; Schoumacher et al., 2010). Invadopodia are rich in actin crosslinking proteins (Schoumacher et al., 2010), and the actin bundling protein fascin stabilizes invadopodia and enhances substrate degradation (Li et al., 2010b). Ultrastructure studies of podosomes show tight clusters of actin filaments (Luxenburg et al., 2007). Thus, actin clusters or bundles may play an important role in the extension of both structures into the substrate.

In addition to activating Arp2/3, the C-terminal WWCA region of N-WASP binds to fast-growing actin filament barbed ends (Co et al., 2007; Egile et al., 1999a; Hu and Kuhn, 2012b; Laurent et al., 1999). For Arp2/3 activation, the central (C) and acidic (A) regions stabilize the short-pitch helix conformation of arp2 and arp3 subunits (Padrick et al., 2011; Xu et al., 2011), while the two Verprolin/WASP homology 2 domains (V, W, or WH2) bind to actin monomers (Chereau et al., 2005; Marchand et al., 2001b) and to actin barbed ends (Gaucher et al., 2012; Rebowski et al., 2008). Thus, N-WASP may also organize actin barbed ends in podosomes and invadopodia independent of its role in Arp2/3 activation.

We recently showed that in the presence of Arp2/3 complex, nanofibers coated with GST-WWCA domains from N-WASP generated both branched and bundled actin networks (Hu and Kuhn, 2012b). This one-dimensional analog of a two-dimensional cell membrane formed actin networks reminiscent of those produced at the leading edge of an invasive cell. In this reconstruction, filament bundles arose spontaneously from the dendritic network and appeared to attach processively to WWCA tethers. This attachment generated enough force to buckle filaments within the bundle. Because N-WASP generated a mix of branched and bundled protruding actin, N-WASP's barbed end binding activity may play an important role in the extension of invadopodia or podosomes into the basement layer. However, it was unclear whether N-WASP attached to barbed ends directly or indirectly through Arp2/3.

Given our observation of bundle tethering to N-WASP coated nanofibers, we sought to determine whether actin filaments could bind processively to tethered WWCA domains in the absence of Arp2/3 and how WWCA binding affects barbed end polymerization rates. Here, we show that N-WASP coated nanofibers bind to *de novo* nucleated actin filament barbed ends in two regimes. Individual barbed ends bound to N-WASP-coated nanofibers grew at or below the diffusion limited polymerization rate, depending on whether the nanofiber acted as a barrier to filament growth. However,clustered barbed ends bound to nanofibers could grow substantially faster than the diffusion-limited polymerization rate. Thus, like Ena/VASP and formin proteins, N-WASP WWCA domains can processively attach to growing barbed end bundles and increase their diffusion-limited elongation rate. This new activity for N-WASP provides an important new mechanism for cell invasion into the substrate.

## Results

### Individual barbed end capture is non processive.

We used TIRF microscopy of single actin filaments (Amann and Pollard, 2001b; Kuhn and Pollard, 2005b; Kuhn and Pollard, 2007) to dissect actin barbed end capture by the C-terminus of N-WASP in the absence of Arp2/3 complex. Glass nanofibers were coated with GST-tagged constructs of the WWCA domain of N-WASP having both native WH2 domains. The first construct tested contained the native poly-proline region (PP) of bovine N-WASP followed by the native WWCA C-terminal Arp2/3 activator domain (Figure 2.1.A). Addition of fluorescently labeled bovine serum albumin (BSA) to coated nanofibers blocked nonspecific binding and highlighted nanofibers for microscopy. Coated nanofibers and fluorescently labeled actin monomers were added to chambers coated with a low concentration of rigor myosin to tether filaments along their length. Myosin attachments appeared as inflection points that served as fiduciary marks to separate barbed and pointed end measurements (Kuhn and Pollard, 2005b).

GST-PP-WWCA coated nanofibers captured growing barbed ends of individual, *de novo* nucleated actin filaments. At low filament densities, we identified two types of barbed end capture with unique behaviors: end-capture parallel to the long axis of the nanofiber or end-capture perpendicular to the long axis. Filament barbed ends that encountered the nanofiber at a shallow angle (Figure 2.1.B) continued to grow along the nanofiber long axis after attachment and were designated as parallel captures. A small fraction of barbed ends (13 ± 24%, N=24 filaments, Mean ± SD) encountered the nanofiber at right angles and remained attached to the same location (**Figure 2.1**.B). These interactions were designated as perpendicular captures.

We measured filament length over time to assay barbed end growth before and after capture. Parallel captured barbed ends grew along the nanofiber at the same rate before and after binding (**Figure 2.1**.C), while perpendicular capture barbed ends grew at a substantially reduced rate while attached to the same location on the nanofiber (Figure 2.1.D). To quantify the slow, saltatory growth of perpendicular-bound barbed ends over time, we determined the smoothed, instantaneous growth rates at each time point. Parallel captured barbed ends in 1.5 $\mu$M actin monomers grew at 10.1 ± 2.3 $s^{-1}$ (N=6 filaments) before capture and at 10.4 ± 1.8 $s^{-1}$ (N=6) after capture (**Figure 2.1**.E-F, I), consistent with theoretical rates for labeled actin (Kuhn and Pollard, 2005b; Pollard, 1986). In contrast, filaments captured perpendicular to the nanofiber slowed from 11.5 ± 2.5 $s^{-1}$ (N=6) to 3.1 ± 2.3 $s^{-1}$ (N=6) after capture (Figure 2.1.G-I). In control experiments, filament barbed ends did not interact with BSA coated nanofibers (Figure 2.7). Thus, the parallel growth along N-WASP coated nanofibers and the substantial reduction in growth of perpendicular capture filaments was due to N-WASP binding rather than non-specific interaction of barbed ends with nanofibers.

**Rapid processive elongation of N-WASP bound barbed ends.**

At high filament densities, some nanofiber-associated filaments grew faster than their neighbors to form prominent buckles and loops. We measured the elongation rates of both nanofiber-associated buckling filaments and unattached background filaments in the same experiment (Table 2.1). Strikingly, buckling barbed ends grew 3.3-fold faster than background filaments. Background barbed ends grew at the theoretical rate (Kuhn and Pollard, 2005b; Pollard, 1986) of 6.89 ± 0.13 $s^{-1}$ (Figure 2.2.B), while buckling barbed ends grew at an average rate of 22.42 ± 0.39 $s^{-1}$ (Figure 2.2.C).

Filament buckling was rare in 1 mM $Mg^{2+}$, but more frequent when $Mg^{2+}$ was raised to induce filament side-to-side association (bundling). Based on previous evidence that filament bundling by divalent cations may mediate processive barbed end attachments to N-WASP (Hu and Kuhn, 2012b), we increased buffer $Mg^{2+}$ concentration to 10 mM to generate actin bundles (Hu and Kuhn, 2012b; Tang and Janmey, 1996). In 10 mM $Mg^{2+}$, nanofibers mediated more frequent rapid filament growth and buckling (Figure 2.2.D) However, high $Mg^{2+}$ did not change speed of accelerated barbed end growth once it began. As with lower $Mg^{2+}$, nanofiber-associated barbed ends grew 3.4-fold faster than unattached barbed ends in 10 mM $Mg^{2+}$.

Accelerated filaments did not remain bundled along their entire length as they grew. Rather, their barbed ends were frequently oriented parallel to the long nanofiber axis and its parallel captured filaments. In some cases, we found accelerated barbed ends that were directly bundled to other filaments (*black arrowheads* in Figure 2.2. A, D). Thus, parallel association of barbed ends (end bundling) likely plays a role in accelerated barbed end growth.

**Profilin bound to the proline-rich region slows barbed end processivity.**

The proline-rich region of PP-WWCA might recruit profilin-actin heterodimers (Mullins et al., 1998b; Suetsugu et al., 1998) for insertion at the barbed end, similar to formin proteins (Romero et al., 2004). To test whether profilin modulated processivity we repeated the barbed end capture experiments with profilin-actin, high $Mg^{2+}$, and short actin seed filaments to overcome the suppression of *de novo* filament nucleation by profilin. Nanofibers generated filament buckles (Figure 2.3.A), but the acceleration was reduced by profilin. Buckling filament barbed ends grew at an average rate of 14.28 ±

0.18 $s^{-1}$ (Figure 2.3.C), compared to 7.4 ± 0.11 $s^{-1}$ for unattached barbed ends (Figure 2.3.B). This 1.9-fold acceleration was significantly lower (p-value < 0.001) than the 3.4-fold acceleration seen in the absence of profilin (Table 2.1).

The proline-rich domain is not required for processivity.

The decrease in profilin-actin assembly rates seen above could be due either to slower incorporation of profilin-actin dimers at the barbed end or through direct interaction between profilin and the proline-rich region of N-WASP. We therefore designed a GST N-WASP construct (Figure 2.1.A) lacking the poly-proline domains to determine its effect on accelerated processivity. We found that GST-WWCA coated nanofibers generated filament buckles in both high (10 mM) and low (1 mM) $Mg^{2+}$ (Figure 2.4) GST-WWCA tethered ends grew 3.14-fold faster than untethered ends in low $Mg^{2+}$ and 3.45-fold faster in high $Mg^{2+}$. These acceleration rates were not significantly different (p-value = 0.1083) in the two $Mg^{2+}$ concentrations tested. The poly-proline region thus does not have a major role in processive barbed end acceleration of actin alone.

To determine whether profilin affected barbed end processivity of GST-WWCA constructs, we repeated the above experiments in the presence of profilin-actin and actin seeds. As with GST-PP-WWCA constructs, GST-WWCA constructs accelerated barbed end assembly in the presence of profilin-actin (Table 2.1). However, the 3.45-fold rate enhancement was equal to the rate enhancement seen in the absence of profilin. Thus, the slower barbed end acceleration rate seen above with construct containing the poly proline region was due to specific interactions between the proline-rich region of N-WASP and profilin-actin.

**Rare processive elongation events were not evident in bulk assays**

Given the rarity of these processive elongation events, we sought to determine whether processive elongation would be evident or hidden in bulk actin polymerization assays under typical conditions (1 mM $Mg^{2+}$). Moderate concentrations of GST-WWCA (200 nM) enhanced the initial polymerization rate of 2.5 μM pyrenyl-actin (Figure 2.5 A-B). However, this enhancement was likely due to GST-WWCA-mediated nucleation rather than barbed end acceleration. Although isolated N-WASP WWCA peptides do not nucleate filaments (Gaucher et al., 2012), dimerization contributed by the GST tag (Lim et al., 1994) effectively doubles the number of WH2 domains available for nucleation. Like the actin nucleators Spire with four WH2 domains (Quinlan et al., 2007) or Cobl's three WH2 domains (Ahuja et al., 2007), GST dimerization could contribute to the weak nucleation activity we found at moderate GST-WWCA concentrations.

In support of a nucleation-based increase in initial rate seen at moderate GST-WWCA concentrations, high concentrations of GST-WWCA (500 nM) abolished the initial rate enhancement, consistent with WWCA sequestration of actin monomers (Gaucher et al., 2012). Furthermore, when GST-WWCA nucleation was overwhelmed with pre-polymerized actin seeds, we found no concentration-dependent rate enhancement (Figure 2.5 C-D). Instead, high concentration of GST-WWCA decreased the actin assembly rate.

This decrease in actin polymerization at high GST-WWCA concentrations could come from monomer sequestration or from N-WASP mediated changes to actin barbed end kinetics. We therefore tested the effects of GST-WWCA on actin depolymerization. A 20-fold dilution of actin filaments prepolymerized from 5 μM ATP-pyrenyl-actin

reduced overall filament concentration to 0.24 μM and free monomer concentration to < 10 nM was used. Under these conditions, monomer binding by GST-WWCA would have little effect on the initial depolymerization rate. Nevertheless, GST-WWCA decreased the actin depolymerization rate (Figure 2.5 E-F), consistent with previous studies of uncomplexed WWCA peptides (Gaucher et al., 2012). The decrease depolymerization was thus likely mediated by GST-WWCA interaction with filament ends rather than by further depleting actin monomers. In support, GST-WWCA also produced a concentration-dependent increase in the final monomer critical concentration (Figure 2.5.G), consistent with its binding to actin barbed-ends.

Taken together, bulk assays support binding of N-WASP to barbed ends but cannot unequivocally show barbed end acceleration. Bulk pyrene actin assays are often difficult to interpret as they only measure the average total filamentous actin content over time. Rare barbed end acceleration events would only contribute a small fraction to total pyrene actin filament mass. Thus, the crucial but rare acceleration activity of N-WASP would only be discernable through TIRF microscopy and could have easily been missed in previous studies.

**Filament bundling increases frequency of N-WASP-mediated barbed end acceleration.**

Although $Mg^{2+}$ did not significantly alter barbed end acceleration rates, nanofiber-mediated buckles appeared earlier in reactions with high (10 mM) $Mg^{2+}$. We therefore scored the buckle initiation time and normalized against the total nanofiber length in each experiment (Figure 2.6). Buckles appeared at significantly higher frequencies in 10 mM $Mg^{2+}$ than they did in 1 mM $Mg^{2+}$ for both N-WASP constructs (Table 2.2). Furthermore,

the N-WASP construct containing the poly-proline region (PP-WWCA) was less efficient than the shorter construct (WWCA) at initiation barbed end acceleration in all cases. Once initiated, both constructs accelerated polymerization to the same extent. This difference in initiation efficiency may lie in the difference between tether lengths. Thus, the range of motion of nearby clustered WWCA domains may play a key role in finding and maintaining contact with bundled filament barbed ends. As both PP-WWCA and WWCA constructs were nonspecifically adhered to glass nanofibers, we cannot rule out differences in the way each construct adhered.

The primary effect of $Mg^{2+}$ on N-WASP processivity was likely due to barbed-end bundling. We previously showed that actin filaments form bundles at cellular (1 mM) $Mg^{2+}$ levels under the same buffer conditions used in the present study (Hu and Kuhn, 2012b). However, the fraction of bundled filaments and the speed of bundle initiation increase significantly in 10 mM $Mg^{2+}$. Furthermore, GST-WWCA coated particles capture significantly more bundled barbed ends than unbundled barbed ends in higher $Mg^{2+}$ or when bundling factors are added. In the present study, N-WASP generated accelerated filament buckles only appeared when filaments density increased and filaments were highly clustered. Adding $Mg^{2+}$ increased the frequency of initiation of processive WWCA-mediated barbed end assembly two- to three-fold without significantly modifying the overall rate of this accelerated assembly. In contrast, increased $Mg^{2+}$ does not increase *de novo* filament nucleation (Hu and Kuhn, 2012b). Barbed ends were generated at the same rate in both high and low $Mg^{2+}$ and the increased rate of buckle initiation in high $Mg^{2+}$ was due to increased availability of bundled barbed ends rather than an increase in total barbed ends. Taken together, polycations influenced

the acceleration of barbed ends by bundling negatively charged filaments and by limiting the diffusion of barbed ends away from N-WASP rather than by increasing the number of available barbed ends or by enhancing the binding of N-WASP to barbed ends. Bundle-mediated cooperativity of barbed ends thus appears to be a key factor in the transition from diffusion limited elongation to fast processive assembly.

## Discussion

Here, we showed that N-WASP-coated nanofibers captured and assembled actin filament barbed ends in two distinct regimes. (1) Individual barbed ends bound to N-WASP assembled at their normal rate when growing along the nanofiber or at a slower rate when growing against the nanofiber. (2) At high filament densities, N-WASP binding promoted rapid, processive barbed end growth. Processive barbed end assembly was rare at low filament densities and could not be discerned with traditional bulk pyrene-actin assembly assays. Processive assembly was relatively rare in the 1 mM $Mg^{2+}$ concentrations used in most actin assays, even at high filament densities. Thus, this novel behavior of N-WASP likely escaped notice as the actin field focused primarily on the Arp2/3 binding activity of N-WASP rather than its interaction with actin filaments.

N-WASP mediated growth of individual barbed ends at or below the diffusion limited polymerization rate fits well with current models of WH2 domain association at the barbed end. WASP family WH2 domains bind to the hydrophobic cleft of actin monomers (Chereau et al., 2005). This binding site is exposed at the barbed end of a filament, allowing WH2-bound actin monomers to add to the barbed end. Once assembled, WH2 domains must dissociate from the hydrophobic cleft to allow further longitudinal actin assembly. Like profilin (Kang et al., 1999; Pollard and Cooper, 1984),

soluble N-WASP WWCA (WCA) activator domains do not prevent barbed end assembly (Egile et al., 1999a), implying that WH2 dissociates somewhere in the assembly process.

In contrast to profilin-actin, it is unclear whether WH2 domains dissociate from the terminal barbed end subunit immediately after WH2-actin addition or after some delay. Our data demonstrated that N-WASP associated actin assembly was much slower than the diffusion limited rate if the nanofiber acted as a barrier to monomer addition (perpendicular attachments). Continuous attachment between N-WASP during periods of slow barbed end growth implies that WH2 dissociation from the barbed end may be linked to subsequent monomer addition. When further monomer addition was restricted, N-WASP remained attached to the barbed end.

Slow growth of barbed ends against a barrier (perpendicular capture) implies a thermal ratchet model of non-processive barbed end assembly by N-WASP. Here, some of the free energy from polymerization goes towards buckling the filament (Dogterom and Yurke, 1997), leading to a decrease in the diffusion limited assembly rate. In the "tethered ratchet" model of motility (Mogilner and Oster, 2003a; Mogilner and Oster, 2003b) and related "cooperative thermal breakage" model (Alberts and Odell, 2004; Soo and Theriot, 2005), non-polymerizing actin barbed ends are transiently attached to the leading edge while polymerizing barbed ends push against the leading edge. Transient filament-to-membrane attachments are broken as the compressive force of polymerization against the membrane is translated through the cross-linked network to the membrane bound filaments. As we have shown, N-WASP can provide this transient attachment to filament barbed ends. Cycles of attachment and detachment were rapid when monomer addition was unrestricted (growth along the nanofiber), while N-WASP

detachment was slower when monomer addition was restricted (growth against the nanofiber).

In the second assembly regime, buckling filaments remained processively attached to the same location on the nanofiber. Rapid and processive barbed end assembly fits closely with the "actoclampin" model of Dickinson and Purich (Dickinson, 2008; Dickinson et al., 2004; Dickinson and Purich, 2002), which posits that a hypothetical membrane bound "actoclampin" molecule maintains constant, processive attachment to the growing barbed end.

The barbed end assembly rate of buckling filaments can be used to distinguish between processive and non-processive polymerization. In the fast-elongation regime, acceleration of barbed ends beyond their natural diffusion-limited rate unequivocally shows processive barbed end assembly by WWCA domains. Like Ena/VASP (Breitsprecher et al., 2008b; Hansen and Mullins, 2010b; Kovar and Pollard, 2004b) and formin family proteins (Kovar and Pollard, 2004b; Otomo et al., 2005; Paul and Pollard, 2009b; Romero et al., 2004), N-WASP WWCA domains can processively attach to growing barbed ends and increase their diffusion-limited elongation rate as originally postulated by Chereau *et al* (Chereau et al., 2005).

Poly-proline regions of WASP family proteins recruit profilin-actin (Suetsugu et al., 1998). We found that N-WASP construct containing this region accelerated profilin-actin polymerization to a lesser extent (1.9-fold) than it did actin alone (3.4-fold). This reduction was likely due to profilin binding to the poly-proline region, as N-WASP constructs lacking this region accelerated barbed end assembly to the same extent with or without profilin. Reduced acceleration could stem from misaligned insertional assembly

of profilin-actin at the barbed end. However, profilin-actin binds to the loading site containing a GPPPP consensus sequence (Mahoney et al., 1997) and the first WH2 domain is a major factor in stabilizing Arp2/3 daughter branches (Mullins, 2000; Suetsugu et al., 1998; Yang et al., 2000). More likely, GPPPP binding to profilin reduces dissociation of profilin from the barbed end required for subsequent longitudinal actin monomer addition. Further experiments with N-WASP constructs lacking one or more GPPPP domains or with different length of linker between the N-terminal GPPPP binding site and the first WH2 domain of N-WASP may shed light on the mechanism of N-WASP mediated profilin-actin insertion at the barbed end.

How is this transition from diffusion-limited elongation to fast processive assembly driven? The active barbed-end binding domains of VASP and WASP proteins are highly homologous (Dominguez, 2009; Ferron et al., 2007), and VASP requires its tetramerization domain to accelerate barbed ends (Bachmann et al., 1999; Breitsprecher et al., 2008b) (Hansen and Mullins, 2010b). Similarly, formin requires dimerization to processively walk along growing barbed ends (Moseley et al., 2004) and clustered WH2 domains from VopL can assembly barbed ends (Namgoong et al., 2011). Membrane clustered WWCA domains could similarly walk along bundled barbed ends and insert actin subunits as previously proposed (Fig. 8 in Hu and Kuhn, 2012b). Although our GST-tagged N-WASP constructs likely formed dimers at the nanofiber surface (Padrick et al., 2008) lending a pseudo-multimerization to our N-WASP, we did not see fast processive elongation until barbed ends clustered as well. In contrast to VASP and formin, which rely on multimerization for processive actin assembly, N-WASP relies on both clustering and bundling provided by extrinsic factors such as polycations. While N-

WASP is less likely to initiate processive assembly than VASP, it is efficient once started. We propose that filament bundling limits diffusion of a barbed end away from WWCA after WWCA dissociation. WWCA is then free to bind additional actin monomers and efficiently re-find the same barbed end for subsequent monomer addition.

Alternatively, the two tandem WH2 domains of N-WASP could provide the two actin binding sites required for processive stepping. While the C-terminal WH2 domain binds to a filament barbed end, the upstream WH2 domain would bind and add a new monomer. Both WH2 domains bind actin monomers (Gaucher et al., 2012; Rebowski et al., 2008), but structures of tandem WH2 domains from N-WASP show that the tandem actin monomers orientation are incompatible with longitudinal dimer formation (Rebowski et al., 2008). We do not preclude an intermediate, low affinity binding state where longitudinal dimer formation ejects the second WH2 from the hydrophobic cleft at the longitudinal dimer interface. However, it is unclear how the short linker between WH2 domains in N-WASP could provide enough flexibility for stepping toward a new binding site during elongation (Dominguez, 2010). Further studies with extended WH2 linkers, with N-WASP constructs lacking one WH2 domain, or with WASP's single WH2 domain should elucidate the mechanism of processive elongation.

We have demonstrated a novel Arp2/3-independent barbed end assembly mechanism by the C-terminal of N-WASP. This new activity provides new insight into the formation of cellular structures by N-WASP. Although actin microspikes are enriched with N-WASP (Nakagawa et al., 2001) and N-WASP overexpression can generate filopodia (Miki et al., 1998a), the involvement of N-WASP in filopodia generation remains controversial (Sarmiento et al., 2008; Snapper et al., 2001; Steffen et al., 2006). However,

N-WASP appears to be required for invadopodia and podosome formation (Co et al., 2007; Linder et al., 1999b; Lorenz et al., 2004b; Mizutani et al., 2002b). We propose that N-WASP promotes transient actin bundles to invasive structures by accelerating their assembly. The simultaneous requirement of both a high density of free barbed ends and their parallel association means that the transition from passive to processive assembly is rare throughout the actin cortex, where free barbed end densities are relatively low. The probability of buckle initiation increases substantially in regions of active barbed end nucleation where barbed ends are also densely packed, such as within podosomes or nascent invadopodia. Once initiated, the force from this accelerated assembly provides an initial push or "spear-tip" for invadopodia to wedge into the basement layer. N-WASP accelerated bundles that do not rapidly dissipate into the dendritic network are then stabilized by crosslinking proteins such as α-actinin and fascin. VASP and formin are then recruited to these sites to extend invadopodia into the basement layer.

**Materials and Methods**

Protein Expression and Purification. Actin was purified from rabbit skeletal muscle actin acetone powder through one round of polymerization and depolymerization followed by gel filtration (Spudich and Watt, 1971b). Actin was labeled with Oregon Green 488 iodoacetamide (Invitrogen) as described (Kuhn and Pollard, 2005b). Actin and labeled actin were stored for 1 month at 4 ºC. Both labeled and unlabeled actins were dialyzed overnight against fresh buffer G (2 mM Tris-Cl pH 8, 0.2 mM ATP, 1 mM $NaN_3$, 0.1 mM $CaCl_2$, 0.5 mM dithiothreitol, DTT) and centrifuged at 38,000 g for 2 hr at 4ºC. Actin concentrations were estimated from extinction coefficients as follows: actin, $E_{290} = 26{,}600\ M^{-1}cm^{-1}$ (Kuhn and Pollard, 2005b); Oregon green actin, $E_{290} = 26{,}600\ M^{-}$

$^{1}cm^{-1}$ using the correction $A^{*}_{290} = A_{290} - 0.16991A_{491}$; Oregon green, $E_{491}$ = 77,800 $M^{-1}cm^{-1}$.

Bovine N-WASP WWCA (A403 - D505) was purified as a GST fusion protein as described (Hu and Kuhn, 2012b). Bovine N-WASP PP-WWCA (A244-D505) starting at the end of the CRIB domain was cloned into the vector pET-41a (Novagen) containing N-terminal GST, His, and S-tags and the sequence was verified. GST-PP-WWCA was expressed in Rosetta DE3pLysS (Novagen) bacteria grown at 37 °C to an $A_{600}$ of 0.8 and induced with 0.5 mM isopropyl β-D-thiogalactopyranoside overnight at 16°C. Bacteria were pelleted, resuspended in TBSE (20 mM Tris, 200 mMNaCl, 1 mM EDTA, 10 mM 2-mercaptoethanol) supplemented with complete EDTA-free protease inhibitors (Roche) and pulse sonicated on ice for a total of 150 seconds. Bacteria were pelleted for 30 min at 46,000 xg, the supernatant was added to glutathione resin (Thermo Scientific), and the resin was washed with 5 volumes of wash buffer (TBSE with 0.1% Thesit). Protein was eluted using 100 mM reduced glutathione, pH 8.0, and gel filtered on a Superdex 200 column (GE Healthcare). GST-PP-WWCA concentration was determined using an extinction coefficient $E_{280}$ = 53080 $M^{-1}cm^{-1}$. Both N-WASP constructs were flash frozen in liquid nitrogen and stored at -80 ºC.

Nanofiber Preparation and Coating. Glass nanofibers (200 nm nominal diameter, Johns Mansville, Denver, CO) were broken into smaller fragments in chloroform in a Dounce homogenizer as previously described (Hu and Kuhn, 2012b). Nanofibers are centrifuged at 3750 rpm for 10 min, excess chloroform drained, and the remaining chloroform evaporated. Nanofibers were washed with deionized water by low-speed centrifugation and sonicated for 1 hour in 1 M KOH in a bath sonicator to remove

contaminants. Nanofibers were washed briefly in deionized water, resuspended in 1 M HCl, sonicated for 1 hour, and incubated overnight in HCl. Cleaned nanofibers were subsequently pelleted by centrifugation and sonicated for 30 minutes each in in deionized water, 1 mM EDTA, 70% ethanol, and absolute ethanol to dry, with pelleting between each step. Cleaned nanofibers were stored in glass containers in absolute ethanol for up to 6 months. For coating, ethanol was removed after centrifugation and the remaining ethanol evaporated. Nanofibers were incubated with 20 $\mu$M N-WASP in coating buffer (10 mM Hepes pH 7.3, 0.1 M KCl, 1 mM $MgCl_2$, 1 mM ATP, 0.1 mM $CaCl_2$, 1 mM $NaN_3$, final pH 7.56) overnight. Fluorescein conjugated bovine serum albumen (FITC-BSA, Invitrogen) was added to a final concentration of 0.02 mg/ml to aid visibility and nanofibers were incubated an additional 5 minutes. Nanofibers were washed 3x with coating buffer and resuspended in coating buffer supplemented with 1 mg/ml low grade BSA (Sigma Aldrich) to block subsequent protein addition. Nanofibers were stored in BSA at 4ºC for up to 5 days before use.

Total Internal Reflection Fluorescence (TIRF) Microscopy. Clean glass slides; coverslips and flow cells were constructed as previously described (Kuhn and Pollard, 2005b). For filament tethering, flow cells were coated with 100 nM n-ethylmaleimide inactivated myosin II for 2 minutes. To prevent non-specific binding flow cells were blocked with 1% w/v BSA for 2 min as described (Kuhn and Pollard, 2005b). Unlabeled Mg-ATP-actin and Mg-ATP-actin labeled with Oregon Green 488 (Invitrogen) were mixed with nanofibers and 2x TIRF buffer (2x: 20 mM Imidazole pH 7, 100 mM KCl, 2 mM $MgCl_2$, 2 mM EGTA, 200 mM DTT, 0.4 mM ATP, 30 mM Glucose, 0.5% Methyl Cellulose 1500 centipoises, 40 $\mu$g/ml catalase, 0.2 mg/ml glucose oxidase) or 2x High

Mg-TIRF buffer (2x: TIRF buffer with 20 mM total $MgCl_2$) to start spontaneous actin assembly. For each experiment 16 $\mu$l of reaction mixture was added to the chamber and the entry and exit ports of flow cell were sealed with warm VALAP (1:1:1 vaseline : lanolin : paraffin).

Actin seeds. Short actin seeds were created as described (Kuhn and Pollard, 2007) by polymerizing 6 $\mu$M unlabeled Mg-ATP-actin at room temperature for 10 minutes in buffer F (buffer G with 10 mM Imidazole pH 7, 50 mM KCl, 0.105 mM $MgCl_2$, 1 mM EGTA). Seeds were diluted 1:20 in buffer F and vortexed immediately at high speed for 60 seconds to shear filaments. Seeds were added to a final concentration of 75 nM.

Image acquisition and analysis. TIRF images were collected on an Olympus upright microscope (BX51WI) using prism-based excitation from a 488 nm solid-state laser (Sapphire, Coherent Santa Clara, CA) and custom optics. Images were captured by a Rolera-MGI EMCCD camera (QImaging, Surrey, BC, Canada) at 10-second intervals using Micro-manager open source acquisition software (Edelstein et al., 2010). Images were analyzed using ImageJ software (Schneider and Rasband, 2012). Actin filament barbed and pointed end lengths were measured against fiduciary marks provided by NEM-Myosin II attachment points as previously described (Kuhn and Pollard, 2005b). We measured the lengths of an average of 10 filaments per experiment and at least 3 experiments per condition unless otherwise indicated.

Pyrenyl-actin assembly assays. Pyrene-actin fluorescence was measured using a fluorescent plate reader (Gemini XPS, Molecular Devices, Sunnyvale, CA). Polymerization was monitored by continuous pyrene fluorescence measurements ($\lambda_{exc}$ = 364 nm, $\lambda_{em}$ = 407 nm) at 22-24 °C. All reactions were carried out in Corning 96 well

half area flat bottom plate. Unseeded actin polymerization assays were monitored over a range of nM concentration of GST-WWCA. The reaction well was prepared by addition of with 1.5 $\mu$l of 100x antifoam (100x: 0.005% antifoam-204, Sigma-Aldrich), 2x initial concentration of Mg KMEI (10x: 500 mM KCl, 10 mM $MgCl_2$, 10 mM EGTA, 100 mM Imidazole, pH 7.0), and buffer G and GST-WWCA. In the preparatory well, 5 $\mu$M Ca-ATP actin (30% pyrene labeled) was mixed 9:1 with ME exchange buffer (10x ME: 10 mM ethylene glycol tetraacetic acid, EGTA, 1 mM $MgCl_2$) and incubated on ice for 2 minutes to form 2x final concentrations of Mg-ATP actin. The reaction was initiated by transferring 75 $\mu$l of actin monomer mixture from the preparatory well to the corresponding row in reaction well for a final concentration of 2.5 $\mu$M monomeric actin in a 150 $\mu$l reaction. The delay from the reaction start until the first data read was recorded manually and added before analysis of kinetic data. Seeded polymerization reactions were similarly produced with 1.5 μM actin (30% pyrene-labeled), varying GST-WWCA and prepolymerized, unlabeled actin seeds. To create actin seeds, 6 $\mu$M Mg-ATP actin was polymerized in F buffer (buffer G with 10 mM Imidazole pH 7, 50 mM KCl, 1.1 mM $MgCl_2$, 2 mM EGTA) for 1 hour at room temperature. Seeds were vortexed (Vortex Genie 2, VWR Scientific Products, West Chester, PA) at maximum speed for 60 seconds to break longer filaments. Short seeds were added to the reaction well to give a final concentration of 0.4 $\mu$M actin seeds in a 150 $\mu$l reaction. For depolymerization assays, actin (5 μM, 88-97% pyrene-labeled) was polymerized overnight. The reaction well was prepared by addition of 7.5 $\mu$l incubated with varying concentrations of GST-WWCA for 10 minutes. A 1.5 $\mu$l drop of 100x antifoam was carefully added along the side of each well. The reaction was diluted 20-fold in F-buffer with 2x slow mixing

strokes and wide-bore pipette tips to minimize filament breakage. After dilution, fluorescence of pyrene-actin was monitored every 15s. Initial rates of actin assembly were determined from linear fits of the initial 400 seconds of depolymerization data.

Buckle occurrence timing. The nanofiber density varied between experiments and therefore influenced the number of nucleation-competent sites in each captured movie. To quantify the frequency of buckle occurrence, we recorded the time after the start of the reaction at which each buckle became visible (buckle initiation). To correct for variations in the number of nucleation sites between experiments, we multiplied the initiation time by the total length of nanofibers in each experiment and divided by the weighted mean of total nanofiber length across all experiments. Normalized initiation times for each condition were combined and sorted to give a cumulative count of the number of buckles. Buckle counts, $C$, were fit to an exponential growth curve, $C\,[1 - \exp(-(t - t_0)/\tau)]$ to find the initiation rate, $\tau$, and delay, $t_0$, for *de novo* filament nucleation.

# TABLES

**Table 2.1. Average filament elongation rate**

| Barbed ends | Tether | Actin | $Mg^{2+}$ | Seeds | Profilin | BE Rate | No. | Rate |
|---|---|---|---|---|---|---|---|---|
| | | *μM* | *mM* | *nM* | *μM* | *subunit•sec*$^{-1}$ | Fil. | Enhancement |
| Tethered | PPWWCA | 1.2 | 1 | — | — | 22.42 ± 0.39 | 10 | 3.25 |
| Free | PPWWCA | 1.2 | 1 | — | — | 6.89 ± 0.13 | 10 | |
| Tethered | PPWWCA | 1 | 10 | — | — | 21.05 ± 0.39 | 10 | 3.44 |
| Free | PPWWCA | 1 | 10 | — | — | 6.12 ± 0.08 | 10 | |
| Tethered | PPWWCA | 1 | 10 | 75 | 1 | 14.28 ± 0.18 | 7 | 1.93 |
| Free | PPWWCA | 1 | 10 | 75 | 1 | 7.40 ± 0.11 | 13 | |
| Tethered | WWCA | 1 | 1 | — | — | 21.45 ± 0.52 | 10 | 3.14 |
| Free | WWCA | 1 | 1 | — | — | 6.83 ± 0.09 | 10 | |
| Tethered | WWCA | 1 | 10 | — | — | 21.74 ± 0.70 | 10 | 3.45 |
| Free | WWCA | 1 | 10 | — | — | 6.29 ± 0.11 | 10 | |
| Tethered | WWCA | 1 | 10 | 75 | 1 | 25.45 ± 1.09 | 10 | 3.45 |
| Free | WWCA | 1 | 10 | 75 | 1 | 7.37± 0.28 | 10 | |

**Table 2.2. Rate of Buckle Occurrence**

| Construct | Actin | $Mg^{2+}$ | Rate |
|---|---|---|---|
| | $\mu M$ | $mM$ | $s^{-1}\mu m^{-1}$ |
| PPWWCA | 1.2 | 1 | $3.9 \pm 1.8 \times 10^{-6}$ |
| PPWWCA | 1 | 10 | $13.8 \pm 0.6 \times 10^{-6}$ |
| WWCA | 1 | 1 | $73.6 \pm 6.7 \times 10^{-6}$ |
| WWCA | 1 | 10 | $134.4 \pm 5.6 \times 10^{-6}$ |

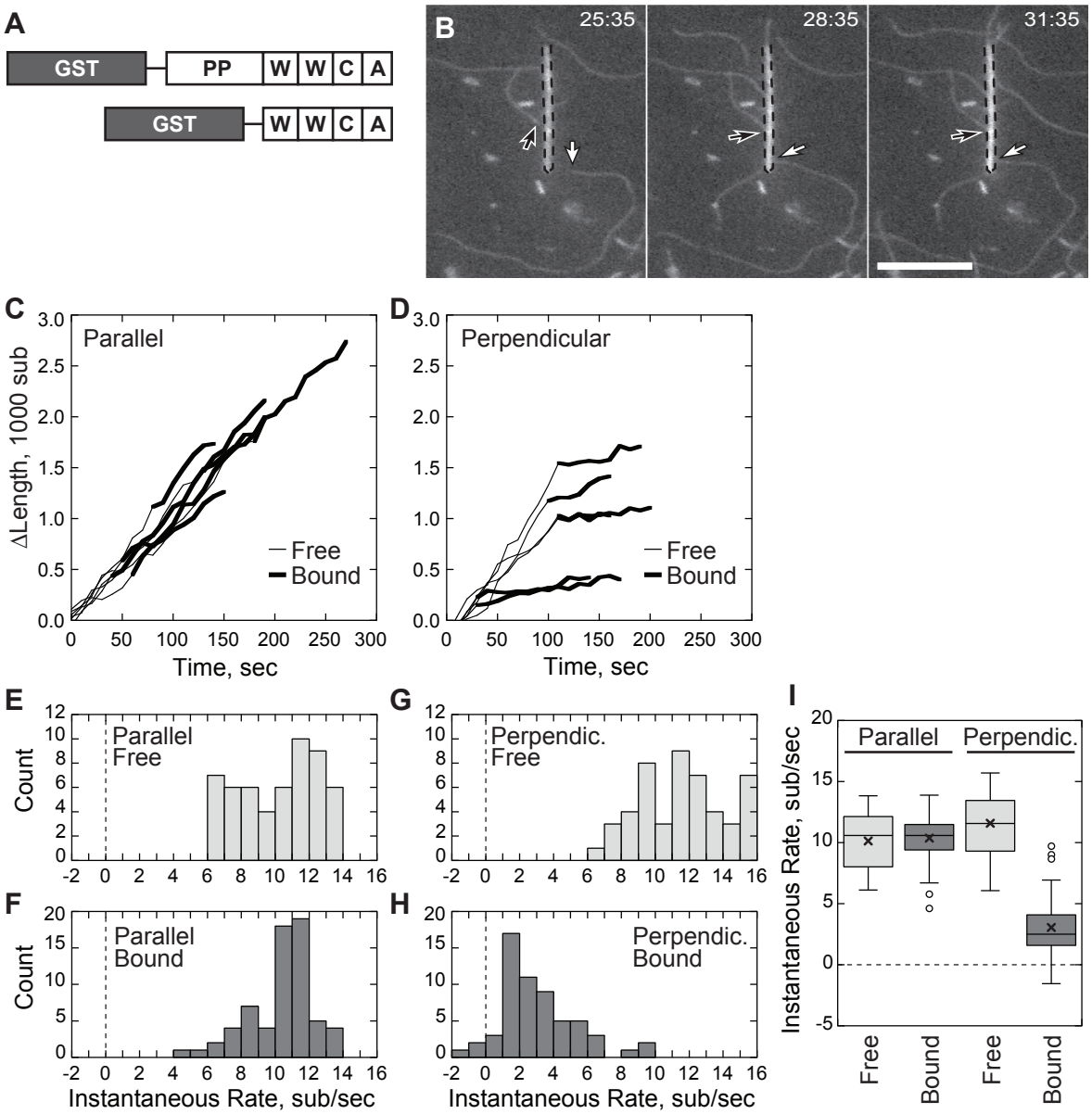


**Figure 2.1**. **Non-bundled filament barbed end capture is not processive.**

Conditions: 1.5 μM (33-40% labeled) Mg-ATP actin, nanofibers coated with 10-20 μM GST-PP-WWCA, 1 mM $MgCl_2$, 10 mM Imidazole pH 7, 50 mM KCl, 1 mM EGTA, 100 mM DTT, 0.2 mM ATP, 0.25% methyl cellulose, 15 mM glucose, 20 μg/mL catalase, 100 μg/mL glucose oxidase. Slides coated with NEM inactivated myosin II. **(A)**

Illustration of the N-WASP constructs used in the study. **(B)** Elongating barbed ends (*arrows*) attached to a GST-PP-WWCA coated FITC-BSA blocked nanofiber (*dashed outline*), polymerizing either perpendicularly (*white arrow*) or parallel (*black arrow*). **(C)** Growth of barbed ends parallel to the nanofiber before and after capture. **(D)** Growth of barbed ends attached perpendicular to the nanofiber before and after capture. **(E-H)** Histogram of smoothed growth rates before (E) and after (F) parallel capture of barbed ends or before (G) and after (H) perpendicular capture. **(I)** Box and whisker plot of growth rates of parallel and perpendicular captured filaments. Scale bar: 10 μm.

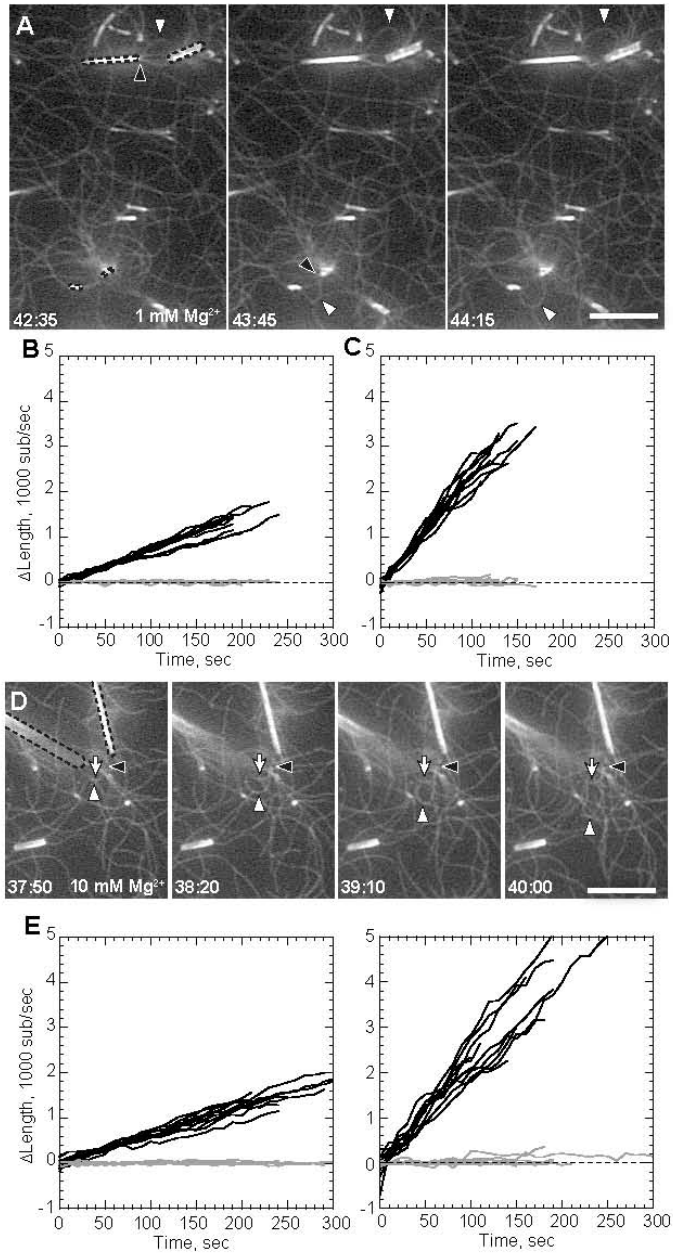


**Figure 2.2 Filament bundling enhances rate of processive elongation**. Conditions as in figure 2.1 except: 1 or 1.2 μM actin as indicated and a total $MgCl_2$ concentration of either 1 mM (A-C) or 10 mM (D-F), (**A**) Processive association of actin filaments to GST-PP-WWCA coated nanofibers (*dotted outlines*) in 1.2 μM Mg-ATP-actin and 1 mM

$Mg^{2+}$ showing buckling of rapidly-elongating filaments (*white arrowheads*) from compression between barbed ends (*black arrowheads*) and NEM myosin attachment points. **(B-C)** Elongation of barbed (*black*) and pointed (*gray*) ends of untethered filaments (B) or tethered buckles (C) in 1 mM $Mg^{2+}$. **(D)** Buckling filament (*white arrowheads*) with barbed end (*black arrowheads*) overlapping a non-buckling filament (white arrow) attached to the end of a nanofiber (*dotted outlines*) in 10 mM $Mg^{2+}$. **(E-F)** Elongation of untethered filaments (E) or tethered filaments (F) in 10 mM $Mg^{2+}$. Barbed end growth rates shown in Table 2.1. Scale bars: 10 μm.

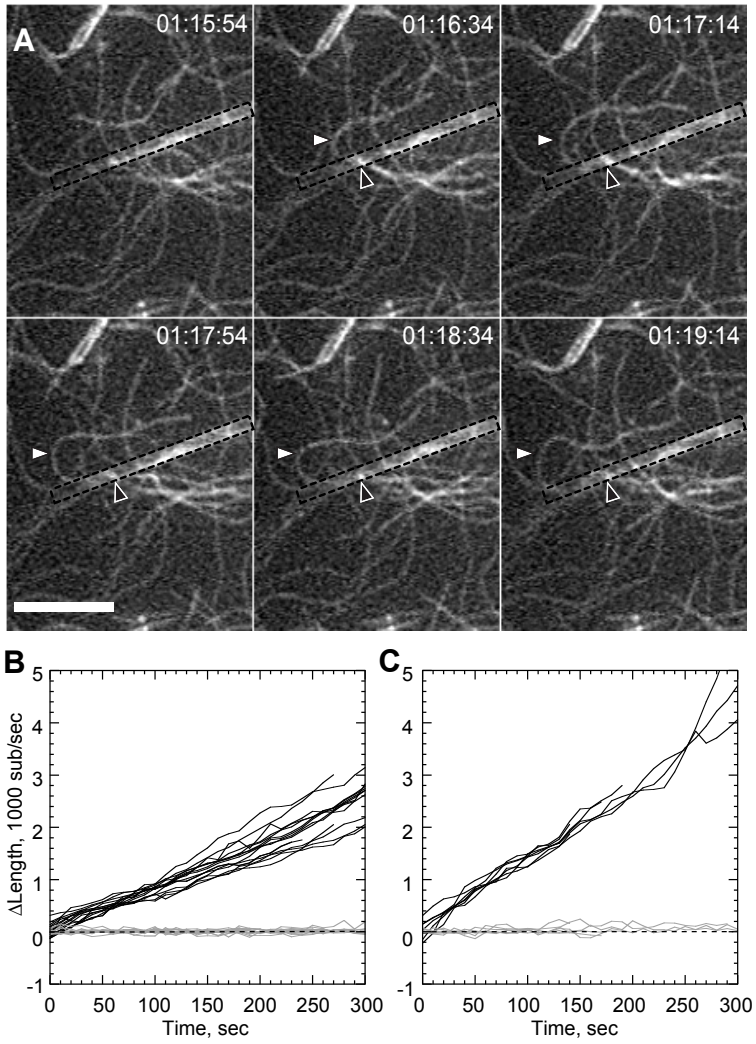


**Figure 2.3**. **Profilin reduces rate of bundle mediated processive elongation.** Conditions as in figure 2.2 with 1 $\mu$M actin, 10 mM total $Mg^{2+}$, 1 $\mu$M Profilin, and 75 nM actin seeds. **(A)** Time-lapse image of sustained processive association of actin filaments on GST-PP-WWCA coated glass nanofibers in presence of profilin. White arrowheads indicate buckling of a rapidly-growing filament. Black arrowheads indicate approximate position of barbed end attachment point. **(B-C)** Elongation of untethered (B) or tethered filaments (C) in 10 mM $Mg^{2+}$. Barbed end growth rates shown in Table 2.1. Scale bar: 10 $\mu$m.

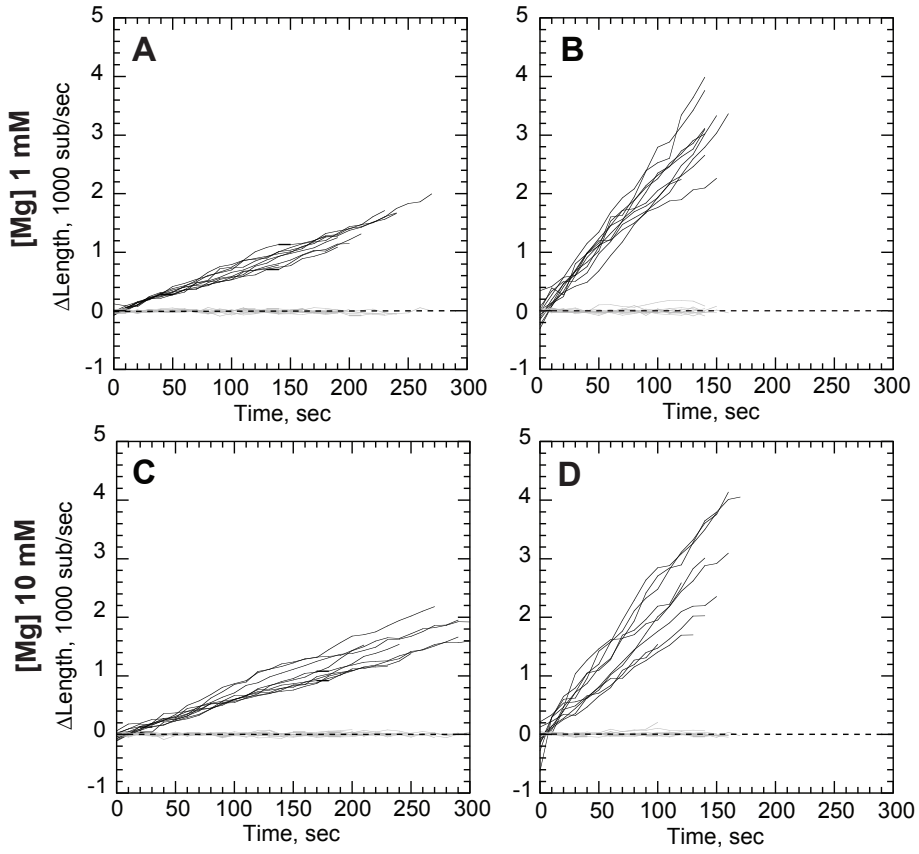


**Figure 2.4**. **N-WASP Proline-rich domains are not required for processive elongation. (A-D)** Conditions as in figure 2.2 except nanofibers coated with GST-WWCA. **(A-B)** Elongation of untethered (A) or tethered filaments (B) in 1 $\mu$M actin and 1 mM $Mg^{2+}$. **(C-D)** Elongation of untethered (C) or tethered filaments (D) in 1 $\mu$M actin 10 mM $Mg^{2+}$. Growth rates shown in Table 2.1.

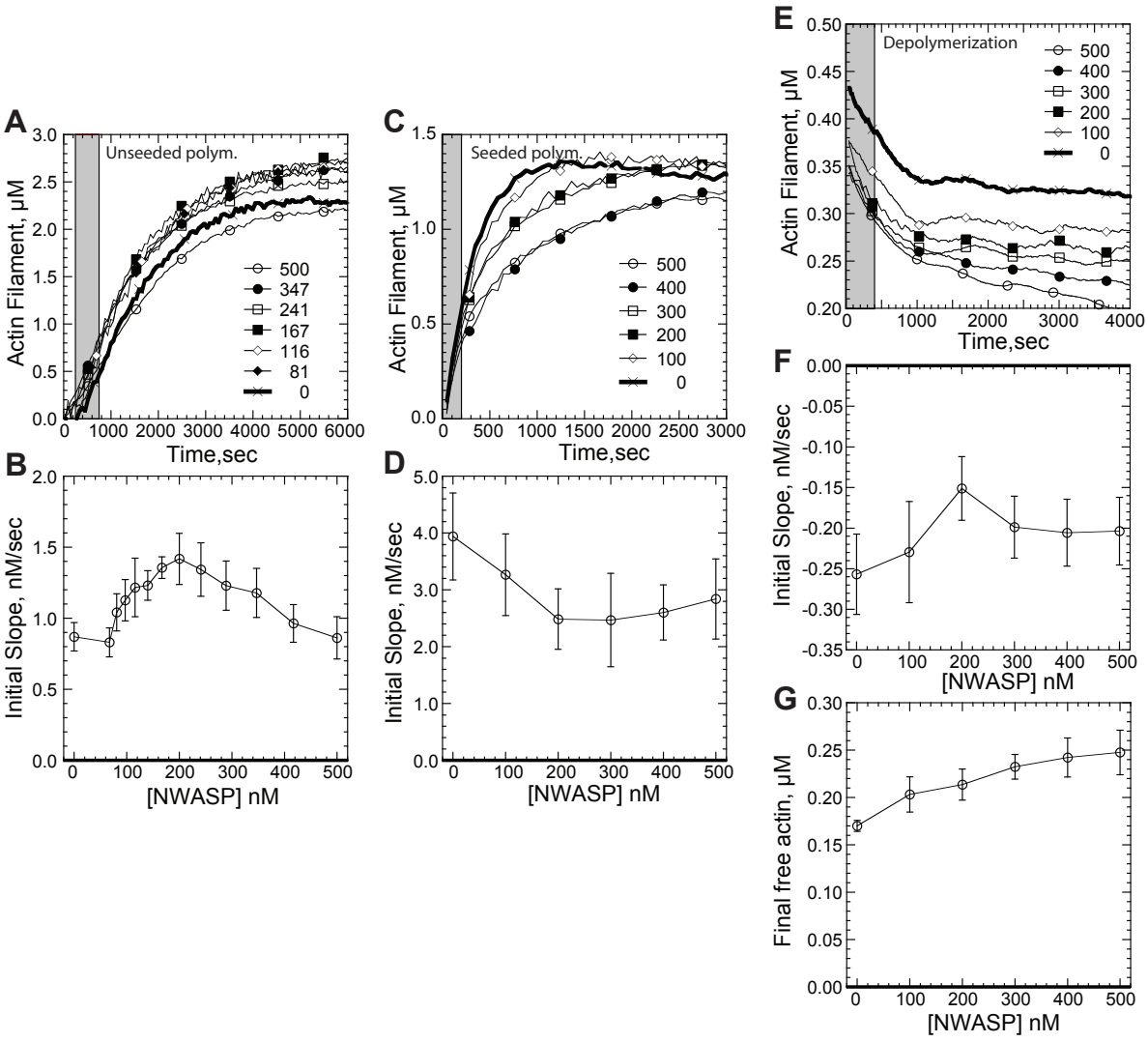


**Figure 2.5. Bulk assays of N-WASP barbed end binding.** Conditions: 1.5 to 5 $\mu$M (30-97% labeled) Mg-ATP actin, 50 mM KCl, 1 mM $MgCl_2$, 1 mM EGTA, 10 mM Imidazole, pH 7.0. (**A**) Representative *de novo* polymerization of 2.5 $\mu$M pyrenyl-actin in the indicated concentration in nM of GST-WWCA. Gray band indicates period for initial slope estimation. (**B**) Average (N=6) *de novo* initial polymerization rates in a range of GST-WWCA concentrations. (**C**) Polymerization of 1.5 $\mu$M pyrenyl-actin from 0.4 $\mu$M seeds. Gray band indicates period for initial slope estimation. (**D**) Average (N=8) initial seeded polymerization rates over a range of nM GST-WWCA concentrations. (**E**) Pyrenyl-actin depolymerization in the presence of indicated nM GST-WWCA. 5 $\mu$M

pyrenyl actin was polymerized then diluted 20-fold in the indicated final nM concentration of GST-WWCA. Gray band indicates period for initial slope estimation. (**F**) Average (N=6) initial seeded polymerization rates over a range of GST-WWCA concentrations. (**G**) Average (N=6) final free actin concentrations over a range of GST-WWCA concentrations.

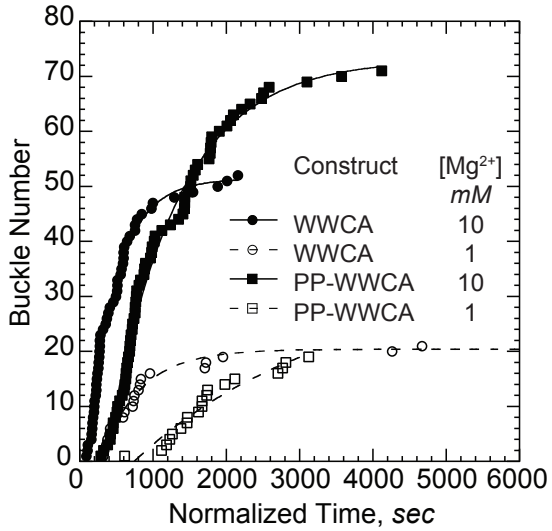


**Figure 2.6. Bundling by $Mg^{2+}$ increases frequency of buckle initiation.** Buckle initiation times were normalized against total nanofiber length in each experiment. Cumulative initiation times over several experiments with the indicated N-WASP construct and $Mg^{2+}$ levels were fit to a delayed exponential to yield an initiation rate (Table 2.2). Buckle formation rates increased with polycation concentration for both constructs. WWCA initiation buckles faster than PP-WWCA.

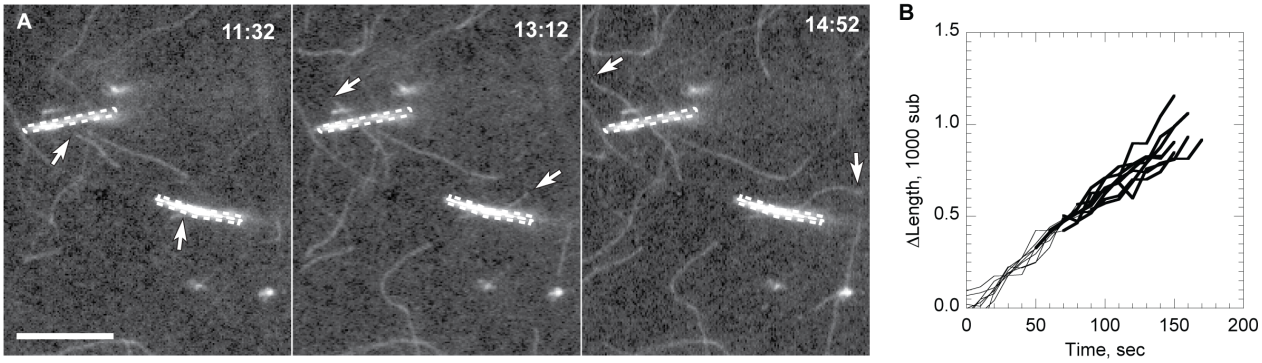


**Figure 2.7. Actin filaments do not interact with control, BSA blocked nanofibers.** Conditions as in figure 2.1 except control nanofibers were blocked only with 1 mg/ml (0.1% FITC labeled) BSA. (A) Time-lapse TIRF microscopy image of barbed end of actin filaments (*white arrow*) growing past BSA coated nanofibers. (B) Barbed end elongation rate of filaments that grew past nanofibers. Growth rates remained the same before (*thin line*) and after (*thick line*) encountering the nanofiber (see Supplementary Movie 6). Scale bar, 10 $\mu$m.

# Chapter 3

# Bundling Mediates N-WASP Processivity


## Abstract

Cells contain a number of dynamic structures including actin filament bundles. These structures play indispensable roles in cell physiology, cell division, motility, adhesion, signaling, etc. Actin bundles may form via cross-linking of individual actin filaments with specific actin-bundling proteins (Puius et al., 1998) or by polycations that "bridge" the gap between negatively charged filaments. We previously showed that N-WASP mediated assembly of actin barbed ends provides an Arp2/3-independent force that likely drives nascent filament bundles into the basement layer during cell invasion (Khanduja and Kuhn, 2013). Extending this idea, we tested the role of reduced and enhanced divalent cation, $Mg^{2+}$ on filament bundling mediated processive acceleration. Based on the previously proposed dependence of processive attachment on filament bundling, we found that the physiological polycation, Spermine also supports N-WASP's processive acceleration of barbed ends. Lastly, we speculate that two WH2 domains are necessary for processivity, as preliminary data shows that a tethered N-WASP construct containing one WH2 domain does not generate processive bundles or filament loops.

## Introduction

Invasive protrusions in cancer cells allow the cell to escape a primary tumor and invade a new niche. After travelling through the vascular and lymphatic systems, the cells exit into a new position and seeds a new tumor – sometimes after lying dormant for months to years (Hanahan and Weinberg, 2011). These invasive protrusions, known as invadopodia, are rich in bundled actin filaments. However, it is unclear whether actin bundling promotes or inhibits cancer metastasis. Rather, cancer cells can adjust the extent of actin bundling to alter their signaling, growth, adhesion and mechanical properties. Typically, mechanical stiffness is directly correlated with invasion (Narumiya et al., 2009) and metastatic potential but there might be exceptions (Swaminathan et al., 2011). Therefore, understanding the mechanism by which actin regulatory proteins promote or utilize actin bundling to succeed in metastasis is still very intriguing and represents an exciting area of research.

Invadopodia are one of the cellular structures that rely on actin bundles for their integrity. Unlike filopodia, invadopodia contain a mixture of bundled and branched actin filaments (Schoumacher et al., 2010). Podosomes are structurally and functionally similar to invadopodia, but occur in non-cancerous cells such as hematopoietic cells, endothelial cells and Src-transformed fibroblasts (Murphy and Courtneidge, 2011). Both, invadopodia and podosomes contain a number of actin-bundling proteins, including fascin (Li et al., 2010a; Schoumacher et al., 2010), α-actinin, formins and Ena/VASP (Murphy and Courtneidge, 2011).

Actin filaments are highly negatively charged biopolymer that are crucial to cell motility and cell shape. They carry a net negative charge of 14 e– per subunit. In cells,

the monovalent cation $K^+$ shields the negative charge of individual subunits to allow them to polymerize. However, polyvalent cations such as $Ca^{2+}$ or $Mg^{2+}$ can also allow whole filaments to overcome the electrostatic repulsion and form parallel or antiparallel bundles (Strzelecka-Gooaszewska et al., 1989). These closely packed bundles can play diverse role in cellular functions.

Actin bundles form either via cross-linking of individual actin filaments with specific actin-bundling proteins or by shielding the negatively charged filaments with polycations that form "bridges" between the filaments. The group of bivalent cross-linking proteins includes fimbrin, α-actinin, spectrin, fascin, filamin. Fascin expression is often upregulated in epithelial cancers and is associated with cancer metastasis and invasion (Machesky and Li, 2010). Actin bundling mediated by Fascin stabilizes filaments and increases their lifetime in filopodia and invadopodia (Li et al., 2010a). Fascin is highly expressed at the invasive front of tumors, and *in vitro* reduction of fascin causes reduced motility and invasion (Hashimoto et al., 2005; Hashimoto et al., 2007; Okada et al., 2007; Schoumacher et al., 2010)

Polycations, including polycationic proteins such as ENA/VASP (Harbeck et al., 2000), and natural and synthetic polyamines, like Spermine and Spermidine induce bundle formation via non-specific electrostatic interactions (Oriol-Audit, 1978; Sowa et al., 2006), by eliminating repulsion between monomeric actin or between actin filaments (Tang and Janmey, 1996). Polycations overcome the 14 e– per subunit negative charge of filamentous actin to promote filament side-to-side association.

Both $Ca^{2+}$ and $Mg^{2+}$ are major divalent cations in cell. Calcium ions are important signaling molecules and they play a role in muscle contraction, cell motility,

fertilization, cell growth and proliferation (Berridge et al., 2000). However, the resting concentration of $Ca^{2+}$ in the cytoplasm is normally maintained in the low range of 10–100 nM. Once activated this level rises to roughly 1000 nM (Berridge et al., 2000). To maintain this low concentration, $Ca^{2+}$ is actively pumped from the cytosol to the extracellular space and into the endoplasmic reticulum (ER), and sometimes in the mitochondria. Magnesium on the other hand is the second most abundant intracellular divalent cation and in mammalian cell its cytosol concentration ranges from 0.5-1.5 mM (Rink et al., 1982; Romani and Scarpa, 1992; Romani and Scarpa, 2000), most of which is bound to negatively charged molecules or ATP (Nadler and Rude, 1995).

Previous studies have shown that multivalent polyamines like Spermine and Spermidine can also promote bundle formation *in vitro* (Grant et al., 1983; Oriol-Audit, 1978; Oriol-Audit, 1982). Spermine, is a small tetravalent cation and is present at millimolar concentrations in proliferating cells (Monti et al., 1996). *In vivo*, these positively charged polyamines are present during processes like neuron repair and sperm activation, processes that reply on actin bundle formation (Aimar and Grant, 1992; Breitbart et al., 1997).

Although N-WASP is primarily described as an Arp2/3 activator, we previously showed that N-WASP WWCA domains could processively attach to growing barbed end bundles and increase their diffusion-limited elongation rate. Furthermore, this activity is independent of Arp2/3. Thick actin bundles generated by 10 mM divalent cation, $Mg^{2+}$, are comparatively more prevalent than those produced in traditional polymerization buffers containing 1 mM $Mg^{2+}$, and these bundles aid in accelerated filament elongation by N-WASP. Given an electrostatic picture of actin bundling, one would expect that a

higher concentration of divalent magnesium or similarly, multivalent linkers would further increase bundling thereby supporting more processive actin elongation by N-WASP. To explore the magnesium dependent bundling in N-WASP mediated processive acceleration we further increased the concentration of magnesium. To test if bundle tethering to N-WASP coated nanofibers could persist in presence of natural polyamines we tested filament bundling and processivity in presence of tetravalent cation, Spermine. Lastly, our preliminary findings indicate that tandem WH2 might be essential in N-WASP processive filament acceleration.

## Results

### Effect of low magnesium concentration on processivity

We adjusted the typical TIRF actin polymerization assay to facilitate a wider range of $Mg^{2+}$ concentrations. Cellular $Mg^{2+}$ concentrations range from 0.5 mM to 1.5 mM (Nureki et al., 2008; Rink et al., 1982; Romani and Scarpa, 1992; Romani and Scarpa, 2000). In *in vitro* actin polymerization assays, the $Ca^{2+}$ bound to the high affinity $Mg^{2+}$ site on actin monomer is first exchanged with $Mg^{2+}$ by addition of Mg-EGTA prior to addition of KCl to polymerize actin. To generate low $Mg^{2+}$ concentrations in our assay, we diluted Ca-ATP-actin monomers into buffer without added $Ca^{2+}$ and reduced Mg-EGTA concentrations 5-fold during the exchange step. Subsequent reducing magnesium in all corresponding buffers regulated total $Mg^{2+}$ concentration in the assay. We calculated free $Mg^{2+}$ concentration from the pH and total buffer $CaCl_2$, EGTA, $MgCl_2$, ATP, and KCl concentrations using existing methods (Bers et al., 1994; Patton et al., 2004).

To test if filament processive attachment could prevail in low magnesium concentration we reduced magnesium concentration in barbed end capture experiments to 0.5 mM and 0.2 mM $Mg^{2+}$. We found that at lower concentrations of $Mg^{2+}$, filament bundle formation was seen after 75 to 90 minutes after the start of the reaction. Although delayed, the inevitable increase in filament density near nanofibers led to filament bundling and resulted in rare processive elongation. Processive elongation was never observed before the point of first filament bundle formation. These results indicate that filament bundling is required for filaments to co-operate for processive elongation on N-WASP.

**Increased divalent cation concentration increases frequency of N-WASP-mediated barbed end acceleration**

We recently showed that filament bundling increases frequency of N-WASP-mediated barbed end acceleration without significantly altering barbed end acceleration rates. We observed that filaments buckles, promoted by filament bundling, appeared at significantly higher frequencies in 10 mM $Mg^{2+}$ than they did in 1 mM $Mg^{2+}$ thereby indicating that bundling play a key role in maintaining barbed end contacts (Khanduja and Kuhn, 2013). To test the bundling effectiveness we doubled the Magnesium concentration from 10 mM to 20 mM in our motility assay. This resulted in faster onset of buckle formation by clustering more filaments on the nanofibers in a shorter time span (Figure 3.1). GST-WWCA coated particles captured significantly more bundled barbed ends than unbundled barbed ends in higher $Mg^{2+}$.

**Processivity persists in presence of cellular polycation, Spermine**

The natural polyamines, Spermidine, and Spermine, are found in almost every living cell at high micromolar to low millimolar concentrations (Russell, 1977; Russell, 1983). Polyamines are synthesized from arginine and s-adenosylmethionine with arginase converting arginine to ornithine, and ornithine decarboxylase (ODC) catalyzing ornithine decarboxylation to form putrescine. Polyamine biosynthesis is up-regulated in actively growing cells most importantly in cancer cells (Erdman et al., 1999; Gerner and Meyskens, 2004; Russell, 1983). During cancer cell transmigration, increased polyamine synthesis appears to be accompanied by cancer invasiveness, as ODC overexpression enhances the invasive characteristics of cancer cells (Kubota et al., 1997). Also, inhibition of polyamine synthesis by the ODC inhibitor, D, L-α-difluoromethylornithine (DFMO) impairs the invasive characteristics of cancer cells (Ashida et al., 1992; Jun et al., 2008; Manni et al., 2005).

Therefore, first we tested if cellular polycations such as spermine may support short filament side-to-side association in *in vitro* TIRF actin polymerization assays. We found that spermine bundles filament at 100 μM, in low $Mg^{2+}$ (0.105mM, Figure 3.2)

To further test if processivity depended on filament bundling rather than magnesium and whether Spermide supports processivity we repeated the barbed end capture experiments with Spermine in low $Mg^{2+}$. We found that the 500 μM tetravalent organic cation Spermine formed thick actin bundles and showed enhanced processivity on N-WASP WWCA coated nanofibers (Figure 3.2). This shows that polycationic bundling of actin filaments *per se*, rather than magnesium, promotes processive acceleration by N-WASP.

**Processivity requires tandem WH2 domain**

Unlike WASP, the C terminus of N-WASP has two tandem WH2 motifs that bind to an actin subunit each. To test if a single actin-binding domain could sustain processivity, I designed a shorter N-WASP construct missing the first native WH2 domain (GST-WCA). To test the activation potency of GST-WCA, we characterized its ability to stimulate Arp2/3 complex mediated actin polymerization. The N-WASP construct with only one WH2 domain had much lower potency as an Arp2/3 activator (Figure 3.3) than did the construct with one two native WH2 domains, consistent with Yamaguchi's result (Yamaguchi et al., 2000)

We repeated barbed end capture experiments in 10 mM $Mg^{2+}$ with N-WASP construct containing single WH2 domain. We found that with a single WH2 domain, N-WASP did not support processive attachment. We therefore conclude that two WH2 motifs are essential for N-WASP mediated processive elongation. However, this shorter N-WASP construct was a less active Arp2/3 nucleator than the WCA domain from WASP, which contains only one native WH2 domain (Figure 3.3). Therefore, it is possible that like its Arp2/3 activation activity, the barbed end binding activity of this shorter construct might have been compromised. Future experiments with WASP and WAVE, nucleators than contain single WH2 domain will further determine whether tandem WH2 domains are absolutely necessary for processive elongation of barbed ends by WASP-family nucleation promoting factors.

## Discussion

N-WASP is a key player in actin cytoskeleton rearrangements. It has been localized in invadopodia and podosomes where it likely controls dynamic attachment and actin turnover at the barbed ends of actin filaments (Lorenz et al., 2004b; Mizutani et al.,

2002b; Murphy and Courtneidge, 2011; Yamaguchi et al., 2005). Our central finding from this study is that filament bundling by both di- and multi-valent cation is essential for maintaining persistent processive attachments between growing barbed ends and N-WASP WCA containing tandem WH2 domains. We found that natural occurring polycation Spermine also supports filament side-to-side association that actively drives processivity. Our preliminary data shows that the two tandem WH2 domains of N-WASP might be necessary to provide the two actin binding sites required for processive stepping.

The natural polyamines are aliphatic cations with multiple functions and are essential for cell growth. In addition, polyamines seem to accelerate tumor invasion and metastasis not only by suppressing immune system activity against established (already existing) tumors but also by enhancing the ability of invasive and metastatic capability of cancer cells. However, the mechanism by which polyamines increase invasive potential remains unclear.

Cancerous cells secrete enzymes that degrade the surrounding extracellular matrix, which is composed of the interstitial matrix and basement membrane that provides additional structural support to cells. Cancer cells are capable of producing numerous proteinases, such as serine proteinase, matrix metalloproteinases (MMP), cathepsins, and plasminogen activator that degrade the extracellular matrix (ECM). A close correlation between increased polyamine synthesis and increased MMP synthesis has also been shown (Matters et al., 2005; Wallon et al., 1994).

Based on the previous known significant role of polyamines in tumor spread and the current findings of enhanced barbed end acceleration through bundling we believe that

polyamines may have a significant role in invasiveness and tumor spread through an actin-based mechanism. Previous studies show that N-WASP is activated at the cell membrane during the initiation of invadopodium formation, thereby implicating N-WASP activity in the initiation of invasion (Lorenz et al., 2004a). Invadopodia emerge from Arp2/3 complex–induced lamellipodial actin meshwork convergent extension. As filaments bundle inside the invadopodia, clustering of N-WASP at the tip of the invadopodia drives accelerated processive barbed end elongation mediated by these bundled filaments. Cytosolic polycation induced bundles might play an important role in specialized focal protrusive structures.

Apart from invadopodia and podosomes, N-WASP is also been found enriched in microspikes (Nakagawa et al., 2001), structures rich with bundled actin. If $Mg^{2+}$ generates short bundles mediate processive attachment, natural bundle formation through polyamines may have important implications for WWCA mediated microspike formation at the leading edge. As bundling increases so would processivity as these filaments co-operate to stabilize the fast growing barbed ends. Filament bundling proteins such as fascin and a-actinin may further help stabilize these nascent clusters.

Our preliminary data also shows that a single WH2 domain does not support co-operative filament processivity. Further studies with extended WH2 linkers, or with WASP/WAVE's single WH2 domain should elucidate the mechanism of processive elongation.

The Wiskott-Aldrich syndrome protein (WASP) and WASP-family verprolin-homologous protein (WAVE) family proteins are fundamental actin-cytoskeleton reorganizers found throughout the eukaryotes (Kurisu and Takenawa, 2009; Stradal et al.,

2004; Takenawa and Miki, 2001). Their conserved function across species is to receive upstream signals from Rho-family small GTPases and deliver them to activate the Arp2/3 complex, leading to rapid actin polymerization. At current count, mammals possess five genes for the WASP and WAVE family proteins: WASP, N-WASP, WAVE1/SCAR1, WAVE2, and WAVE3 (Deeks and Hussey, 2005; Millard et al., 2004b; Stradal and Scita, 2006; Takenawa and Suetsugu, 2007b; Vartiainen and Machesky, 2004). These contain a N-terminal regulatory region and a conserved C-terminal functional domain (Fig 3.4). Structure-based multiple sequence alignment of the WCA (verprolin homology (WH2)/central/acidic) region of these WH2-domain containing proteins indicates a high levels of sequence identity between their C term domains. The WH2 domains might be evolutionarily independent protein-binding sequences but their sequence similarity could be indicative of a shared common function. A highly homologous protein, VASP, requires its tetramerization domain to accelerate barbed ends (Bachmann et al., 1999; Breitsprecher et al., 2008b). Similarly, Formins dimerize and remain processively attached to growing barbed ends. Dimerization of WASP/WAVE has been shown to greatly enhance it Arp2/3 activation activity (Padrick et al., 2008). Similarly, dimerization of WASP/WAVE family WCA domains at the leading edge could act synergistically with filament bundling to enhance accelerated processive binding to barbed ends.

Our understanding of WASP and SCAR/WAVE proteins is growing quickly, but there is still a lot that is left to discover. Newly discovered WASP-family members such as WASH (Wiskott-Aldrich syndrome protein and Scar homolog)(Linardopoulou et al., 2007), WHAMM (WASP homolog associated with actin, membranes, and

microtubules)(Campellone et al., 2008) and JMY (a WHAMM homolog)(Zuchero et al., 2009) have broadened the range of roles of the family, interacting proteins and pathways are only beginning to be discovered. In light of the processive barbed end elongation activity of N-WASP, these newly discovered WASP-family members should be examined for similar Arp2/3-independent behaviors.

## Materials and Methods

Protein Expression and Purification. Actin was purified from rabbit skeletal muscle actin acetone powder through one round of polymerization and depolymerization followed by gel filtration (Spudich and Watt, 1971a). Actin was labeled with Oregon Green 488 iodoacetamide (Invitrogen) as described {Kuhn, 2005 #123. Unlabeled and labeled actin was stored for up to 1 month at 4 ºC. Both labeled and unlabeled actins were dialyzed overnight against fresh buffer G (2 mM Tris-Cl pH 8, 0.2 mM ATP, 1 mM $NaN_3$, 0.1 mM $CaCl_2$, 0.5 mM dithiothreitol, DTT) and centrifuged at 38,000 g for 2 hr at 4ºC before use to remove storage precipitates. Actin concentrations were estimated from extinction coefficients as follows: actin, $E_{290} = 26{,}600\ M^{-1}cm^{-1}$ (Kuhn and Pollard, 2005b); Oregon green actin, $E_{290} = 26{,}600\ M^{-1}cm^{-1}$ using the correction $A^*_{290} = A_{290} - 0.16991A_{491}$; Oregon green, $E_{491} = 77{,}800\ M^{-1}cm^{-1}$.

Bovine N-WASP WWCA (A403 - D505) was purified as a GST fusion protein as described {Hu, 2012 #101}. Bovine N-WASP WCA (G433-D505) was designed to contain the second WH2 domain (G433-V450) and the first W domain was WH1 (N405-K421) removed. The construct was cloned into the vector pGEX2 (Novagen) containing N-terminal GST and the sequence was verified. GST-WCA was expressed in Rosetta DE3pLysS (Novagen) bacteria grown at 37 °C to an $A_{600}$ of 0.8 and induced with 0.5 mM

isopropyl β-D-thiogalactopyranoside overnight at 16°C. Bacteria were pelleted, resuspended in TBSE (20 mM Tris, 200 mMNaCl, 1 mM EDTA, 10 mM 2-mercaptoethanol) supplemented with complete EDTA-free protease inhibitors (Roche) and pulse sonicated on ice for a total of 150 seconds. Bacteria were pelleted for 30 min at 46,000 xg, the supernatant was added to glutathione resin (Thermo Scientific), and the resin was washed with 5 volumes of wash buffer (TBSE with 0.1% Thesit). Protein was eluted using 50 mM reduced glutathione, pH 8.0 followed by anion exchange chromatography on a Source Q (GE Healthcare, Piscataway, NJ) column. GST-WCA concentration was determined using an extinction coefficient $E_{280}$ = 46030 $M^{-1}cm^{-1}$. Both N-WASP constructs were flash frozen in liquid nitrogen and stored at -80 ºC.

Nanofiber Preparation and Coating. Glass nanofibers (200 nm nominal diameter, Johns Mansville, Denver, CO) were broken into smaller fragments in chloroform in a Dounce homogenizer as previously described (Hu and Kuhn, 2012a). Nanofibers are centrifuged at 3750 X g for 10 min, excess chloroform drained, and the remaining chloroform evaporated. Nanofibers were washed with deionized water by low-speed centrifugation and sonicated for 1 hour in 1 M KOH in a bath sonicator to remove contaminants. Nanofibers were washed briefly in deionized water, resuspended in 1 M HCl, sonicated for 1 hour, and incubated overnight in HCl. Cleaned nanofibers were subsequently pelleted by centrifugation and sonicated for 30 minutes each in in deionized water, 1 mM EDTA, 70% ethanol, and absolute ethanol to dry, with pelleting between each step. Cleaned nanofibers were stored in glass containers in absolute ethanol for up to 6 months. For coating, ethanol was removed after centrifugation and the remaining ethanol evaporated. Nanofibers were incubated with 20 $\mu$M N-WASP in coating buffer

(10 mM Hepes pH 7.3, 0.1 M KCl, 1 mM $MgCl_2$, 1 mM ATP, 0.1 mM $CaCl_2$, 1 mM $NaN_3$, final pH 7.56) overnight. Fluorescein conjugated bovine serum albumen (FITC-BSA, Invitrogen) was added to a final concentration of 0.02 mg/ml to aid visibility and nanofibers were incubated an additional 5 minutes. Nanofibers were washed 3x with coating buffer and resuspended in coating buffer supplemented with 1 mg/ml low grade BSA (Sigma Aldrich) to block subsequent protein addition. Nanofibers were stored in BSA at 4ºC for up to 5 days before use.

Testing processivity in low Magnesium and Spermine. For low $Mg^{2+}$ motility buffers, we made the following changes for the reaction. For each experiment we diluted fresh Ca-ATP actin into buffer G without $Ca^{2+}$. We mixed actin 9:1 with 10x low magnesium exchange buffer (10x lowME: 2 mM EGTA, 0.2 mM MgCl2) for 2 minutes to form 4x final concentration of actin. We diluted all proteins in buffer G with no added $Ca^{2+}$, or $Mg^{2+}$, or EGTA. We reduced $MgCl_2$ in 2x TIRF buffer from 2 mM to 0.2 mM to form 2x low-Mg TIRF buffer. The final total concentration of $Mg^{2+}$, $Ca^{2+}$, EGTA, and ATP were 0.105 mM, 5 μM, 1.05 mM, and 0.2 mM, respectively. Free $Mg^{2+}$, $Ca^{2+}$, and ATP concentrations were calculated using MaxChelator software (Bers et al., 1994; Patton et al., 2004) available at the following address maxchelator.stanford.edu. For filament bundling with spermine, all buffers were preparated as above. Spermine (100 μM or 500 μM) was added right before the start of reaction

Total Internal Reflection Fluorescence (TIRF) Microscopy. Clean glass slides; coverslips and flow cells were constructed as previously described (Kuhn and Pollard, 2005b)(Kuhn and Pollard, 2005b)(Kuhn and Pollard 2005)(Kuhn and Pollard, 2005a). For filament tethering, flow cells were coated with 100 nM n-ethylmaleimide inactivated

myosin II for 2 minutes. To prevent non-specific binding flow cells were blocked with 1% w/v BSA for 2 min as described (Kuhn and Pollard, 2005a). Unlabeled Mg-ATP-actin and Mg-ATP-actin labeled with Oregon Green 488 (Invitrogen) were mixed with nanofibers and either 2x Low-Mg TIRF buffer (above), 2x TIRF buffer (2x: 20 mM Imidazole pH 7, 100 mM KCl, 2 mM $MgCl_2$, 2 mM EGTA, 200 mM DTT, 0.4 mM ATP, 30 mM Glucose, 0.5% Methyl Cellulose 1500 centipoises, 40 $\mu$g/ml catalase, 0.2 mg/ml glucose oxidase) or 2x High Mg-TIRF buffer (2x: TIRF buffer with 20 mM total $MgCl_2$) to start spontaneous actin assembly. For each experiment 16 $\mu$l of reaction mixture was added to the chamber and the entry and exit ports of flow cell were sealed with warm VALAP (1:1:1 vaseline : lanolin : paraffin).

Image acquisition and analysis. TIRF images were collected on an Olympus upright microscope (BX51WI) using prism-based excitation from a 488 nm solid-state laser (Sapphire, Coherent Santa Clara, CA) and custom optics. Images were captured by a Rolera-MGI EMCCD camera (QImaging, Surrey, BC, Canada) at 10-second intervals using Micro-manager open source acquisition software (Edelstein et al., 2010). Images were analyzed using ImageJ software (Schneider and Rasband, 2012). Actin filament barbed and pointed end lengths were measured against fiduciary marks provided by NEM-Myosin II attachment points as previously described (Kuhn and Pollard, 2005b).

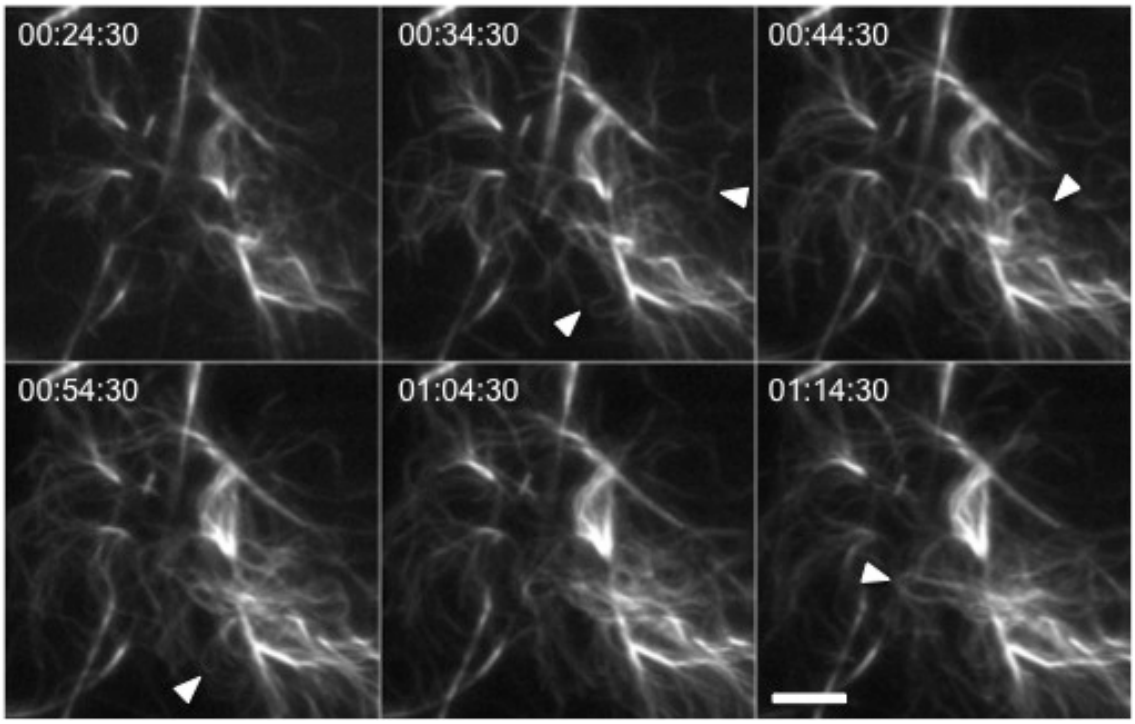


**Figure 3.1 Doubling $Mg^{2+}$ increases frequency of loops.** Conditions: 1uM Mg-ATP actin (40% labeled), nanofibers coated with 20 $\mu$M GST-WWCA, 20 mM $MgCl_2$, 10 mM Imidazole pH 7, 50 mM KCl, 1 mM EGTA, 100 mM DTT, 0.2 mM ATP, 0.25% methyl cellulose, 15 mM glucose, 20 $\mu$g/mL catalase, 100 $\mu$g/mL glucose oxidase. Time-lapse TIRF microscopy movie of sustained rapid elongation of actin filaments with barbed ends attached to GST-WWCA nanofibers in 20mM $Mg^{2+}$. Buckling filaments (*white arrowheads*) with barbed ends attached to nanofibers. Scale bar 10um

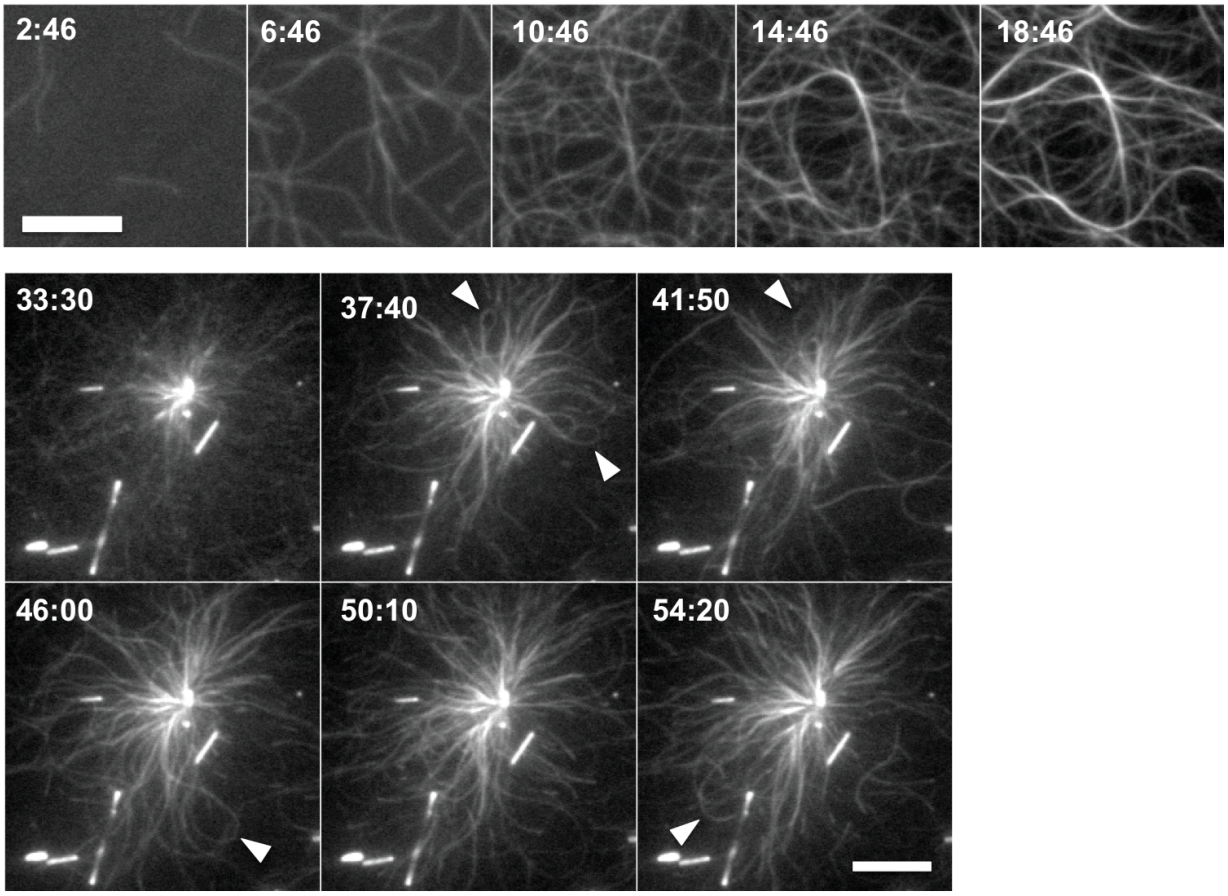


**Figure 3.2 Spermine supports bundle mediated processive elongation.**

Conditions as in figure 3.1 but with 1 μM actin, 0.105 mM $Mg^{2+}$ (A) 100 $\mu$M Spermine without GST-N-WASP coated nanofiber (B) 500 $\mu$M Spermine. (A) Time lapse TIRF images of *de novo* nucleated actin filaments forming bundles. (B) Buckling filaments (*white arrowheads*) with barbed ends attached to GST-N-WASP coated nanofibers in presence of Spermine.

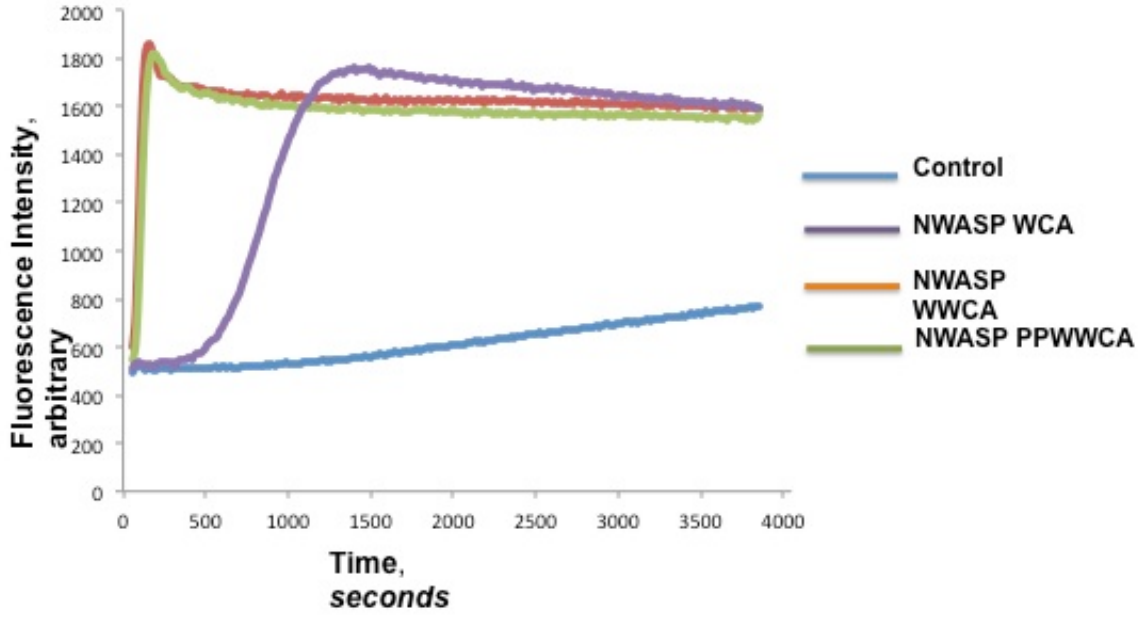


**Figure 3.3: Arp2/3 Nucleation Activity of N-WASP**. Conditions: 1.5uM Actin (30% labeled), 40nM Arp2/3, 100 nM of indicated N-WASP construct. Pyrene assay to test Arp2/3 nucleation activity of N-WASP-WWCA, N-WASP-PPWWCA and N-WASP-WCA. N-WASP-WCA was active but has lower activation potency

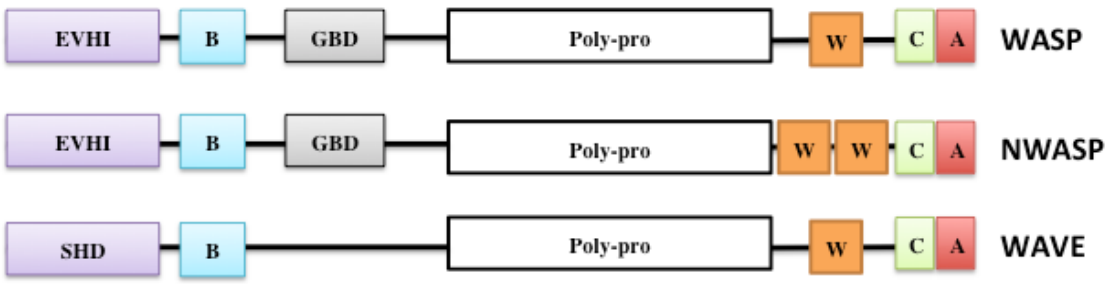


**Figure 3.4 Domain organization of WASP/Scar proteins** *EVH1*, Ena/Vasp homology 1 domain; *B*, basic region; *GBD*, GTPase-binding domain; *Poly Pro*, proline-rich region; *SHD*, Scar homology domain; *WH2*, verprolin-like or WASP homology 2 domain; *C*, central or connecting domain; *A*, acidic domain.


**Figure 3.5 Structure-based WASP family sequence alignment.** Structure-based multiple sequence alignment of the WCA (verprolin homology (WH2)/central/acidic) region of WH2-domain containing proteins. The alignment was constructed using ClustalW and BOXSHADE3.21 (http://www.ch.embnet.org/software/BOX_form.html). Accession numbers are WAVE1 (Q8R5H6), WAVE2 (Q8BH43), WAVE3 (Q8VHI6), WASP (P70315), N-WASP (BAA20128).

# Chapter 4

# Conclusions and Future Directions

## Conclusions

Metastasis represents the most lethal aspect of cancerous cell and also arguably one of the most exciting frontiers of scientific and biomedical investigation. As the study of tumor metastasis advances we are beginning to understand the role of the actin cytoskeleton and key proteins that might be involved in the process. Discoveries of unique protein pathways involved in invasion and metastasis will provide new targets for therapeutic development.

The present work demonstrates that like Ena/VASP (Breitsprecher et al., 2008b; Hansen and Mullins, 2010b) and Formin (Kovar and Pollard, 2004b; Shemesh et al., 2005) family proteins, N-WASP WWCA domains can processively attach to growing barbed bundles and increase their diffusion-limited elongation rate in the absence of Arp2/3 complex. N-WASP can thus regulate assembly of actin filaments by directly enhancing filament elongation in a processive manner.

My thesis describes a novel actin polymerization activity of N-WASP that is independent of its canonical role as an Arp2/3 complex activator. Localized activity of N-WASP is considered critical for podosomes formation (Linder et al., 1999b; Mizutani et al., 2002b) and invasion of the metastatic cancer cell (Lorenz et al., 2004a; Yamaguchi et al., 2005). We used TIRF microscopy to show how nanofibers coated with WWCA domains of N-WASP interact with individual *de novo* nucleated actin filament barbed ends. In chapter 2, we show that individual filaments captured perpendicularly by N-WASP-coated nanofibers grew at or below the diffusion limited polymerization rate.

However, clustered barbed ends bound to nanofibers could grow substantially faster than the diffusion-limited polymerization rate. This rapid processive elongation of N-WASP bound barbed ends was due to filament bundling by the divalent cation $Mg^{2+}$. When filaments overlapped at the nanofiber surface, several nanofiber-connected barbed ends switched from slow to fast growth. Measurements showed that these N-WASP-assembled barbed ends grew 3.4-fold faster than background filaments. While the poly-proline domains reduce the rate of processive acceleration in the presence of profilin, the processive acceleration mediated by N-WASP WWCA domains alone remains unaffected. We further showed that increasing $Mg^{2+}$ to promote filament bundling dramatically increases the frequency of accelerated buckle formation. My study points to a significant requirement of divalent cation, magnesium for processive motility.

Magnesium is primarily found within cells (Elin, 1988). Intracellular magnesium concentrations increase upon cell stimulation and differ in each cell types (Gunther, 2006). Magnesium has numerous functions inside the cell. It is a co-factor to >300 enzyme reactions and a counter-ion for ATP (Saris et al., 2000; Swaminathan, 2003). Its membrane functions include cell adhesion and transmembrane transport including transport of calcium and potassium ions. In muscle contraction, magnesium stimulates calcium re-uptake by the calcium activated ATPase (Saris et al., 2000). It is also believed that magnesium has a role in insulin secretion (Reis et al., 2000). My research has focused on a new role of divalent cation and the direct participation of $Mg^{2+}$ in the processive motility.

The 3rd chapter further explores the role of polycations in N-WASP mediated processivity. Because N-WASP mediated filament acceleration is dependent on filament

bundling, reducing divalent cation substantially delays filament bundling and the appearance of processive elongation. In contrast, 20 mM magnesium accelerates filament bundling and concomitantly increases the initiation of processive elongation. Other physiological polycations such as Spermine show similar actin filament bundling and processivity activity, which indicates that cellular polyamines play an important role in N-WASP induced invadopodia formation. Our preliminary results also showed that N-WASP constructs with only a single WH2 domain did not support filament barbed end processivity. However, this must be confirmed with WASP and WAVE, which natively contain only one WH2 domain.

Based on previous studies and my thesis I believe two distinct types of filamentous actin networks possibly cooperate to form invadopodia - a branched actin network that forms the base of invadopodia and a parallel array of bundled filaments along the length of the invadopodial protrusive shaft that is responsible for its elongation, degradation of, and invasion into ECM.

Invadopodia are initiated by assembly of dendritic network into bundled actin networks and then mature by processive elongation of individual filaments in actin bundles. These two actin networks are driven by different molecular components, but N-WASP has an essential role to play in both. The branched array of actin filaments at the base of invadopodia is driven by N-WASP activated Arp2/3 nucleated branch filament network (Lorenz et al., 2004a; Schoumacher et al., 2010; Yamaguchi et al., 2005). N-WASP is activated by the Rho GTPase Cdc42, WIP and Nck1 - all of which localize to the invadopodia and have been shown to be necessary for its formation (Yamaguchi et al., 2005). Invadopodia elongation is suggested to be driven by arrays of parallel bundled

filaments internally present along the length of invadopodia shaft (Schoumacher et al., 2010). Actin polymerization occurs at the barbed end of an actin filament and N-WASP is known to bind to the barbed end of filaments (Egile et al., 1999a; Hu and Kuhn, 2012b; Khanduja and Kuhn, 2013). In invadopodia, the actin severing protein cofilin has been shown to be responsible for the generation of free barbed ends; that drive protrusion of this structure (Oser et al., 2009). Accelerated extension of these barbed ends is driven by N-WASP, which is present at the tip of these invasive bundled actin structures. The bundling activity is coordinated by bundling proteins, Fascin (Li et al., 2010a), and polycations whose biosynthesis is known to be up-regulated in actively growing cells, including cancer cells (Erdman et al., 1999). We propose that the membrane clustered N-WASP provide a multimerization effect to hold the barbed ends oriented perpendicular to the membrane and accelerate their elongation. This means that at the tip of invadopodia, multiple WCA domains from adjacent N-WASP could cooperate to attach to filament barbed ends. The bundling factors provide sturdiness to a protrusive structure and limits filaments from diffusing away. N-WASP thus acts synergistically with filament bundling to enhance processive binding to barbed ends. We hence believe that N-WASP has a crucial role to play at internal periphery of the cell, from initiating the nucleation of a branched network to the accelerating ability of invasive and metastatic capability of cancer cells.

We propose that this novel Arp2/3-independent mechanism for N-WASP has important implications for invadopodia and podosome formation. N-WASP promotes transient actin bundles to invasive structures by accelerating their assembly. The force from this accelerated filament assembly provides an initial push or “spear-tip” for

invadopodia to wedge into the basement layer. This report on a novel Arp2/3-independent actin polymerizing function of N-WASP is the first step towards a detailed dissection of the mechanism of accelerated actin polymerization by N-WASP and its role in forming invasive cell protrusions.

## Future Directions

To further confirm the proposed mechanism for N-WASP mediated cell invasion into the substrate, future lab members will work on providing more direct microscopic evidence and testing of this model in cells. Several other newly discovered actin regulating proteins like WAVE, WHAMM, WASH and JMY (a WHAMM homolog) contain WH2 domains that might play similar roles in processive acceleration of the filament-barbed ends. The C termini of these players should be tested for processive actin assembly under similar conditions. The work presented here opens up a set of new questions that can be addressed by further experiments,both *in vivo* and *in vitro*, that will help us define the exact role and significance of this new mechanism for N-WASP. Some potential experiments are listed as below.

**Does $Mg^{2+}$ affect Acidic (A) domain binding to barbed ends?**

Both the WH2 and acidic domains of N-WASP bind to actin monomers with low affinity (Marchand et al., 2001b) and polycation concentrations were never explored in my research. Thus, the role that polycations play in binding to the C-terminal domain of N-WASP needs to be further investigated. Like actin filaments, the acidic domain of WCA activators is negatively charged at cellular pH. Actin filaments carry a negative 14e- per subunit charge and multivalent cations could play a role in overcoming ionic

repulsion between and the acidic domain and filament barbed ends. Although the monovalent salt concentration (KCl) in these experiments is high enough to partially shield these repulsive ionic interactions, we cannot discount the possibility that excessive $Mg^{2+}$ or other polycations in these assays binds acidic domains to actin filaments. This can be tested using truncated version of N-WASP, GST-WWC without the acidic domain (or A domain constructs with acidic residues mutated to neutral or basic) to test if N-WASP WWC domains retain the ability to enhance barbed ends rates in the presence of high $Mg^{2+}$.

**Test barbed end-binding affinities to N-WASP**

If WCA domains (containing a single WH2) do not support processive elongation, this effect is likely due to a lower affinity for actin barbed ends. While previously, the actin monomer binding affinities to WASP WCA domains have been measured (Marchand et al., 2001b), the filament barbed end affinities have never been measured. The Kuhn lab has found that fluorescence anisotropic assays can measure binding of rhodamine-labeled N-WASP to actin filament barbed end (Hu and Kuhn, manuscript in preparation). A main requirement for these assays is the careful shearing of barbed ends by repetitive pipetting or vortexing to generate a reproducible range of filament end concentrations. Actin is polymerized for short span of time, diluted and mechanically sheared for various times. The resultant short filaments should be used immediately in two separate reactions. In first reaction one tests binding affinities by mixing these sheared filaments with rhodamine tagged N-WASP WWCA. The binding of WWCA to the barbed end would produce shifts in the reaction. A second reaction uses the other half of the seeds to estimate barbed end concentration in the first reaction. Unlabeled WCA

form WASP and WAVE would be used in competition assays with rhodamine labeled WWCA to estimate the unlabeled peptide's binding affinity. If a low concentration of rhodamine tagged N-WASP was titrated against a range of concentrations of the untagged barbed ends it will help us measure the affinity of the labeled WCA to barbed end. Decreased affinity of WCA compared to PP-WWCA or WWCA could help explain why N-WASP WCA domains do not processively bind to growing filaments.

**Discover role of ATP hydrolysis in processive elongation.**

It was previously reported that ATP hydrolysis is crucial for Formin processivity (Romero et al., 2004; Romero et al., 2007), However, several other studies found that ATP hydrolysis played no role in Formin mediated actin assembly (Kovar et al., 2006; Paul and Pollard, 2009a). So far, the only other processive filament elongator is the VASP family of proteins that contain FAB domains – domains that have WH2-like actin binding properties. The clamped elongation model by (Dickinson and Purich, 2002) suggests that altered affinities from the FAB to ATP and ADP actin are essential for tracking the barbed end. The role of ATP hydrolysis for VASP processivity still remains controversial, and it needs to be explored for the new processive accelerator N-WASP. This can be achieved by either substitution of a nonhydrolyzable ATP analog or measurement of the time course of γ-phosphate release from ATP-actin filaments in the presence of N-WASP coated nanofibers and polycations. A non-hydrolysable ATP analog might prevent or reduce the accelerated processivity. If the addition of actin onto barbed ends of filaments were directly coupled to the release of γ-phosphate from ATP-actin subunits then we would know that the hydrolysis of ATP provides the necessary energetic requirements for processive elongation by N-WASP.

**Quantify filament bundling with AFM**

One of the major challenges we faced during our study was the quantification of bundling that mediates processivity. Due to the limited resolution of TIRF, the overlapping fluorescence of nanofiber and filament bundles made it hard to quantify filament density. We therefore need a nanometer-resolution method that would help us measure number of filaments in a bundle that initiates processivity. For this we can use Atomic Force Microscopy (AFM), which is a very high-resolution type of scanning probe microscopy. TIRF observed filament bundling and processive acceleration could be flash fixed. We can relocate the same field on AFM and digitally correlate the TIRF data where we see filament buckling to the number of filaments in a bundle that help initiate it to better understand the quantitative role of bundling in processivity.

**Testing the role of polycations *in vivo***

In addition to its biochemical properties and *in vitro* function, *in vivo* studies can provide insight into precise role of N-WASP based cell motility, cancer and its interaction with other proteins.

Though we showed that motility *in vitro* requires polycations, the requirement of polyvalent cations such as Magnesium or Spermine for motility *in vivo* remains unclear. High cellular $Mg^{2+}$ levels have been linked to angiogenesis and endothelial cell migration. Magnesium has also been associated to integrin-mediated cell attachments that provide traction for motile cells (Takeichi and Okada, 1972). Our study points to a direct role of divalent cations *in vitro*. Therefore it is essential to find out how increased cellular magnesium would affect the cytoskeleton machinery *in vivo*.

The biosynthesis of polyamines such as Spermine is highly up-regulated in actively growing cells, including cancer cells (Gerner and Meyskens, 2004; Russell, 1977; Russell, 1983). A major factor that directly influences the prognosis of patients with malignant disease is the capability of cancer cells to invade surrounding tissues and organs and evade immune cell defenses to metastasize to distant organs. In animal experiments, inhibition of polyamine synthesis has shown to not only reduce tumor growth but also a reduced amount of metastasis, resulting in prolonged survival of tumor bearing animals (Kingsnorth et al., 1983; Klein et al., 1985; Manni et al., 2005). Inhibition of polyamine uptake has been shown to reduce cancer metastasis (Aziz et al., 1996). Because of the exquisite sensitivity of N-WASP processivity to polyamines, N-WASP mediated invasiveness could play an important role in mediating increased invasiveness due to polyamine upregulation. Detailed *in vivo* experiments (described below) would define the link between N-WASP, polycations, and invasiveness of cancer cells.

Polycation induced cancer invasion could be used in tissue culture using cell lines or clinically derived primary cancer cells to track tumor evolution and tumor response to therapy in cancer cells or in patients. If N-WASP played a role in polycation-mediated invasion, then tumor cell lines or primary tumor cells from cancer patients would likely show increased invadopodia formation and invasiveness on basement membranes *in vitro*. We would expect that knockdown of native N-WASP using antisense morpholinos would decrease invadopodia formation and substrate invasion in high-polycation expressing cells. Reintroduction of exogenous full-length GFP-N-WASP should restore invadopodia formation. However, based on its lack of processivity, exogenous GFP-N-

WASP containing only a single WH2 would likely not restore invadopodia formation. We would fine-tune this approach with *in vitro* processivity experiments to design a version of N-WASP that activates Arp2/3 but does not processively elongate filament ends. We would use this construct to distinguish between N-WASP important role as Arp2/3 activation activity and its processive elongation activity *in vivo*. Such measurements could be translated into therapeutic efficacy.

We can also test if the bundling dependent attachment model could inhibit polyamine synthesis or availability inside cancer cells. This can be achieved by treating cells with DL-α-difluoromethylornithine (DFMO), an inhibitor of ornithine decarboxylase (ODC) that catalyzes the first rate-limiting step in polyamine biosynthesis. If N-WASP based invasiveness depends solely on bundling by these polyamines we should observe a decreased amount of metastasis, resulting in prolonged survival of tumor bearing animals. Supplementation with polyamines should show a reverse effect. The requirement for polyamines could further be tested in TIRF assays with N-WASP coated nanofibers in tumor cell extracts supplemented with fluorescent actin and a range of polyamine concentrations.

Other methods could include binding ligands of physiological polyamines. If polyamine binding proteins, such as spermine binding protein, were overexpressed in cancer cells we should see reduced motility. Depletion of these physiological polycations should attenuate cellular protrusions. If no major effects are observed knockdown of actin bundling proteins, such as fascin, α-actinin, will be performed to reduce filament bundling.

## Larger Significance

After this newly identified function of N-WASP we wonder about the larger significance of the WCA protein sequence. N-WASP belongs to extensive WASP family proteins, mostly defined by their catalytic WCA domain. WCA domains contain single or tandem WH2 domains; key known function of which is to bind monomeric actin. The phylogenetic analysis indicates that initially WASP contained only one WH2 domain and during early metazoan evolution the WH2 domain got duplicated and later lost during vertebrate evolution in WASP (Veltman and Insall, 2010). The earliest known function of WASP was its role in endocytosis and vesicle trafficking from which it has evolved and acquired new roles in regulation of the actin cytoskeleton.

As actin remained highly conserved across species during evolution so did the WASP's actin binding WH2 motif. WH2 domain contains a key LLxxIR consensus sequence that binds between actin subdomain 1 and 3; is found in all WASP subfamily and seems to have remained conserved (Hertzog et al., 2004; Veltman and Insall, 2010). A spacer region whose sequence is not so highly conserved amongst WASP subfamilies follows WH2 domain. This is followed by a central region, which plays a role in autoinhibition (Kim et al., 2000) and Arp2/3 binding (Marchand et al., 2001a). A key region in this domain forms α-helix and has different motifs in each WASP subfamilies (Veltman and Insall, 2010). Amongst subfamilies there is a high degree of sequence conservation in this α-helix suggesting that their role could be subfamily specific. The following domain, a low complexity acidic region is enriched in acidic residues. In WASP, SCAR, and WHAMM/JMY the acidic residue follows immediately after the

central region but in WASH there is a separation of acidic and central region by a spacer of about 100 residues, the function of which still remains unknown.

Recently two new subfamilies of WASP have been identified namely, which we called WAML and WAWH (Kollmar et al., 2012) and further research will help us understand the larger significance of conserved protein sequences. My research focuses on a fascinating new found function of N-WASP's WCA domain and it would be interesting to further study the conserved role of modular domains containing consensus sequence amongst subfamilies.

## References


Ahuja, R., R. Pinyol, N. Reichenbach, L. Custer, J. Klingensmith, M.M. Kessels, and B. Qualmann. 2007. Cordon-bleu is an actin nucleation factor and controls neuronal morphology. *Cell*. 131:337-350.

Aimar, C., and N. Grant. 1992. The role of calcium, polyamines and centrosomes in the formation and organization of cleavage furrows in amphibian eggs. *Biol Cell*. 76:23-31.

Alberts, J.B., and G.M. Odell. 2004. In silico reconstitution of Listeria propulsion exhibits nano-saltation. *PLoS Biol*. 2:e412.

Amann, K.J., and T.D. Pollard. 2001a. Direct real-time observation of actin filament branching mediated by Arp2/3 complex using total internal reflection fluorescence microscopy. *P Natl Acad Sci USA*. 98:15009-15013.

Amann, K.J., and T.D. Pollard. 2001b. Direct real-time observation of actin filament branching mediated by Arp2/3 complex using total internal reflection fluorescence microscopy. *Proc Natl Acad Sci U S A*. 98:15009-15013.

Ashida, Y., J. Kido, F. Kinoshita, M. Nishino, K. Shinkai, H. Akedo, and H. Inoue. 1992. Putrescine-dependent invasive capacity of rat ascites hepatoma cells. *Cancer Res*. 52:5313-5316.

Aziz, S.M., M.N. Gillespie, P.A. Crooks, S.F. Tofiq, C.P. Tsuboi, J.W. Olson, and M.P. Gosland. 1996. The potential of a novel polyamine transport inhibitor in cancer chemotherapy. *The Journal of pharmacology and experimental therapeutics*. 278:185-192.

Bachmann, C., L. Fischer, U. Walter, and M. Reinhard. 1999. The EVH2 domain of the vasodilator-stimulated phosphoprotein mediates tetramerization, F-actin binding, and actin bundle formation. *J Biol Chem*. 274:23549-23557.

Baldassarre, M., I. Ayala, G. Beznoussenko, G. Giacchetti, L.M. Machesky, A. Luini, and R. Buccione. 2006. Actin dynamics at sites of extracellular matrix degradation. *Eur J Cell Biol*. 85:1217-1231.

Bear, J.E., J.F. Rawls, and C.L. Saxe, 3rd. 1998. SCAR, a WASP-related protein, isolated as a suppressor of receptor defects in late Dictyostelium development. *J Cell Biol*. 142:1325-1335.

Berridge, M.J., P. Lipp, and M.D. Bootman. 2000. The versatility and universality of calcium signalling. *Nat Rev Mol Cell Biol*. 1:11-21.

Bers, D.M., C.W. Patton, and R. Nuccitelli. 1994. A practical guide to the preparation of Ca2+ buffers. *Methods Cell Biol*. 40:3-29.

Blanchoin, L., K.J. Amann, H.N. Higgs, J.B. Marchand, D.A. Kaiser, and T.D. Pollard. 2000. Direct observation of dendritic actin filament networks nucleated by Arp2/3 complex and WASP/Scar proteins. *Nature*. 404:1007-1011.

Blanchoin, L., and T.D. Pollard. 1999. Mechanism of interaction of Acanthamoeba actophorin (ADF/Cofilin) with actin filaments. *The Journal of biological chemistry*. 274:15538-15546.

Blanchoin, L., and T.D. Pollard. 2002. Hydrolysis of ATP by polymerized actin depends on the bound divalent cation but not profilin. *Biochemistry*. 41:597-602.

Boczkowska, M., G. Rebowski, M.V. Petoukhov, D.B. Hayes, D.I. Svergun, and R. Dominguez. 2008. X-ray scattering study of activated Arp2/3 complex with bound actin-WCA. *Structure*. 16:695-704.

Bray, D. 2001. Cell Movements From Molecules to Motility. Garland Publishing, New York.

Breitbart, H., S. Rubinstein, and Y. Lax. 1997. Regulatory mechanisms in acrosomal exocytosis. *Reviews of reproduction*. 2:165-174.

Breitsprecher, D., A.K. Kiesewetter, J. Linkner, C. Urbanke, G.P. Resch, J.V. Small, and J. Faix. 2008a. Clustering of VASP actively drives processive, WH2 domain-mediated actin filament elongation. *The EMBO journal*. 27:2943-2954.

Breitsprecher, D., A.K. Kiesewetter, J. Linkner, C. Urbanke, G.P. Resch, J.V. Small, and J. Faix. 2008b. Clustering of VASP actively drives processive, WH2 domain-mediated actin filament elongation. *EMBO J*. 27:2943-2954.

Breitsprecher, D., A.K. Kiesewetter, J. Linkner, M. Vinzenz, T.E. Stradal, J.V. Small, U. Curth, R.B. Dickinson, and J. Faix. 2011. Molecular mechanism of Ena/VASP-mediated actin-filament elongation. *EMBO J*. 30:456-467.

Buccione, R., J.D. Orth, and M.A. McNiven. 2004. Foot and mouth: podosomes, invadopodia and circular dorsal ruffles. *Nat Rev Mol Cell Biol*. 5:647-657.

Bugyi, B., and M.F. Carlier. 2010. Control of actin filament treadmilling in cell motility. *Annu Rev Biophys*. 39:449-470.

Campellone, K.G., N.J. Webb, E.A. Znameroski, and M.D. Welch. 2008. WHAMM is an Arp2/3 complex activator that binds microtubules and functions in ER to Golgi transport. *Cell*. 134:148-161.

Campellone, K.G., and M.D. Welch. 2010. A nucleator arms race: cellular control of actin assembly. *Nat Rev Mol Cell Biol*. 11:237-251.

Carlier, M.F., D. Pantaloni, and E.D. Korn. 1986a. The effects of Mg2+ at the high-affinity and low-affinity sites on the polymerization of actin and associated ATP hydrolysis. *J Biol Chem*. 261:10785-10792.

Carlier, M.F., D. Pantaloni, and E.D. Korn. 1986b. Fluorescence measurements of the binding of cations to high-affinity and low-affinity sites on ATP-G-actin. *J Biol Chem*. 261:10778-10784.

Carlsson, L., L.E. Nystrom, I. Sundkvist, F. Markey, and U. Lindberg. 1977. Actin polymerizability is influenced by profilin, a low molecular weight protein in non-muscle cells. *J Mol Biol*. 115:465-483.

Chambers, A.F., A.C. Groom, and I.C. MacDonald. 2002. Dissemination and growth of cancer cells in metastatic sites. *Nat Rev Cancer*. 2:563-572.

Chereau, D., F. Kerff, P. Graceffa, Z. Grabarek, K. Langsetmo, and R. Dominguez. 2005. Actin-bound structures of Wiskott-Aldrich syndrome protein (WASP)-homology domain 2 and the implications for filament assembly. *Proc Natl Acad Sci USA*. 102:16644-16649.

Co, C., D.T. Wong, S. Gierke, V. Chang, and J. Taunton. 2007. Mechanism of Actin Network Attachment to Moving Membranes: Barbed End Capture by N-WASP WH2 Domains. *Cell*. 128:901-913.

Cooper, J.A., S.B. Walker, and T.D. Pollard. 1983. Pyrene actin: documentation of the validity of a sensitive assay for actin polymerization. *Journal of muscle research and cell motility*. 4:253-262.

Deeks, M.J., and P.J. Hussey. 2005. Arp2/3 and SCAR: plants move to the fore. *Nat Rev Mol Cell Biol*. 6:954-964.

Derry, J.M., H.D. Ochs, and U. Francke. 1994. Isolation of a novel gene mutated in Wiskott-Aldrich syndrome. *Cell*. 79:following 922.

Dickinson, R.B. 2008. A Multi-Scale Mechanistic Model for Actin-Propelled Bacteria. *Cel. Mol. Bioeng.* 1:110-121.

Dickinson, R.B., L. Caro, and D. Purich. 2004. Force Generation by Cytoskeletal Filament End-Tracking Proteins. *Biophysical Journal*. 87:2838-2854.

Dickinson, R.B., and D.L. Purich. 2002. Clamped-filament elongation model for actin-based motors. *Biophysical Journal*. 82:605-617.

Dogterom, M., and B. Yurke. 1997. Measurement of the force-velocity relation for growing microtubules. *Science*. 278:856-860.

Dominguez, R. 2009. Actin filament nucleation and elongation factors--structure-function relationships. *Crit Rev Biochem Mol Biol*. 44:351-366.

Dominguez, R. 2010. The WASP-Homology 2 Domain and Cytoskeleton Assembly. *Actin-based Motility*:255-277.

dos Remedios, C.G., D. Chhabra, M. Kekic, I.V. Dedova, M. Tsubakihara, D.A. Berry, and N.J. Nosworthy. 2003. Actin binding proteins: regulation of cytoskeletal microfilaments. *Physiol Rev*. 83:433-473.

Duncan, M.C., M.J. Cope, B.L. Goode, B. Wendland, and D.G. Drubin. 2001. Yeast Eps15-like endocytic protein, Pan1p, activates the Arp2/3 complex. *Nat Cell Biol*. 3:687-690.

Edelstein, A., N. Amodaj, K. Hoover, R. Vale, and N. Stuurman. 2010. Computer control of microscopes using μManager. *Curr Protoc Mol Biol*. Chapter 14:Unit14.20.

Egile, C., T.P. Loisel, V. Laurent, R. Li, D. Pantaloni, P.J. Sansonetti, and M.-F. Carlier. 1999a. Activation of the CDC42 effector N-WASP by the Shigella flexneri IcsA protein promotes actin nucleation by Arp2/3 complex and bacterial actin-based motility. *J Cell Biol*. 146:1319-1332.

Egile, C., T.P. Loisel, V. Laurent, R. Li, D. Pantaloni, P.J. Sansonetti, and M.F. Carlier. 1999b. Activation of the CDC42 effector N-WASP by the Shigella flexneri IcsA protein promotes actin nucleation by Arp2/3 complex and bacterial actin-based motility. *J Cell Biol*. 146:1319-1332.

Elin, R.J. 1988. Magnesium metabolism in health and disease. *Disease-a-month : DM*. 34:161-218.

Erdman, S.H., N.A. Ignatenko, M.B. Powell, K.A. Blohm-Mangone, H. Holubec, J.M. Guillen-Rodriguez, and E.W. Gerner. 1999. APC-dependent changes in expression of genes influencing polyamine metabolism, and consequences for gastrointestinal carcinogenesis, in the Min mouse. *Carcinogenesis*. 20:1709-1713.

Ferron, F., G. Rebowski, S.H. Lee, and R. Dominguez. 2007. Structural basis for the recruitment of profilin–actin complexes during filament elongation by Ena/VASP. *EMBO J*. 26:4597-4606.

Frieden, C. 1983. Polymerization of actin: mechanism of the Mg2+-induced process at pH 8 and 20 degrees C. *Proc Natl Acad Sci U S A*. 80:6513-6517.

Friedl, P., and D. Gilmour. 2009. Collective cell migration in morphogenesis, regeneration and cancer. *Nat Rev Mol Cell Biol*. 10:445-457.

Gaszner, B., M. Nyitrai, N. Hartvig, T. Koszegi, B. Somogyi, and J. Belagyi. 1999. Replacement of ATP with ADP affects the dynamic and conformational properties of actin monomer. *Biochemistry*. 38:12885-12892.

Gaucher, J.-F., C. Mauge, D. Didry, B. Guichard, L. Renault, and M.-F. Carlier. 2012. Interactions of isolated C-terminal fragments of Neural Wiskott-Aldrich Syndrome Protein (N-WASP) with actin and Arp2/3 complex. *Journal of Biological Chemistry*.

Gavazzi, I., M.V. Nermut, and P.C. Marchisio. 1989. Ultrastructure and gold-immunolabelling of cell-substratum adhesions (podosomes) in RSV-transformed BHK cells. *J Cell Sci*. 94 ( Pt 1):85-99.

Gerner, E.W., and F.L. Meyskens, Jr. 2004. Polyamines and cancer: old molecules, new understanding. *Nat Rev Cancer*. 4:781-792.

Gimona, M., R. Buccione, S.A. Courtneidge, and S. Linder. 2008. Assembly and biological role of podosomes and invadopodia. *Curr Opin Cell Biol*. 20:235-241.

Goldschmidt-Clermont, P.J., M.I. Furman, D. Wachsstock, D. Safer, V.T. Nachmias, and T.D. Pollard. 1992. The control of actin nucleotide exchange by thymosin beta 4 and profilin. A potential regulatory mechanism for actin polymerization in cells. *Molecular biology of the cell*. 3:1015-1024.

Goley, E.D., and M.D. Welch. 2006. The ARP2/3 complex: an actin nucleator comes of age. *Nat Rev Mol Cell Biol*. 7:713-726.

Grant, N.J., C. Oriol-Audit, and M.J. Dickens. 1983. Supramolecular forms of actin induced by polyamines; an electron microscopic study. *Eur J Cell Biol*. 30:67-73.

Gunther, T. 2006. Concentration, compartmentation and metabolic function of intracellular free Mg2+. *Magnes Res*. 19:225-236.

Hanahan, D., and R.A. Weinberg. 2000. The hallmarks of cancer. *Cell*. 100:57-70.

Hanahan, D., and R.A. Weinberg. 2011. Hallmarks of cancer: the next generation. *Cell*. 144:646-674.

Hansen, S.D., and R.D. Mullins. 2010a. VASP is a processive actin polymerase that requires monomeric actin for barbed end association. *The Journal of cell biology*. 191:571-584.

Hansen, S.D., and R.D. Mullins. 2010b. VASP is a processive actin polymerase that requires monomeric actin for barbed end association. *J Cell Biol*. 191:571-584.

Harbeck, B., S. Huttelmaier, K. Schluter, B.M. Jockusch, and S. Illenberger. 2000. Phosphorylation of the vasodilator-stimulated phosphoprotein regulates its interaction with actin. *J Biol Chem*. 275:30817-30825.

Hashimoto, Y., T. Ito, H. Inoue, T. Okumura, E. Tanaka, S. Tsunoda, M. Higashiyama, G. Watanabe, M. Imamura, and Y. Shimada. 2005. Prognostic significance of fascin overexpression in human esophageal squamous cell carcinoma. *Clin Cancer Res*. 11:2597-2605.

Hashimoto, Y., M. Parsons, and J.C. Adams. 2007. Dual actin-bundling and protein kinase C-binding activities of fascin regulate carcinoma cell migration downstream of Rac and contribute to metastasis. *Mol Biol Cell*. 18:4591-4602.

Hertzog, M., C. van Heijenoort, D. Didry, M. Gaudier, J. Coutant, B. Gigant, G. Didelot, T. Preat, M. Knossow, E. Guittet, and M.F. Carlier. 2004. The beta-thymosin/WH2 domain; structural basis for the switch from inhibition to promotion of actin assembly. *Cell*. 117:611-623.

Holmes, K.C., D. Popp, W. Gebhard, and W. Kabsch. 1990. Atomic model of the actin filament. *Nature*. 347:44-49.

Hu, X., and J.R. Kuhn. 2012a. Actin filament attachments for sustained motility in vitro are maintained by filament bundling. *PLoS One*. 7:e31385.

Hu, X., and J.R. Kuhn. 2012b. Actin filament attachments for sustained motility in vitro are maintained by filament bundling. *PLoS ONE*. 7:e31385.

Innocenti, M., A. Zucconi, A. Disanza, E. Frittoli, L.B. Areces, A. Steffen, T.E.B. Stradal, P.P. Di Fiore, M.F. Carlier, and G. Scita. 2004. Abi1 is essential for the formation and activation of a WAVE2 signalling complex. *Nature Cell Biology*. 6:319-327.

Jun, J.Y., J.W. Griffith, R. Bruggeman, S. Washington, L.M. Demers, M.F. Verderame, and A. Manni. 2008. Effects of polyamine depletion by alpha-difluoromethylornithine on in vitro and in vivo biological properties of 4T1 murine mammary cancer cells. *Breast cancer research and treatment*. 107:33-40.

Kang, F., D.L. Purich, and F.S. Southwick. 1999. Profilin promotes barbed-end actin filament assembly without lowering the critical concentration. *J Biol Chem*. 274:36963-36972.

Kaverina, I., T.E. Stradal, and M. Gimona. 2003. Podosome formation in cultured A7r5 vascular smooth muscle cells requires Arp2/3-dependent de-novo actin polymerization at discrete microdomains. *J Cell Sci*. 116:4915-4924.

Kessels, M.M., A.E. Engqvist-Goldstein, D.G. Drubin, and B. Qualmann. 2001. Mammalian Abp1, a signal-responsive F-actin-binding protein, links the actin cytoskeleton to endocytosis via the GTPase dynamin. *J Cell Biol*. 153:351-366.

Khanduja, N., and J.R. Kuhn. 2013. Processive acceleration of actin barbed end assembly by N-WASP. *Mol Biol Cell*.

Kim, A.S., L.T. Kakalis, N. Abdul-Manan, G.A. Liu, and M.K. Rosen. 2000. Autoinhibition and activation mechanisms of the Wiskott-Aldrich syndrome protein. *Nature*. 404:151-158.

Kingsnorth, A.N., P.P. McCann, K.A. Diekema, J.S. Ross, and R.A. Malt. 1983. Effects of alpha-difluoromethylornithine on the growth of experimental Wilms' tumor and renal adenocarcinoma. *Cancer Res*. 43:4031-4034.

Klein, S., J.J. Miret, I.D. Algranati, and E.S. de Lustig. 1985. Effect of alpha-difluoromethylornithine in lung metastases before and after surgery of primary adenocarcinoma tumors in mice. *Biol Cell*. 53:33-36.

Kollmar, M., D. Lbik, and S. Enge. 2012. Evolution of the eukaryotic ARP2/3 activators of the WASP family: WASP, WAVE, WASH, and WHAMM, and the proposed new family members WAWH and WAML. *BMC Res Notes*. 5:88.

Korn, E.D., M.F. Carlier, and D. Pantaloni. 1987. Actin polymerization and ATP hydrolysis. *Science*. 238:638-644.

Kovar, D.R., E.S. Harris, R. Mahaffy, H.N. Higgs, and T.D. Pollard. 2006. Control of the assembly of ATP- and ADP-actin by formins and profilin. *Cell*. 124:423-435.

Kovar, D.R., and T.D. Pollard. 2004a. Insertional assembly of actin filament barbed ends in association with formins produces piconewton forces. *Proceedings of the National Academy of Sciences of the United States of America*. 101:14725-14730.

Kovar, D.R., and T.D. Pollard. 2004b. Insertional assembly of actin filament barbed ends in association with formins produces piconewton forces. *Proc Natl Acad Sci USA*. 101:14725-14730.

Kubota, S., H. Kiyosawa, Y. Nomura, T. Yamada, and Y. Seyama. 1997. Ornithine decarboxylase overexpression in mouse 10T1/2 fibroblasts: cellular transformation and invasion. *Journal of the National Cancer Institute*. 89:567-571.

Kuhn, J.R., and T.D. Pollard. 2005a. Real-time measurements of actin filament polymerization by total internal reflection fluorescence microscopy. *Biophys J*. 88:1387-1402.

Kuhn, J.R., and T.D. Pollard. 2005b. Real-time measurements of actin filament polymerization by total internal reflection fluorescence microscopy. *Biophysical Journal*. 88:1387-1402.

Kuhn, J.R., and T.D. Pollard. 2007. Single molecule kinetic analysis of actin filament capping. Polyphosphoinositides do not dissociate capping proteins. *J Biol Chem*. 282:28014-28024.

Kurisu, S., and T. Takenawa. 2009. The WASP and WAVE family proteins. *Genome Biol*. 10:226.

Lai, F.P., M. Szczodrak, J. Block, J. Faix, D. Breitsprecher, H.G. Mannherz, T.E. Stradal, G.A. Dunn, J.V. Small, and K. Rottner. 2008. Arp2/3 complex interactions and actin network turnover in lamellipodia. *EMBO J*. 27:982-992.

Lassing, I., and U. Lindberg. 1985. Specific interaction between phosphatidylinositol 4,5-bisphosphate and profilactin. *Nature*. 314:472-474.

Laurent, V., T.P. Loisel, B. Harbeck, A. Wehman, L. Gröbe, B.M. Jockusch, J. Wehland, F.B. Gertler, and M.-F. Carlier. 1999. Role of proteins of the Ena/VASP family in actin-based motility of Listeria monocytogenes. *J Cell Biol*. 144:1245-1258.

Li, A., J.C. Dawson, M. Forero-Vargas, H.J. Spence, X. Yu, I. Konig, K. Anderson, and L.M. Machesky. 2010a. The actin-bundling protein fascin stabilizes actin in invadopodia and potentiates protrusive invasion. *Curr Biol*. 20:339-345.

Li, A., J.C. Dawson, M. Forero-Vargas, H.J. Spence, X. Yu, I. König, K. Anderson, and L.M. Machesky. 2010b. The actin-bundling protein fascin stabilizes actin in invadopodia and potentiates protrusive invasion. *Curr Biol*. 20:339-345.

Li, A., Y. Ma, X. Yu, R.L. Mort, C.R. Lindsay, D. Stevenson, D. Strathdee, R.H. Insall, J. Chernoff, S.B. Snapper, I.J. Jackson, L. Larue, O.J. Sansom, and L.M. Machesky. 2011. Rac1 drives melanoblast organization during mouse development by orchestrating pseudopod- driven motility and cell-cycle progression. *Dev Cell*. 21:722-734.

Lim, K., J.X. Ho, K. Keeling, G.L. Gilliland, X. Ji, F. Rüker, and D.C. Carter. 1994. Three-dimensional structure of Schistosoma japonicum glutathione S-transferase fused with a six-amino acid conserved neutralizing epitope of gp41 from HIV. *Protein Sci.* 3:2233-2244.

Linardopoulou, E.V., S.S. Parghi, C. Friedman, G.E. Osborn, S.M. Parkhurst, and B.J. Trask. 2007. Human subtelomeric WASH genes encode a new subclass of the WASP family. *PLoS Genet*. 3:e237.

Linder, S., and M. Aepfelbacher. 2003. Podosomes: adhesion hot-spots of invasive cells. *Trends Cell Biol*. 13:376-385.

Linder, S., H. Higgs, K. Hüfner, K. Schwarz, U. Pannicke, and M. Aepfelbacher. 2000. The polarization defect of Wiskott-Aldrich syndrome macrophages is linked to dislocalization of the Arp2/3 complex. *J Immunol*. 165:221-225.

Linder, S., D. Nelson, M. Weiss, and M. Aepfelbacher. 1999a. Wiskott-Aldrich syndrome protein regulates podosomes in primary human macrophages. *Proc Natl Acad Sci U S A*. 96:9648-9653.

Linder, S., D. Nelson, M. Weiss, and M. Aepfelbacher. 1999b. Wiskott-Aldrich syndrome protein regulates podosomes in primary human macrophages. *Proc Natl Acad Sci USA*. 96:9648-9653.

Lorenz, M., H. Yamaguchi, Y. Wang, R.H. Singer, and J. Condeelis. 2004a. Imaging sites of N-wasp activity in lamellipodia and invadopodia of carcinoma cells. *Current biology : CB*. 14:697-703.

Lorenz, M., H. Yamaguchi, Y. Wang, R.H. Singer, and J. Condeelis. 2004b. Imaging sites of N-wasp activity in lamellipodia and invadopodia of carcinoma cells. *Curr Biol*. 14:697-703.

Luxenburg, C., D. Geblinger, E. Klein, K. Anderson, D. Hanein, B. Geiger, and L. Addadi. 2007. The architecture of the adhesive apparatus of cultured osteoclasts: from podosome formation to sealing zone assembly. *PLoS ONE*. 2:e179.

Machesky, L.M., and R.H. Insall. 1998. Scar1 and the related Wiskott-Aldrich syndrome protein, WASP, regulate the actin cytoskeleton through the Arp2/3 complex. *Curr Biol*. 8:1347-1356.

Machesky, L.M., and R.H. Insall. 1999. Signaling to actin dynamics. *J Cell Biol*. 146:267-272.

Machesky, L.M., and A. Li. 2010. Fascin: Invasive filopodia promoting metastasis. *Communicative & integrative biology*. 3:263-270.

Machesky, L.M., R.D. Mullins, H.N. Higgs, D.A. Kaiser, L. Blanchoin, R.C. May, M.E. Hall, and T.D. Pollard. 1999. Scar, a WASp-related protein, activates nucleation of actin filaments by the Arp2/3 complex. *Proceedings of the National Academy of Sciences of the United States of America*. 96:3739-3744.

Mahaffy, R.E., and T.D. Pollard. 2008. Influence of phalloidin on the formation of actin filament branches by Arp2/3 complex. *Biochemistry*. 47:6460-6467.

Mahoney, N.M., P.A. Janmey, and S.C. Almo. 1997. Structure of the profilin-poly-L-proline complex involved in morphogenesis and cytoskeletal regulation. *Nat Struct Biol*. 4:953-960.

Mahoney, N.M., D.A. Rozwarski, E. Fedorov, A.A. Fedorov, and S.C. Almo. 1999. Profilin binds proline-rich ligands in two distinct amide backbone orientations. *Nature structural biology*. 6:666-671.

Manni, A., S. Washington, X. Hu, J.W. Griffith, R. Bruggeman, L.M. Demers, D. Mauger, and M.F. Verderame. 2005. Effects of polyamine synthesis inhibitors on primary tumor features and metastatic capacity of human breast cancer cells. *Clin Exp Metastasis*. 22:255-263.

Marchand, J.B., D.A. Kaiser, T.D. Pollard, and H.N. Higgs. 2001a. Interaction of WASP/Scar proteins with actin and vertebrate Arp2/3 complex. *Nat Cell Biol*. 3:76-82.

Marchand, J.B., D.A. Kaiser, T.D. Pollard, and H.N. Higgs. 2001b. Interaction of WASP/Scar proteins with actin and vertebrate Arp2/3 complex. *Nat Cell Biol*. 3:76-82.

Matters, G.L., A. Manni, and J.S. Bond. 2005. Inhibitors of polyamine biosynthesis decrease the expression of the metalloproteases meprin alpha and MMP-7 in hormone-independent human breast cancer cells. *Clin Exp Metastasis*. 22:331-339.

Mehlen, P., and A. Puisieux. 2006. Metastasis: a question of life or death. *Nat Rev Cancer*. 6:449-458.

Melki, R., S. Fievez, and M.F. Carlier. 1996. Continuous monitoring of Pi release following nucleotide hydrolysis in actin or tubulin assembly using 2-amino-6-mercapto-7-methylpurine ribonucleoside and purine-nucleoside phosphorylase as an enzyme-linked assay. *Biochemistry*. 35:12038-12045.

Metzler, W.J., A.J. Bell, E. Ernst, T.B. Lavoie, and L. Mueller. 1994. Identification of the poly-L-proline-binding site on human profilin. *J Biol Chem*. 269:4620-4625.

Miki, H., K. Miura, and T. Takenawa. 1996. N-WASP, a novel actin-depolymerizing protein, regulates the cortical cytoskeletal rearrangement in a PIP2-dependent manner downstream of tyrosine kinases. *EMBO J*. 15:5326-5335.

Miki, H., T. Sasaki, Y. Takai, and T. Takenawa. 1998a. Induction of filopodium formation by a WASP-related actin-depolymerizing protein N-WASP. *Nature*. 391:93-96.

Miki, H., S. Suetsugu, and T. Takenawa. 1998b. WAVE, a novel WASP-family protein involved in actin reorganization induced by Rac. *The EMBO journal*. 17:6932-6941.

Miki, H., and T. Takenawa. 1998. Direct binding of the verprolin-homology domain in N-WASP to actin is essential for cytoskeletal reorganization. *Biochemical and biophysical research communications*. 243:73-78.

Millard, T.H., S.J. Sharp, and L.M. Machesky. 2004a. Signalling to actin assembly via the WASP (Wiskott-Aldrich syndrome protein)-family proteins and the Arp2/3 complex. *Biochem J*. 380:1-17.

Millard, T.H., S.J. Sharp, and L.M. Machesky. 2004b. Signalling to actin assembly via the WASP (Wiskott-Aldrich syndrome protein)-family proteins and the Arp2/3 complex. *Biochem J*. 380:1-17.

Mitchison, T.J., and L.P. Cramer. 1996. Actin-based cell motility and cell locomotion. *Cell*. 84:371-379.

Mizutani, K., H. Miki, H. He, H. Maruta, and T. Takenawa. 2002a. Essential role of neural Wiskott-Aldrich syndrome protein in podosome formation and degradation of extracellular matrix in src-transformed fibroblasts. *Cancer Res*. 62:669-674.

Mizutani, K., H. Miki, H. He, H. Maruta, and T. Takenawa. 2002b. Essential role of neural Wiskott-Aldrich syndrome protein in podosome formation and degradation of extracellular matrix in src-transformed fibroblasts. *Cancer Res*. 62:669-674.

Mockrin, S.C., and E.D. Korn. 1980. Acanthamoeba profilin interacts with G-actin to increase the rate of exchange of actin-bound adenosine 5'-triphosphate. *Biochemistry*. 19:5359-5362.

Mogilner, A., and G. Oster. 1996. Cell motility driven by actin polymerization. *Biophys J*. 71:3030-3045.

Mogilner, A., and G. Oster. 2003a. Force Generation by Actin Polymerization II: The Elastic Ratchet and Tethered Filaments. *Biophys J*. 84:1591-1605.

Mogilner, A., and G. Oster. 2003b. Polymer motors: pushing out the front and pulling up the back. *Curr Biol*. 13:R721-733.

Monti, M.G., L. Pernecco, R. Manfredini, C. Frassineti, D. Barbieri, G. Marverti, and S. Ghiaroni. 1996. Inhibition of cell growth by accumulated spermine is associated with a transient alteration of cell cycle progression. *Life sciences*. 58:2065-2072.

Moseley, J.B., I. Sagot, A.L. Manning, Y. Xu, M.J. Eck, D. Pellman, and B.L. Goode. 2004. A conserved mechanism for Bni1- and mDia1-induced actin assembly and dual regulation of Bni1 by Bud6 and profilin. *Mol Biol Cell*. 15:896-907.

Mueller, S.C., and W.T. Chen. 1991. Cellular invasion into matrix beads: localization of beta 1 integrins and fibronectin to the invadopodia. *J Cell Sci*. 99 ( Pt 2):213-225.

Mullins, R.D. 2000. How WASP-family proteins and the Arp2/3 complex convert intracellular signals into cytoskeletal structures. *Curr Opin Cell Biol*. 12:91-96.

Mullins, R.D., J.A. Heuser, and T.D. Pollard. 1998a. The interaction of Arp2/3 complex with actin: nucleation, high affinity pointed end capping, and formation of branching networks of filaments. *Proceedings of the National Academy of Sciences of the United States of America*. 95:6181-6186.

Mullins, R.D., J.A. Heuser, and T.D. Pollard. 1998b. The interaction of Arp2/3 complex with actin: nucleation, high affinity pointed end capping, and formation of branching networks of filaments. *Proc Natl Acad Sci U S A*. 95:6181-6186.

Mullins, R.D., W.F. Stafford, and T.D. Pollard. 1997. Structure, subunit topology, and actin-binding activity of the Arp2/3 complex from Acanthamoeba. *J Cell Biol*. 136:331-343.

Murphy, D.A., and S.A. Courtneidge. 2011. The 'ins' and 'outs' of podosomes and invadopodia: characteristics, formation and function. *Nature reviews. Molecular cell biology*. 12:413-426.

Nadler, J.L., and R.K. Rude. 1995. Disorders of magnesium metabolism. *Endocrinology and metabolism clinics of North America*. 24:623-641.

Nakagawa, H., H. Miki, M. Ito, K. Ohashi, T. Takenawa, and S. Miyamoto. 2001. N-WASP, WAVE and Mena play different roles in the organization of actin cytoskeleton in lamellipodia. *J Cell Sci*. 114:1555-1565.

Namgoong, S., M. Boczkowska, M.J. Glista, J.D. Winkelman, G. Rebowski, D.R. Kovar, and R. Dominguez. 2011. Mechanism of actin filament nucleation by Vibrio VopL and implications for tandem W domain nucleation. *Nat Struct Mol Biol*. 18:1060-1067.

Narumiya, S., M. Tanji, and T. Ishizaki. 2009. Rho signaling, ROCK and mDia1, in transformation, metastasis and invasion. *Cancer metastasis reviews*. 28:65-76.

Nureki, O., M. Hattori, and R. Ishitani. 2008. [Mechanism of cellular magnesium balance regulation by a magnesium transporter]. *Seikagaku. The Journal of Japanese Biochemical Society*. 80:933-939.

Okada, K., T. Shimura, K. Asakawa, S. Hashimoto, Y. Mochida, T. Suehiro, and H. Kuwano. 2007. Fascin expression is correlated with tumor progression of extrahepatic bile duct cancer. *Hepato-gastroenterology*. 54:17-21.

Oosawa, F. 1983. Macromolecular assembly of actin. In Muscle and Nonmuscle Motility. *Academic Press*:151–216.

Oriol-Audit, C. 1978. Polyamine-induced actin polymerization. *Eur J Biochem*. 87:371-376.

Oriol-Audit, C. 1982. Actin-polyamines interaction : relationship between physicochemical properties and cytokinesis induction. *Biochem Biophys Res Commun*. 105:1096-1101.

Oser, M., H. Yamaguchi, C.C. Mader, J.J. Bravo-Cordero, M. Arias, X. Chen, V. Desmarais, J. van Rheenen, A.J. Koleske, and J. Condeelis. 2009. Cortactin regulates cofilin and N-WASp activities to control the stages of invadopodium assembly and maturation. *J Cell Biol*. 186:571-587.

Otomo, T., D.R. Tomchick, C. Otomo, S.C. Panchal, M. Machius, and M.K. Rosen. 2005. Structural basis of actin filament nucleation and processive capping by a formin homology 2 domain. *Nature*. 433:488-494.

Padrick, S.B., H.-C. Cheng, A.M. Ismail, S.C. Panchal, L.K. Doolittle, S. Kim, B.M. Skehan, J. Umetani, C.A. Brautigam, J.M. Leong, and M.K. Rosen. 2008. Hierarchical regulation of WASP/WAVE proteins. *Mol Cell*. 32:426-438.

Padrick, S.B., L.K. Doolittle, C.A. Brautigam, D.S. King, and M.K. Rosen. 2011. Arp2/3 complex is bound and activated by two WASP proteins. *Proc Natl Acad Sci USA*. 108:E472-479.

Padrick, S.B., and M.K. Rosen. 2010. Physical mechanisms of signal integration by WASP family proteins. *Annu Rev Biochem*. 79:707-735.

Patton, C., S. Thompson, and D. Epel. 2004. Some precautions in using chelators to buffer metals in biological solutions. *Cell Calcium*. 35:427-431.

Paul, A.S., and T.D. Pollard. 2009a. Energetic requirements for processive elongation of actin filaments by FH1FH2-formins. *J Biol Chem*. 284:12533-12540.

Paul, A.S., and T.D. Pollard. 2009b. Review of the mechanism of processive actin filament elongation by formins. *Cell Motil Cytoskeleton*. 66:606-617.

Peskin, C.S., G.M. Odell, and G.F. Oster. 1993. Cellular motions and thermal fluctuations: the Brownian ratchet. *Biophys J*. 65:316-324.

Pollard, T.D. 1986. Rate constants for the reactions of ATP- and ADP-actin with the ends of actin filaments. *J Cell Biol*. 103:2747-2754.

Pollard, T.D., L. Blanchoin, and R.D. Mullins. 2000a. Molecular mechanisms controlling actin filament dynamics in nonmuscle cells. *Annual review of biophysics and biomolecular structure*. 29:545-576.

Pollard, T.D., L. Blanchoin, and R.D. Mullins. 2000b. Molecular mechanisms controlling actin filament dynamics in nonmuscle cells. *Annu Rev Biophys Biomol Struct*. 29:545-576.

Pollard, T.D., and G.G. Borisy. 2003. Cellular motility driven by assembly and disassembly of actin filaments. *Cell*. 112:453-465.

Pollard, T.D., and J.A. Cooper. 1984. Quantitative analysis of the effect of Acanthamoeba profilin on actin filament nucleation and elongation. *Biochemistry (Mosc)*. 23:6631-6641.

Pollard, T.D., and J.A. Cooper. 2009. Actin, a central player in cell shape and movement. *Science*. 326:1208-1212.

Pollitt, A.Y., and R.H. Insall. 2009. WASP and SCAR/WAVE proteins: the drivers of actin assembly. *J Cell Sci*. 122:2575-2578.

Puius, Y.A., N.M. Mahoney, and S.C. Almo. 1998. The modular structure of actin-regulatory proteins. *Curr Opin Cell Biol*. 10:23-34.

Quinlan, M.E., S. Hilgert, A. Bedrossian, R.D. Mullins, and E. Kerkhoff. 2007. Regulatory interactions between two actin nucleators, Spire and Cappuccino. *J Cell Biol*. 179:117-128.

Ramesh, N., I.M. Anton, J.H. Hartwig, and R.S. Geha. 1997. WIP, a protein associated with wiskott-aldrich syndrome protein, induces actin polymerization and redistribution in lymphoid cells. *Proc Natl Acad Sci U S A*. 94:14671-14676.

Rebowski, G., M. Boczkowska, D.B. Hayes, L. Guo, T.C. Irving, and R. Dominguez. 2008. X-ray scattering study of actin polymerization nuclei assembled by tandem W domains. *Proc Natl Acad Sci USA*. 105:10785-10790.

Reis, M.A., F.G. Reyes, M.J. Saad, and L.A. Velloso. 2000. Magnesium deficiency modulates the insulin signaling pathway in liver but not muscle of rats. *The Journal of nutrition*. 130:133-138.

Rink, T.J., R.Y. Tsien, and T. Pozzan. 1982. Cytoplasmic pH and free Mg2+ in lymphocytes. *J Cell Biol*. 95:189-196.

Robinson, R.C., K. Turbedsky, D.A. Kaiser, J.B. Marchand, H.N. Higgs, S. Choe, and T.D. Pollard. 2001. Crystal structure of Arp2/3 complex. *Science*. 294:1679-1684.

Rodal, A.A., O. Sokolova, D.B. Robins, K.M. Daugherty, S. Hippenmeyer, H. Riezman, N. Grigorieff, and B.L. Goode. 2005. Conformational changes in the Arp2/3 complex leading to actin nucleation. *Nat Struct Mol Biol*. 12:26-31.

Rohatgi, R., H.Y. Ho, and M.W. Kirschner. 2000. Mechanism of N-WASP activation by CDC42 and phosphatidylinositol 4, 5-bisphosphate. *J Cell Biol*. 150:1299-1310.

Rohatgi, R., L. Ma, H. Miki, M. Lopez, T. Kirchhausen, T. Takenawa, and M.W. Kirschner. 1999. The interaction between N-WASP and the Arp2/3 complex links Cdc42-dependent signals to actin assembly. *Cell*. 97:221-231.

Romani, A., and A. Scarpa. 1992. Regulation of cell magnesium. *Arch Biochem Biophys*. 298:1-12.

Romani, A.M., and A. Scarpa. 2000. Regulation of cellular magnesium. *Front Biosci*. 5:D720-734.

Romero, S., C.L. Clainche, D. Didry, C. Egile, D. Pantaloni, and M.-F. Carlier. 2004. Formin is a processive motor that requires profilin to accelerate actin assembly and associated ATP hydrolysis. *Cell*. 119:419-429.

Romero, S., D. Didry, E. Larquet, N. Boisset, D. Pantaloni, and M.-F. Carlier. 2007. How ATP hydrolysis controls filament assembly from profilin-actin: implication for formin processivity. *J Biol Chem*. 282:8435-8445.

Russell, D.H. 1977. Clinical relevance of polyamines as biochemical markers of tumor kinetics. *Clinical chemistry*. 23:22-27.

Russell, D.H. 1983. Clinical relevance of polyamines. *Critical reviews in clinical laboratory sciences*. 18:261-311.

Saris, N.E., E. Mervaala, H. Karppanen, J.A. Khawaja, and A. Lewenstam. 2000. Magnesium. An update on physiological, clinical and analytical aspects. *Clinica chimica acta; international journal of clinical chemistry*. 294:1-26.

Sarmiento, C., W. Wang, A. Dovas, H. Yamaguchi, M. Sidani, M. El-Sibai, V. Desmarais, H.A. Holman, S. Kitchen, J.M. Backer, A. Alberts, and J. Condeelis. 2008. WASP family members and formin proteins coordinate regulation of cell protrusions in carcinoma cells. *J Cell Biol*. 180:1245-1260.

Schneider, C.A., and W.S. Rasband. 2012. NIH Image to ImageJ: 25 years of image analysis. *Nature Methods*.

Schoumacher, M., R.D. Goldman, D. Louvard, and D.M. Vignjevic. 2010. Actin, microtubules, and vimentin intermediate filaments cooperate for elongation of invadopodia. *J Cell Biol*. 189:541-556.

Shemesh, T., T. Otomo, M.K. Rosen, A.D. Bershadsky, and M.M. Kozlov. 2005. A novel mechanism of actin filament processive capping by formin: solution of the rotation paradox. *The Journal of cell biology*. 170:889-893.

Small, J.V., G. Isenberg, and J.E. Celis. 1978a. Polarity of Actin at Leading-Edge of Cultured-Cells. *Nature*. 272:638-639.

Small, J.V., G. Isenberg, and J.E. Celis. 1978b. Polarity of actin at the leading edge of cultured cells. *Nature*. 272:638-639.

Snapper, S.B., F. Takeshima, I. Antón, C.H. Liu, S.M. Thomas, D. Nguyen, D. Dudley, H. Fraser, D. Purich, M. Lopez-Ilasaca, C. Klein, L. Davidson, R. Bronson, R.C. Mulligan, F. Southwick, R. Geha, M.B. Goldberg, F.S. Rosen, J.H. Hartwig, and F.W. Alt. 2001. N-WASP deficiency reveals distinct pathways for cell surface projections and microbial actin-based motility. *Nat Cell Biol*. 3:897-904.

Soo, F.S., and J.A. Theriot. 2005. Adhesion controls bacterial actin polymerization-based movement. *Proc Natl Acad Sci USA*. 102:16233-16238.

Sowa, G.Z., D.S. Cannell, A.J. Liu, and E. Reisler. 2006. Polyamine-induced bundling of F-actin. *J Phys Chem B*. 110:22279-22284.

Spudich, J.A., and S. Watt. 1971a. The regulation of rabbit skeletal muscle contraction. I. Biochemical studies of the interaction of the tropomyosin-troponin complex with actin and the proteolytic fragments of myosin. *J Biol Chem*. 246:4866-4871.

Spudich, J.A., and S. Watt. 1971b. The regulation of rabbit skeletal muscle contraction. I. Biochemical studies of the interaction of the tropomyosin-troponin complex with actin and the proteolytic fragments of myosin. *J Biol Chem*. 246:4866-4871.

Steffen, A., J. Faix, G.P. Resch, J. Linkner, J. Wehland, J.V. Small, K. Rottner, and T.E. Stradal. 2006. Filopodia formation in the absence of functional WAVE- and Arp2/3-complexes. *Mol Biol Cell*. 17:2581-2591.

Stradal, T.E., K. Rottner, A. Disanza, S. Confalonieri, M. Innocenti, and G. Scita. 2004. Regulation of actin dynamics by WASP and WAVE family proteins. *Trends Cell Biol*. 14:303-311.

Stradal, T.E.B., and G. Scita. 2006. Protein complexes regulating Arp2/3-mediated actin assembly. *Curr Opin Cell Biol*. 18:4-10.

Straub, F.B. 1942. Actin. *Stud. Szeged*:3-15.

Strzelecka-Gooaszewska, H., G. Boguta, S. Zmorzynski, and J. Moraczewska. 1989. Biochemical and theoretical approach to localization of metal-ion-binding sites in the actin primary structure. *Eur J Biochem*. 182:299-305.

Suetsugu, S., H. Miki, and T. Takenawa. 1998. The essential role of profilin in the assembly of actin for microspike formation. *EMBO J*. 17:6516-6526.

Suetsugu, S., H. Miki, and T. Takenawa. 1999. Identification of two human WAVE/SCAR homologues as general actin regulatory molecules which associate with the Arp2/3 complex. *Biochem Biophys Res Commun*. 260:296-302.

Suraneni, P., B. Rubinstein, J.R. Unruh, M. Durnin, D. Hanein, and R. Li. 2012. The Arp2/3 complex is required for lamellipodia extension and directional fibroblast cell migration. *The Journal of cell biology*. 197:239-251.

Swaminathan, R. 2003. Magnesium metabolism and its disorders. *The Clinical biochemist. Reviews / Australian Association of Clinical Biochemists*. 24:47-66.

Swaminathan, V., K. Mythreye, E.T. O'Brien, A. Berchuck, G.C. Blobe, and R. Superfine. 2011. Mechanical stiffness grades metastatic potential in patient tumor cells and in cancer cell lines. *Cancer Res*. 71:5075-5080.

Takeichi, M., and T.S. Okada. 1972. Roles of magnesium and calcium ions in cell-to-substrate adhesion. *Exp Cell Res*. 74:51-60.

Takenawa, T., and H. Miki. 2001. WASP and WAVE family proteins: key molecules for rapid rearrangement of cortical actin filaments and cell movement. *J Cell Sci*. 114:1801-1809.

Takenawa, T., and S. Suetsugu. 2007a. The WASP-WAVE protein network: connecting the membrane to the cytoskeleton. *Nat Rev Mol Cell Biol*. 8:37-48.

Takenawa, T., and S. Suetsugu. 2007b. The WASP-WAVE protein network: connecting the membrane to the cytoskeleton. *Nat Rev Mol Cell Biol*. 8:37-48.

Tang, J.X., and P.A. Janmey. 1996. The polyelectrolyte nature of F-actin and the mechanism of actin bundle formation. *J Biol Chem*. 271:8556-8563.

Tarone, G., D. Cirillo, F.G. Giancotti, P.M. Comoglio, and P.C. Marchisio. 1985. Rous sarcoma virus-transformed fibroblasts adhere primarily at discrete protrusions of the ventral membrane called podosomes. *Exp Cell Res*. 159:141-157.

Uruno, T., J. Liu, P. Zhang, Y. Fan, C. Egile, R. Li, S.C. Mueller, and X. Zhan. 2001. Activation of Arp2/3 complex-mediated actin polymerization by cortactin. *Nat Cell Biol*. 3:259-266.

Vartiainen, M.K., and L.M. Machesky. 2004. The WASP-Arp2/3 pathway: genetic insights. *Curr Opin Cell Biol*. 16:174-181.

Veltman, D.M., and R.H. Insall. 2010. WASP family proteins: their evolution and its physiological implications. *Mol Biol Cell*. 21:2880-2893.

Wallon, U.M., L.R. Shassetz, A.E. Cress, G.T. Bowden, and E.W. Gerner. 1994. Polyamine-dependent expression of the matrix metalloproteinase matrilysin in a human colon cancer-derived cell line. *Molecular carcinogenesis*. 11:138-144.

Weaver, A.M., A.V. Karginov, A.W. Kinley, S.A. Weed, Y. Li, J.T. Parsons, and J.A. Cooper. 2001. Cortactin promotes and stabilizes Arp2/3-induced actin filament network formation. *Curr Biol*. 11:370-374.

Weed, S.A., A.V. Karginov, D.A. Schafer, A.M. Weaver, A.W. Kinley, J.A. Cooper, and J.T. Parsons. 2000. Cortactin localization to sites of actin assembly in lamellipodia requires interactions with F-actin and the Arp2/3 complex. *J Cell Biol*. 151:29-40.

Wegner, A. 1976. Head to tail polymerization of actin. *J Mol Biol*. 108:139-150.

Weigelt, B., J.L. Peterse, and L.J. van 't Veer. 2005. Breast cancer metastasis: markers and models. *Nat Rev Cancer*. 5:591-602.

Xu, X.-P., I. Rouiller, B.D. Slaughter, C. Egile, E. Kim, J.R. Unruh, X. Fan, T.D. Pollard, R. Li, D. Hanein, and N. Volkmann. 2011. Three-dimensional reconstructions of Arp2/3 complex with bound nucleation promoting factors. *EMBO J*. 31:236-247.

Yamaguchi, H., M. Lorenz, S. Kempiak, C. Sarmiento, S. Coniglio, M. Symons, J. Segall, R. Eddy, H. Miki, T. Takenawa, and J. Condeelis. 2005. Molecular mechanisms of invadopodium formation: the role of the N-WASP-Arp2/3 complex pathway and cofilin. *J Cell Biol*. 168:441-452.

Yamaguchi, H., H. Miki, S. Suetsugu, L. Ma, M.W. Kirschner, and T. Takenawa. 2000. Two tandem verprolin homology domains are necessary for a strong activation of Arp2/3 complex-induced actin polymerization and induction of microspike formation by N-WASP. *Proc Natl Acad Sci U S A*. 97:12631-12636.

Yang, C., M. Huang, J. DeBiasio, M. Pring, M. Joyce, H. Miki, T. Takenawa, and S.H. Zigmond. 2000. Profilin enhances Cdc42-induced nucleation of actin polymerization. *J Cell Biol*. 150:1001-1012.

Zuchero, J.B., A.S. Coutts, M.E. Quinlan, N.B. Thangue, and R.D. Mullins. 2009. p53-cofactor JMY is a multifunctional actin nucleation factor. *Nat Cell Biol*. 11:451-459.